Relaxation and decoherence in quantum spin system

Yuan, Shengjun

Relaxation and Decoherence in Quantum Spin System

Shengjun Yuan

2008

To my parents and my wife

University of Groningen
Zernike Institute
for Advanced Materials

Zernike Institute PhD thesis series 2008-01
ISSN 1570-1530

The work described in this thesis was performed at the Department of Applied Physics of the Rijksuniversiteit Groningen, the Netherlands.

ISBN electronic version: 978-90-367-3303-8
ISBN printed version: 978-90-367-3302-1

RIJKSUNIVERSITEIT GRONINGEN

Relaxation and Decoherence in Quantum Spin System

Proefschrift

ter verkrijging van het doctoraat in de
Wiskunde en Natuurwetenschappen
aan de Rijksuniversiteit Groningen
op gezag van de
Rector Magnificus, dr. F. Zwarts,
in het openbaar te verdedigen op
vrijdag 18 januari 2008
om 14:45 uur

door

Shengjun Yuan

geboren op 16 april 1979
te Enshi, Hubei, China

Promotor: Prof.dr. H.A. De Raedt

Beoordelingscommissie: Prof.dr. S. Miyashita
Prof.dr. M.I. Katsnelson
Prof.dr.ir. P.H.M. van Loosdrecht

Contents

Chapter 1

Introduction

Quantum spin systems are of much interest recently, not only because of their relevance to magnetic (nano) materials in general but also because of their relation to the quantum computation and quantum information in particular. The quantum computer promises to be more powerful than classical computers in solving some particular problems such as integer factorization, database search, and simulation of quantum systems. Quantum information combines communications and cryptography and is considered to be absolute secure. In the physical realization of quantum computation and quantum information, one major problem is keeping the components of the computer or communication channel in a coherent quantum state. The interaction with the external world reduces the coherence (phase relations) between the states of the quantum system. This effect, called decoherence, destroys the unitary transformations that are essential for quantum information processing. Therefore, the study of relaxation and decoherence in quantum spin systems is necessary to understand the basic phenomena that are at play.

Quantum spin systems are rather complicated many-body systems and except for some special cases their time evolution cannot be calculated analytically. With the help of powerful modern computers and efficient algorithms, we can simulate the dynamics of the system directly by solving the time-dependent Schrödinger equation. A lot of useful information can be extracted from these simulations, information that may be relevant for the development of a theory or experimental study of these systems.

In this thesis, we will focus on two different quantum spin problems. The first concerns the relaxation and decoherence of a central system of two spins

that is coupled to a spin-bath environment. This problem is not only related to the progress of the physical realization of quantum computer and quantum information, but also addresses fundamental conjectures of decoherence theory. Another topic is the stability of domain wall and its interaction with spin waves in spin 1/2 chain, which is relevant to the critical phenomena and quantum communication in quantum spin systems.

The contents of each chapter are the following:

In Chapter 2, we present the details of the physical model and the algorithms that we use to perform the computer simulations.

In Chapter 3, we study the relaxation and decoherence in a system of two antiferromagnetically coupled spins that interact with a spin-bath environment, which is initially prepared in its ground state. Systems are considered that range from the rotationally invariant to highly anisotropic spin models, for instance, the couplings among the bath spins or between them and the central two spins, can be isotropic Heisenberg or Ising-like. The interactions have different topologies and values of parameters that are fixed or allowed to fluctuate randomly. We explore the conditions under which the two-spin system clearly shows an evolution from the initial spin-up -spin-down state towards the maximally entangled singlet state. We demonstrate that frustration and, especially, glassiness of the spin environment strongly enhances decoherence of the two-spin system.

In Chapter 4, we continue the study of decoherence of two coupled spins that interact with a frustrated spin-bath environment in its ground state. The central system can be either ferromagnetic or antiferromagnetic. The conditions under which the two-spin system relaxes from the initial spin-up - spin-down state towards its ground state are determined. It is demonstrated that the symmetry of the coupling between the two-spin system and the environment has an important effect on the relaxation process. In particular, we show that if this coupling conserves the magnetization, the two-spin system readily relaxes to its ground state whereas a non-conserving coupling prevents the two-spin system from coming close to its ground state.

In Chapter 5, we study decoherence of two coupled spins that interact with a chaotic spin-bath environment which initially is prepared in a random superposition of all the basis states of the environment. This state corresponds to the equilibrium density matrix of the environment at infinite temperature. It is shown that connectivity of spins in the bath is of crucial importance for decoherence of the central system. The previously found phenomenon of

two-step decoherence (V. V. Dobrovitski et al, Phys. Rev. Lett. **90**, 210401 (2003)) turns out to be typical for the bath with a slow enough dynamics or no internal interactions. For a generic random system with chaotic dynamics, a conventional exponential relaxation to the pointer states takes place. Our results confirm a conjecture that for weak enough interactions, the pointer states are eigenstates of the central system.

In Chapter 6, we demonstrate that magnetic chains with uniaxial anisotropy support stable structures, separating ferromagnetic domains of opposite magnetization. These structures, domain walls in a quantum system, are shown to remain stable if they interact with a spin wave. The value of the phase shift of spin waves passing through a domain wall was found to be proportional to the angle by which the magnetization of domain wall rotates in the film plane (R. Hertel et al, Phys. Rev. Lett. **93** 257202 (2004)). We find that a domain wall transmits the longitudinal component of the spin excitations only. Our results suggest that continuous, classical spin models described by Landau-Lifshitz-Gilbert equation cannot be used to describe spin wave-domain wall interaction in microscopic magnetic systems.

In Chapter 7, we study the real-time domain-wall dynamics near a quantum critical point of the one-dimensional anisotropic ferromagnetic spin 1/2 chain. It is known that the ground state of this model in the subspace of total magnetization zero supports domain wall structures. However, if we let the system evolve in time from an initial state with a domain wall structure and this initial state is not an eigenstate, it must contain some excited states. Therefore, the question whether the domain wall structure will survive in the stationary (long-time) regime is nontrivial. In this chapter, we focus on the dynamic stability of the domain wall in the Heisenberg-Ising ferromagnetic chain, and by numerical simulation, we find the domain wall is dynamically stable in the Heisenberg-Ising model. Near the quantum critical point, the width of the domain wall diverges as $(\Delta - 1)^{-1/2}$. We also show that the domain wall profiles rapidly become very stable as we move away from the quantum critical point.

Chapter 2

Model and Algorithm

The measurement of the spin component of particles such as electrons, protons, and neutrons along any direction yield either $\hbar/2$ or $-\hbar/2$, and we call these particles as spin 1/2 particles. The state corresponds to the outcome $\hbar/2$ is convenient to be named as spin up ($|\uparrow\rangle$) and $-\hbar/2$ as spin down ($|\downarrow\rangle$). Mathematically, the states

$$|\uparrow\rangle = |0\rangle = \begin{pmatrix} 1 \\ 0 \end{pmatrix}, \text{ and } |\downarrow\rangle = |1\rangle = \begin{pmatrix} 0 \\ 1 \end{pmatrix} \tag{2.1}$$

are the eigenstates of z component of the spin 1/2 operator $\mathbf{S} = (S^x, S^y, S^z)$ with eigenvalues $+1/2$ and $-1/2$. Here S^x, S^y, S^z are defined (in units such that $\hbar = 1$) by

$$S^x = \frac{1}{2}\begin{pmatrix} 0 & 1 \\ 1 & 0 \end{pmatrix}, S^y = \frac{1}{2}\begin{pmatrix} 0 & i \\ -i & 0 \end{pmatrix}, \text{ and } S^z = \frac{1}{2}\begin{pmatrix} 1 & 0 \\ 0 & -1 \end{pmatrix}. \tag{2.2}$$

In general, the wavefunction of a single spin 1/2 particle can be written as a linear combination of the spin up and spin down by

$$|\phi\rangle = a(\uparrow)|\uparrow\rangle + a(\downarrow)|\downarrow\rangle, \tag{2.3}$$

where $a(\uparrow)$ and $a(\downarrow)$ are complex numbers, and it is convenient to normalize $\langle\phi|\phi\rangle = 1$:

$$|a(\uparrow)|^2 + |a(\downarrow)|^2 = 1. \tag{2.4}$$

Similarly, the state of a spin 1/2 system with N spins can be represented by

$$\begin{aligned} |\phi\rangle = {} & a(\uparrow\uparrow \ldots \uparrow\uparrow)|\uparrow\uparrow \ldots \uparrow\uparrow\rangle + a(\uparrow\uparrow \ldots \uparrow\downarrow)|\uparrow\uparrow \ldots \uparrow\downarrow\rangle + \ldots \\ & + a(\downarrow\downarrow \ldots \downarrow\uparrow)|\downarrow\downarrow \ldots \downarrow\uparrow\rangle + a(\downarrow\downarrow \ldots \downarrow\downarrow)|\downarrow\downarrow \ldots \downarrow\downarrow\rangle. \end{aligned} \tag{2.5}$$

Let spin up (down) corresponds to the state 0 (1) as Eq.(2.1), then

$$\begin{aligned}|\phi\rangle &= a(00...00)\,|00...00\rangle + a(00...01)\,|00...01\rangle + ... \\ &+ a\,(11...10)\,|11...10\rangle + a\,(11...11)\,|11...11\rangle \\ &= \sum_{k=0}^{2^N-1} a_k\,|k\rangle\,. \end{aligned} \tag{2.6}$$

Here we denote the spins from right to left, which means in the translations of notations, from spin up (down) to a binary number, the first bit in the binary number corresponds to the $1st$ spin, and the last bit to the N-th spin. The coefficients a_k are complex numbers, and it is convenient to normalize $\langle\phi|\phi\rangle = 1$:

$$\sum_{k=0}^{2^N-1} |a_k|^2 = 1. \tag{2.7}$$

Generally, the Hamiltonian of a spin 1/2 system with N coupled spins is represented by

$$H\,(t) = -\sum_{i,j=1}^{N}\sum_{\alpha=x,y,z} J_{i,j}^{\alpha}(t) S_i^{\alpha} S_j^{\alpha} - \sum_{i=1}^{N}\sum_{\alpha=x,y,z} h_i^{\alpha}(t) S_i^{\alpha}, \tag{2.8}$$

where the exchange integrals $J_{i,j}^{\alpha}$ determine the strength of the interaction between the α components of spins i and j, and $\mathbf{h}_i = (h_i^x, h_i^y, h_i^z)$ is the external magnetic field applied on the $i-th$ spin.

To calculate the time evolution of this system we need solve the TDSE

$$i\frac{\partial}{\partial t}\,|\phi(t)\rangle = H\,(t)\,|\phi(t)\rangle\,, \tag{2.9}$$

which has the solution

$$|\phi(t)\rangle = U\,(t)\,|\phi(0)\rangle = e^{-i\int H(t)dt}\,|\phi(0)\rangle\,. \tag{2.10}$$

If the Hamiltonian is time independent, Eq.(2.10) becomes

$$|\phi(t)\rangle = U\,(t)\,|\phi(0)\rangle = e^{-itH}\,|\phi(0)\rangle\,. \tag{2.11}$$

If the Hamiltonian is time dependent, we can choose a relevant small time step τ, during which the Hamiltonian can be regarded as a constant, then the relation of the wave function at time $t+\tau$ and t can be represented as

$$|\phi(t+\tau)\rangle = U\,(\tau)\,|\phi(t)\rangle \simeq e^{-i\tau H(t)}\,|\phi(t)\rangle\,. \tag{2.12}$$

Equations (2.11) and (2.10) have the similar expression, and there are several numerical algorithms to calculate them. In the following sections we will give a brief introduction to the algorithms that we used in our simulation.

2.1 Spin 1/2 Operations

First we consider the single spin 1/2 operation $|\phi'\rangle = S_m^\alpha |\phi\rangle$, where $\alpha = x, y, z$:

$$\left|\phi'\right\rangle = S_m^\alpha |\phi\rangle = \sum_{k=0}^{2^N-1} a'_k |k\rangle . \tag{2.13}$$

It follows from Eq.(2.2) that the coefficients a' and a have the rules:

(i) for S_m^z

$$\begin{aligned} a'(*...0_m...*) &= +\frac{1}{2} a(*...0_m...*) , \\ a'(*...1_m...*) &= -\frac{1}{2} a(*...1_m...*) ; \end{aligned} \tag{2.14}$$

(ii) for S_m^x

$$\begin{aligned} a'(*...0_m...*) &= +\frac{1}{2} a(*...1_m...*) , \\ a'(*...1_m...*) &= +\frac{1}{2} a(*...0_m...*) ; \end{aligned} \tag{2.15}$$

(iii) for S_m^y

$$\begin{aligned} a'(*...0_m...*) &= -\frac{i}{2} a(*...1_m...*) , \\ a'(*...1_m...*) &= +\frac{i}{2} a(*...0_m...*) . \end{aligned} \tag{2.16}$$

The bit strings on the left and right hand sides of each equation above are identical except for the m-th bit.

The two spin 1/2 operation $|\phi''\rangle = S_m^\alpha S_n^\alpha |\phi\rangle = \sum_{k=0}^{2^N-1} a''_k |k\rangle$ can also be constructed similarly:

(i) for $S_m^z S_n^z$

$$\begin{aligned}
a'\left(*...0_m...0_n...*\right) &= +\frac{1}{4}a\left(*...0_m...0_n...*\right), \\
a'\left(*...0_m...1_n...*\right) &= -\frac{1}{4}a\left(*...0_m...1_n...*\right), \\
a'\left(*...1_m...0_n...*\right) &= -\frac{1}{4}a\left(*...1_m...0_n...*\right), \\
a'\left(*...1_m...1_n...*\right) &= +\frac{1}{4}a\left(*...1_m...1_n...*\right); \qquad (2.17)
\end{aligned}$$

(ii) for $S_m^x S_n^x$

$$\begin{aligned}
a'\left(*...0_m...0_n...*\right) &= +\frac{1}{4}a\left(*...1_m...1_n...*\right), \\
a'\left(*...0_m...1_n...*\right) &= +\frac{1}{4}a\left(*...1_m...0_n...*\right), \\
a'\left(*...1_m...0_n...*\right) &= +\frac{1}{4}a\left(*...0_m...1_n...*\right), \\
a'\left(*...1_m...1_n...*\right) &= +\frac{1}{4}a\left(*...0_m...0_n...*\right); \qquad (2.18)
\end{aligned}$$

(iii) for $S_m^y S_n^y$

$$\begin{aligned}
a'\left(*...0_m...0_n...*\right) &= -\frac{1}{4}a\left(*...1_m...1_n...*\right), \\
a'\left(*...0_m...1_n...*\right) &= +\frac{1}{4}a\left(*...1_m...0_n...*\right), \\
a'\left(*...1_m...0_n...*\right) &= +\frac{1}{4}a\left(*...0_m...1_n...*\right), \\
a'\left(*...1_m...1_n...*\right) &= -\frac{1}{4}a\left(*...0_m...0_n...*\right). \qquad (2.19)
\end{aligned}$$

Similarly, the bit strings on the left and right sides of each equation above are identical except the m-th and n-th bits.

Next we will discuss how to construct the time evolution operator $U(t)$ in a form by which we can perform the single and two spin 1/2 operations direct to the wave function $|\phi\rangle$.

2.2 Chebyshev Polynomial Algorithm

The Chebyshev polynomial algorithm is based on the numerically exact polynomial decomposition of the operator $U(t) = e^{-itH}$.

Firstly we need the polynomial decomposition of e^{-izx}, where x is a real number in the range $[-1, 1]$.

Let $x \equiv \cos\theta$, since [1]

$$\cos(zx) = J_0(z) + 2\sum_{m=1}^{\infty}(-1)^m J_{2m}(z)\cos(2m\theta), \tag{2.20}$$

$$\sin(zx) = 2\sum_{m=0}^{\infty}(-1)^m J_{2m+1}(z)\cos\{(2m+1)\theta\}, \tag{2.21}$$

where $J_m(z)$ is the Bessel function of integer order m, we have

$$\begin{aligned}
e^{-izx} &= \cos(zx) - i\sin(zx) \\
&= J_0(z) - 2iJ_1(z)\cos\theta \\
&+ 2\sum_{m=1}^{\infty}(-1)^m\left[J_{2m}(z)\cos(2m\theta) - iJ_{2m+1}(z)\cos\{(2m+1)\theta\}\right] \\
&= J_0(z) - 2iJ_1(z)\cos\theta \\
&+ 2\sum_{m=1}^{\infty}\left[i^{2m}J_{2m}(z)\cos(2m\theta) - i^{2m+1}J_{2m+1}(z)\cos\{(2m+1)\theta\}\right] \\
&= J_0(z) + 2\sum_{m=1}^{\infty}(-i)^m J_m(z)\cos(m\theta) \\
&= J_0(z) + 2\sum_{m=1}^{\infty}(-i)^m J_m(z)T_m(x),
\end{aligned} \tag{2.22}$$

where $T_m(x) = \cos[m\arccos(x)]$ is the Chebyshev polynomial of the first kind [1]. $T_m(x)$ obeys the following recurrence relation:

$$T_{m+1}(x) + T_{m-1}(x) = 2xT_m(x). \tag{2.23}$$

The Bessel function $\{J_m(z)\}$ can be numerically generated by using the following recurrence relation and associated series [1]

$$J_{m-1}(z) = \frac{2m}{z}J_m(z) + J_{m+1}(z), \tag{2.24}$$

$$J_0(z) + 2J_2(z) + 2J_4(z) + 2J_6(z) + \cdots = 1. \tag{2.25}$$

The recurrence relation Eq.(2.24) should only be used in the decreasing way in the program, otherwise the result will not converge [2]. $|J_m(z)|$ vanishes very rapidly if m becomes larger than z [3], and therefore we can find a fix M such

that for all $m \geq M$, we have $|J_m(z)| < \epsilon$. Here ϵ is a small positive number, for example 10^{-15}, which determines the accuracy of the approximation of the generated $\{J_m(z)\}$.

We will derive an expression of M in the following.

From [1], the Bessel functions $J_m(mz)$ have upper bounds [2]

$$|J_m(mz)| \leq \left| \frac{z^m \exp\left[m\sqrt{1-z^2}\right]}{\left[1+\sqrt{1-z^2}\right]^m} \right|, \tag{2.26a}$$

and similarly we have

$$|J_m(z)| \leq \left| \frac{\left(\frac{z}{m}\right)^m \exp\left[m\sqrt{1-\left(\frac{z}{m}\right)^2}\right]}{\left[1+\sqrt{1-\left(\frac{z}{m}\right)^2}\right]^m} \right|, \text{for } m \geq |z|. \tag{2.27}$$

Since for $z > 0$, $1+\sqrt{1-(z/m)^2} < 2$ and therefore from Eq.(2.27) we get

$$\ln|J_m(z)| < m\ln(\frac{z}{2m}) + \sqrt{m^2-z^2} < m\left[\ln(\frac{z}{2m})+1\right], \tag{2.28}$$

which implies that

$$|J_m(z)| < e^{m\left[\ln(\frac{z}{2m})+1\right]}. \tag{2.29}$$

The inequality $|J_m(z)| < \epsilon$ holds when $\exp\left\{m\left[\ln(\frac{z}{2m})+1\right]\right\} \leq \epsilon$, which is equivalent to

$$m\left[\ln(\frac{z}{2m})+1\right] \leq \ln\epsilon, \tag{2.30}$$

where ϵ is a small positive number and can be denoted as $\epsilon \equiv \exp(-\alpha)$, where $\alpha > 1$. Equation (2.30) becomes

$$\ln(\frac{z}{2m})+1 \leq -\frac{\alpha}{m}, \tag{2.31}$$

since $m \geq z$, Eq.(2.31) also holds if

$$\ln(\frac{z}{2m})+1 \leq -\frac{\alpha}{z}, \tag{2.32}$$

or

$$m \geq \frac{1}{2}ze^{\left(1+\frac{\alpha}{z}\right)} = \frac{1}{2}ze^{\left(1-\frac{\ln\epsilon}{z}\right)}. \tag{2.33}$$

Therefore, we can introduce

$$M \equiv z\exp\left[1-(\ln\epsilon)/z\right]/2, \tag{2.34}$$

then, for all $m \geq M$, we have $|J_m(z)| < \epsilon$. Now Eq.(2.22) can be written as:

$$e^{-izx} \simeq J_0(z) + 2\sum_{m=1}^{M} (-i)^m J_m(z) T_m(x). \tag{2.35}$$

In practice, the generation of $\{J_m(z)\}$ is very fast, even if ϵ equals the numerical precision of the machine.

We can now derive the polynomial decomposition of the operator $U(t) = e^{-itH}$. Since the Hamiltonian H has a complete set of eigenvectors $|E_n\rangle$ with real valued eigenvalues E_n, we can expand the wave function $|\phi(0)\rangle$ as a superposition of the $|E_n\rangle$

$$|\phi(0)\rangle = \sum_{n=1}^{2^N} |E_n\rangle \langle E_n|\phi(0)\rangle, \tag{2.36}$$

and therefore

$$|\phi(t)\rangle = e^{-itH}|\phi(0)\rangle = \sum_{n=1}^{2^N} e^{-itE_n}|E_n\rangle \langle E_n|\phi(0)\rangle. \tag{2.37}$$

Now we introduce $\|H\|_b$ as a positive number which is not smaller than the maximum of the eigenvalues E_n, that is

$$\|H\|_b \geq \|H\|_m \equiv \max\{E_n\}, \tag{2.38}$$

and introduce new variables $\hat{t} \equiv t\|H\|_b$ and $\hat{E}_n \equiv E_n/\|H\|_b$, where $\hat{E}_n$ are the eigenvalues of a modified Hamiltonian $\hat{H} \equiv H/\|H\|_b$, that is

$$\hat{H}|E_n\rangle = \hat{E}_n|E_n\rangle. \tag{2.39}$$

Now we can rewrite Eq.(2.37) as

$$|\phi(t)\rangle = \sum_{n=1}^{2^N} e^{-i\hat{t}\hat{E}_n}|E_n\rangle \langle E_n|\phi(0)\rangle. \tag{2.40}$$

Here $\left|\hat{E}_n\right| \leq 1$, which means that $\hat{E}_n$ has the same value interval of x in Eq.(2.22). Then we can use Eq.(2.22) to decompose the operator $e^{-i\hat{t}\hat{E}_n}$. By using the inequality

$$\left\|\sum_{n=1}^{N} X_n\right\| \leq \sum_{n=1}^{N} \|X_n\|, \tag{2.41}$$

and the elementary bounds

$$\|s_k^\alpha\| = \frac{1}{2}, \ \left\|s_k^\alpha s_{k'}^{\alpha'}\right\| = \frac{1}{4}, \tag{2.42}$$

with the Hamiltonian H of Eq.(2.8) we find

$$\|H\|_m \leq \frac{1}{4}\sum_{i,j=1}^{N}\sum_{\alpha=x,y,z}\left|J_{i,j}^\alpha(t)\right| + \frac{1}{2}\sum_{i=1}^{N}\sum_{\alpha=x,y,z}\left|h_i^\alpha(t)\right|. \tag{2.43}$$

Then we introduce $\|H\|_b$

$$\|H\|_b \equiv \frac{1}{4}\sum_{i,j=1}^{N}\sum_{\alpha=x,y,z}\left|J_{i,j}^\alpha(t)\right| + \frac{1}{2}\sum_{i=1}^{N}\sum_{\alpha=x,y,z}\left|h_i^\alpha(t)\right|. \tag{2.44}$$

Now we use Eq.(2.35) to rewrite Eq.(2.40) as

$$\begin{aligned}
|\phi(t)\rangle &\simeq \sum_{n=1}^{2^N}\left[J_0(\hat{t}) + 2\sum_{m=1}^{M_n}(-i)^m J_m\left(\hat{t}\right) T_m\left(\hat{E}_n\right)\right]|E_n\rangle\langle E_n|\phi(0)\rangle \\
&= J_0(\hat{t})\,|\phi(0)\rangle + 2\sum_{m=1}^{M}(-i)^m J_m\left(\hat{t}\right)\sum_{n=1}^{2^N} T_m\left(\hat{E}_n\right)|E_n\rangle\langle E_n|\phi(0)\rangle \\
&= \left[J_0(\hat{t})\hat{T}_0\left(\hat{H}\right) + 2\sum_{m=1}^{M} J_m\left(\hat{t}\right)\hat{T}_m\left(\hat{H}\right)\right]|\phi(0)\rangle,
\end{aligned} \tag{2.45}$$

where

$$M_n \equiv \hat{E}_n \exp\left[1 - (\ln\epsilon)/\hat{E}_n\right]/2, M \equiv \max\{M_n\}, \tag{2.46}$$

and

$$\hat{T}_m\left(\hat{H}\right) = (-i)^m T_m\left(\hat{H}\right) = (-i)^m \sum_{n=1}^{2^N} T_m\left(\hat{E}_n\right)|E_n\rangle\langle E_n|, \tag{2.47}$$

is a 2^N-dimensional matrix, with diagonal elements $\hat{T}_m(\hat{E}_n)$, the modified Chebyshev polynomial, which is related with the Chebyshev polynomial $T_m(\hat{E}_n)$ by

$$\hat{T}_m\left(\hat{E}_n\right) = (-i)^m T_m\left(\hat{E}_n\right). \tag{2.48}$$

The first two matrices $\hat{T}_m$ are given by

$$\hat{T}_0\left(\hat{H}\right)|\phi\rangle = I\,|\phi\rangle\,, \hat{T}_1\left(\hat{H}\right)|\phi\rangle = -i\hat{H}\,|\phi\rangle\,. \tag{2.49}$$

From Eq.(2.23), we have the recurrence relation of the Chebyshev polynomial $T_m\left(\hat{E}_n\right)$

$$T_{m+1}\left(\hat{E}_n\right) + T_{m-1}\left(\hat{E}_n\right) = 2\hat{E}_n T_m\left(\hat{E}_n\right), \tag{2.50}$$

and therefore we can get the following recurrence relation for the matrix $\hat{T}_m\left(\hat{H}\right)$

$$\begin{aligned}\hat{T}_{m+1}\left(\hat{H}\right)|\phi\rangle &= (-i)^{m+1}\sum_{n=1}^{2^N}\left[2\hat{E}_n T_m\left(\hat{E}_n\right) - T_{m-1}\left(\hat{E}_n\right)\right]|E_n\rangle\langle E_n|\phi\rangle \\ &= (-i)^{m+1}\left[2\hat{H}T_m\left(\hat{H}\right) - T_{m-1}\left(\hat{H}\right)\right]|\phi\rangle \\ &= -2i\hat{H}\hat{T}_m\left(\hat{H}\right)|\phi\rangle + \hat{T}_{m-1}\left(\hat{H}\right)|\phi\rangle, \end{aligned} \tag{2.51}$$

for $m \geq 1$.

By using the recurrence relation Eq.(2.51) together with Eq.(2.49), we can get $\{\hat{T}_m\left(\hat{H}\right)|\phi(0)\rangle,\ m = 0, 1, ..., M\}$, and performing the sum in Eq.(2.45), the wave function at time t can be obtained.

2.3 Suzuki-Trotter Product-Formula Algorithm

In the previous section, we introduce the Chebyshev polynomial to reduce the exponential operation ($e^{-itH}|\phi\rangle$) into linear operations ($\hat{H}|\phi\rangle$). In the following, we will introduce Suzuki-Trotter product-formula algorithm to compute the matrix exponential directly. The basic idea of this algorithm is to decompose the time evolution operator into several independent exponential operation, which can be applied to the wave function separately and directly.

The Suzuki-Trotter product-formula algorithm is based on a systematic approximation of the unitary matrix exponential [4, 5],

$$U(t) = e^{-itH} = e^{-it(H_1+H_2+\cdots+H_N)} = \lim_{m\to\infty}\left(\prod_{n=1}^{N} e^{-itH_n/m}\right)^m, \tag{2.52}$$

and generalizations thereof [6–8]. For understanding why Eq.(2.52) holds,

one can compare two Taylor series

$$\begin{aligned} e^{(H_1+H_2)/m} &= 1+\frac{(H_1+H_2)}{m}+\frac{(H_1+H_2)^2}{2m^2}+O\left(\frac{1}{m^3}\right) \\ &= 1+\frac{(H_1+H_2)}{m}+\frac{H_1^2+H_1H_2+H_2H_1+H_2^2}{2m^2} \\ &\quad +O\left(\frac{1}{m^3}\right), \end{aligned} \tag{2.53}$$

and

$$e^{H_1/m}e^{H_2/m}=1+\frac{(H_1+H_2)}{m}+\frac{H_1^2+2H_1H_2+H_2^2}{2m^2}+O\left(\frac{1}{m^3}\right). \tag{2.54}$$

It is clear that for sufficiently large m, two expressions above are equal up to terms of $O\left([H_1,H_2]/m^2\right)$, then we have

$$e^{H_1+H_2}=\lim_{m\to\infty}(e^{H_1/m}e^{H_2/m})^m. \tag{2.55}$$

One can also show that [5]

$$\left\|e^{H_1+H_2}-\left(e^{H_1/m}e^{H_2/m}\right)^m\right\|\leq\frac{1}{2m}\left\|[H_1,H_2]\right\|e^{(\|H_1\|+\|H_2\|)}, \tag{2.56}$$

and

$$\begin{aligned} &\left\|e^{H_1+H_2+\cdots+H_N}-\left(e^{H_1/m}e^{H_2/m}...e^{H_2/m}\right)^m\right\| \\ \leq\ &\frac{1}{2m}\sum_{1\leq i\leq j\leq N}\left\|[H_i,H_j]\right\|e^{(\|H_1\|+\|H_2\|+...+\|H_N\|)}. \end{aligned} \tag{2.57}$$

Equation (2.52) suggests that for a short time interval

$$U_1(\tau)=e^{-i\tau H_1}\cdots e^{-i\tau H_n}\cdots e^{-i\tau H_N} \tag{2.58}$$

is a good approximation to $U(\tau)$ if τ is sufficiently small. If all H_n in Eq.(2.58) are Hermitian, then $U_1(\tau)$ is unitary and the algorithm based on Eq.(2.58) is unconditionally stable. We have

$$\left\|U(\tau)-U_1(\tau)\right\|\leq\frac{\tau^2}{2}\sum_{i<j}\left\|[H_i-H_j]\right\|, \tag{2.59}$$

therefore $U_1(\tau)$ may be a good approximation to $U(\tau)$ if we use small time steps τ such that $\tau\left\|H\right\|\ll 1$. It also follows from Eq.(2.59) that the Taylor

series of $U(\tau)$ and $U_1(\tau)$ are identical up to first order in τ and we call $U_1(\tau)$ a first-order approximation of $U(\tau)$.

The Suzuki-Trotter product-formula approach provides a simple, systematic procedure to improve the accuracy of the approximation of $U(\tau)$ without changing its fundamental properties. We can introduce higher-order approximations, for example, the unitary matrix

$$U_2(\tau) = U_1^+(-\tau/2)\,U_1(\tau/2) = e^{-i\tau H_N/2}\cdots e^{-i\tau H_1/2}e^{-i\tau H_1/2}\cdots e^{-i\tau H_N/2} \tag{2.60}$$

is a second-order approximation of $U(\tau)$ [6–8], and we have [9]

$$\|U(\tau) - U_2(\tau)\| \leq c_2\tau^2, \tag{2.61}$$

where c_2 is a positive constant. A fourth-order approximation can be constructed as [6, 8]

$$U_4(\tau) = U_2(a\tau)\,U_2(a\tau)\,U_2((1-4a)\tau)\,U_2(a\tau)\,U_2(a\tau), \tag{2.62}$$

where $a = 1/\left(4 - 4^{1/3}\right)$, and we have

$$\|U(\tau) - U_4(\tau)\| \leq c_4\tau^4, \tag{2.63}$$

where c_4 is a positive constant. Equations (2.59), (2.61) and (2.63) give the rigorous error bounds of the approximations, and the approximation Eq.(2.60) and Eq.(2.62) have proven to be very useful for a wide range of different applications [7–15]. The crucial step to apply the Suzuki-Trotter product-formula algorithm in our spin system is how to choose the Hermitian matrixes $\{H_n\}$ such that the operators $e^{-i\tau H_n}$ can be calculated efficiently.

We first decompose the Hamiltonian H in Eq.(2.8) into two parts:

$$H_a(t) = -\sum_{j=1}^{N}\sum_{\alpha=x,y,z} h_j^\alpha(t)S_j^\alpha, \tag{2.64}$$

$$H_b(t) = -\sum_{j,k=1}^{N}\sum_{\alpha=x,y,z} J_{j,k}^\alpha(t)S_j^\alpha S_k^\alpha, \tag{2.65}$$

where $H_a(t)$ contains the external time-dependent fields and $H_b(t)$ contains the exchange coupling of the spins.

For $H_a(t)$, we consider the case when the external field changes slowly such that in each small time step τ the external field can be regarded as a constant.

Since the spin operators with different spin labels commute, that is $[S_i^\alpha, S_j^\alpha] = 0$, and using the fact that

$$e^{A+B} = e^A e^B \quad \text{if } [A,B] = 0, \tag{2.66}$$

we have

$$\begin{aligned} U_a(\tau) &= e^{-i\tau H_a(t)} = \exp\left[i\tau \sum_{j=1}^{N} \sum_{\alpha=x,y,z} h_j^\alpha(t) S_j^\alpha \right] \\ &= \prod_{j=1}^{N} \exp\left[i\tau \sum_{\alpha=x,y,z} h_j^\alpha(t) S_j^\alpha \right] = \prod_{j=1}^{N} \exp\left[i\tau \mathbf{S}_j \cdot \mathbf{h}_j(t) \right]. \end{aligned} \tag{2.67}$$

We introduce $\widehat{\mathbf{h}}_j(t) \equiv \mathbf{h}_j(t)/h_j(t)$, where $h_j(t) = \|\mathbf{h}_j(t)\|$. Then $\mathbf{S}_j \cdot \widehat{\mathbf{h}}_j(t)$ is the projection of $\mathbf{S}_j$ on the direction $\widehat{\mathbf{h}}_j(t)$ and it is easy to prove that

$$\begin{aligned} & \exp\left[i\tau \mathbf{S}_j \cdot \mathbf{h}_j(t) \right] \\ = \; & \cos\left(\frac{\tau h_j(t)}{2} \right) + 2i \mathbf{S}_j \cdot \widehat{\mathbf{h}}_j(t) \sin\left(\frac{\tau h_j(t)}{2} \right) \\ = \; & \begin{pmatrix} \cos\left(\frac{\tau h_j(t)}{2}\right) + \frac{i h_j^z(t)}{h_j(t)} \sin\left(\frac{\tau h_j(t)}{2}\right) & \frac{i h_j^x(t) + h_j^y(t)}{h_j(t)} \sin\left(\frac{\tau h_j(t)}{2}\right) \\ \frac{i h_j^x(t) - h_j^y(t)}{h_j(t)} \sin\left(\frac{\tau h_j(t)}{2}\right) & \cos\left(\frac{\tau h_j(t)}{2}\right) - \frac{i h_j^z(t)}{h_j(t)} \sin\left(\frac{\tau h_j(t)}{2}\right) \end{pmatrix}. \end{aligned} \tag{2.68}$$

For $H_b(t)$, the pair-product decomposition is defined by [5, 16]

$$\begin{aligned} U_b(\tau) &= e^{-i\tau H_b(t)} = \exp\left[i\tau \sum_{j,k=1}^{N} \sum_{\alpha=x,y,z} J_{j,k}^\alpha(t) S_j^\alpha S_k^\alpha \right] \\ &= \prod_{j,k=1}^{N} \exp\left[i\tau \sum_{\alpha=x,y,z} J_{j,k}^\alpha(t) S_j^\alpha S_k^\alpha \right], \end{aligned} \tag{2.69}$$

and each factor can be calculated analytically as

$$\begin{aligned} & \exp\left[i\tau \sum_{\alpha=x,y,z} J_{j,k}^\alpha(t) S_j^\alpha S_k^\alpha \right] \\ = \; & \begin{pmatrix} e^{ia\tau}\cos b\tau & 0 & 0 & i e^{ia\tau}\sin b\tau \\ 0 & e^{-ia\tau}\cos c\tau & i e^{-ia\tau}\sin c\tau & 0 \\ 0 & i e^{-ia\tau}\sin c\tau & e^{-ia\tau}\cos c\tau & 0 \\ i e^{ia\tau}\sin b\tau & 0 & 0 & e^{ia\tau}\cos b\tau \end{pmatrix}_{jk}, \end{aligned} \tag{2.70}$$

where $a = J^z_{j,k}(t)/4$, $b = \left[J^x_{j,k}(t) - J^y_{j,k}(t)\right]/4$ and $c = \left[J^x_{j,k}(t) + J^y_{j,k}(t)\right]/4$. The matrix in Eq.(2.68) is just a single spin 1/2 operation. Equation (2.70) is more complicated but can be performed in a similar manner as two spin 1/2 operation, therefore we will not give a more detailed description.

2.4 Exact Diagonalization Algorithm

In this and the following section, we will discuss the algorithms which will perform the operation $U(t)|\phi\rangle$ without using the single or two spin 1/2 operations: the exact diagonalization algorithm and short-iterative Lanczos algorithm.

The Hamiltonian H in Eq.(2.8) is a 2^N-dimensional Hermitian matrix, and it has a complete set of eigenvectors and real-valued eigenvalues. We can find a unitary matrix Ω ($\Omega^+\Omega = I$) to diagonalize H as [17]

$$\Omega^+ H \Omega = \widetilde{H}, \tag{2.71}$$

where $\widetilde{H}$ is a diagonal matrix. Then, the time evolution operator becomes

$$\begin{aligned} U(t) = e^{-itH} = e^{-it\Omega\widetilde{H}\Omega^+} &= \sum_{n=0}^{\infty} \frac{\left(-it\Omega\widetilde{H}\Omega^+\right)^n}{n!} \\ &= \sum_{n=0}^{\infty} \frac{(-it)^n \left(\Omega\widetilde{H}\Omega^+\right)_1 \left(\Omega\widetilde{H}\Omega^+\right)_2 \cdots \left(\Omega\widetilde{H}\Omega^+\right)_{n-1} \left(\Omega\widetilde{H}\Omega^+\right)_n}{n!} \\ &= \Omega \sum_{n=0}^{\infty} \frac{\left(-it\widetilde{H}\right)^n}{n!} \Omega^+ = \Omega e^{-it\widetilde{H}} \Omega^+. \end{aligned} \tag{2.72}$$

The elements of matrix $\widetilde{H}$ are non-zero only along the diagonal:

$$\widetilde{H} = \begin{bmatrix} m_1 & 0 & \cdots & 0 & \cdots & 0 & 0 \\ 0 & m_2 & \cdots & 0 & \cdots & 0 & 0 \\ \vdots & \vdots & \ddots & \vdots & \ddots & \vdots & \vdots \\ 0 & 0 & \cdots & m_k & \cdots & 0 & 0 \\ \vdots & \vdots & \ddots & \vdots & \ddots & \vdots & \vdots \\ 0 & 0 & \cdots & 0 & \cdots & m_{2^N-1} & 0 \\ 0 & 0 & \cdots & 0 & \cdots & 0 & m_{2^N} \end{bmatrix}, \tag{2.73}$$

and the operator $e^{-it\widetilde{H}}$ can be expanded in a series

$$
\begin{aligned}
e^{-it\widetilde{H}} &= \sum_{n=0}^{\infty} \frac{(-it)^n}{n!} \widetilde{H}^n \\
&= \sum_{n=0}^{\infty} \frac{(-it)^n}{n!} \begin{bmatrix}
m_1^n & 0 & \cdots & 0 & \cdots & 0 & 0 \\
0 & m_2^n & \cdots & 0 & \cdots & 0 & 0 \\
\vdots & \vdots & \ddots & \vdots & \ddots & \vdots & \vdots \\
0 & 0 & \cdots & m_k^n & \cdots & 0 & 0 \\
\vdots & \vdots & \ddots & \vdots & \ddots & \vdots & \vdots \\
0 & 0 & \cdots & 0 & \cdots & m_{2^N-1}^n & 0 \\
0 & 0 & \cdots & 0 & \cdots & 0 & m_{2^N}^n
\end{bmatrix} \\
&= \begin{bmatrix}
e^{-itm_1} & 0 & \cdots & 0 & \cdots & 0 & 0 \\
0 & e^{-itm_2} & \cdots & 0 & \cdots & 0 & 0 \\
\vdots & \vdots & \ddots & \vdots & \ddots & \vdots & \vdots \\
0 & 0 & \cdots & e^{-itm_k} & \cdots & 0 & 0 \\
\vdots & \vdots & \ddots & \vdots & \ddots & \vdots & \vdots \\
0 & 0 & \cdots & 0 & \cdots & e^{-itm_{2^N-1}} & 0 \\
0 & 0 & \cdots & 0 & \cdots & 0 & e^{-itm_{2^N}}
\end{bmatrix}.
\end{aligned}
\tag{2.74}
$$

It is clear that if we find the unitary matrix Ω and the eigenvalues $\{m_k\}$ of H, the time evolution operator $U(t)$ can be performed by simple matrix multiplications. Diagonalizing the Hermitian matrix H is straightforward: we use a standard linear algebra package such as LAPACK.

The algorithm based on exact diagonalization is simple, but it needs a lot of memory to store and perform the diagonalization. The memory and CPU time of the direct diagonalization scale as D^2 and D^3 respectively [17–19]. Thus we can use this technique for small systems (up to $L \approx 13$) only.

2.5 Lanczos Algorithm

The basic idea of the Lanczos algorithm [3, 20] is to use the Lanczos recursion to project the Hamiltonian onto a new basis in which H is a tri-diagonal matrix and can be diagonalized easily.

Let $|\phi(0)\rangle$ be a randomly selected initial state. We denote the Lanczos vector by $|\phi_i\rangle$ ($i = 0, 1, 2, ..., j$ where $j \leq D$), and introduce scalars by

$$\alpha_i \equiv \langle\phi_i| H |\phi_i\rangle , \beta_{i+1} \equiv \langle\phi_{i+1}| H |\phi_i\rangle , \tag{2.75}$$

and

$$\beta_1 = 0, |\phi_0\rangle = 0, \text{ and } |\phi_1\rangle = |\phi(0)\rangle / \sqrt{\langle\phi(0)|\phi(0)\rangle}. \tag{2.76}$$

We generate the Lanczos vectors as

$$\beta_{i+1} |\phi_{i+1}\rangle = H |\phi_i\rangle - \alpha_i |\phi_i\rangle - \beta_i |\phi_{i-1}\rangle . \tag{2.77}$$

We will now proof that

$$\langle\phi_i|\phi_{i'}\rangle = \delta \left(i - i'\right) . \tag{2.78}$$

By construction we have $\langle\phi_1|\phi_1\rangle = 1$, and it is easy to show that $\langle\phi_1|\phi_2\rangle = 0$ and $\langle\phi_2|\phi_2\rangle = 1$ (multiply $\langle\phi_1|$ or $\langle\phi_2|$ on both sides of Eq.(2.77) and take $i = 1$). That means Eq.(2.78) is true for $i \leq 2$. Assume Eq.(2.78) is true for $i, i' \leq k$ ($k \geq 2$), that is, $\langle\phi_i|\phi_{i'}\rangle = \delta (i - i')$ for $i, i' \leq k$, we will show that it is also true for $i, i' \leq k + 1$, which means that we need prove

$$\langle\phi_i|\phi_{k+1}\rangle = \delta (k + 1 - i) \text{ for } i \leq k + 1. \tag{2.79}$$

First, from Eq.(2.77) we have that

$$\beta_{i+1} \langle\phi_k|\phi_{i+1}\rangle = \langle\phi_k| H |\phi_i\rangle - \alpha_i \langle\phi_k|\phi_i\rangle - \beta_i \langle\phi_k|\phi_{i-1}\rangle , \tag{2.80}$$

and for $i \leq k - 2$, $\langle\phi_k|\phi_{i+1}\rangle = \langle\phi_k|\phi_i\rangle = \langle\phi_k|\phi_{i-1}\rangle = 0$, therefore

$$\langle\phi_k| H |\phi_i\rangle = 0 \text{ for } i \leq k - 2. \tag{2.81}$$

From Eq.(2.77), we have that

$$\beta_{k+1} \langle\phi_i|\phi_{k+1}\rangle = \langle\phi_i| H |\phi_k\rangle - \alpha_k \langle\phi_i|\phi_k\rangle - \beta_k \langle\phi_i|\phi_{k-1}\rangle , \tag{2.82}$$

1) for $i \leq k - 2$, $\langle\phi_i| H |\phi_k\rangle = \langle\phi_i|\phi_k\rangle = \langle\phi_i|\phi_{k-1}\rangle = 0$, therefore

$$\langle\phi_i|\phi_{k+1}\rangle = 0 \text{ for } i \leq k - 2; \tag{2.83}$$

2) for $i = k - 1$, $\langle\phi_i| H |\phi_k\rangle = \beta_k$, $\langle\phi_i|\phi_k\rangle = 0$, therefore

$$\langle\phi_i|\phi_{k+1}\rangle = 0 \text{ for } i = k - 1; \tag{2.84}$$

3) for $i = k$, $\langle\phi_i| H |\phi_k\rangle = \alpha_k$, $\langle\phi_i|\phi_{k-1}\rangle = 0$, therefore

$$\langle\phi_i|\phi_{k+1}\rangle = 0 \text{ for } i = k; \tag{2.85}$$

4) for $i = k+1$, $\langle\phi_i| H |\phi_k\rangle = \beta_{k+1}$, $\langle\phi_i|\phi_k\rangle = \langle\phi_i|\phi_{k-1}\rangle = 0$, therefore

$$\langle\phi_i|\phi_{k+1}\rangle = 1 \text{ for } i = k+1. \tag{2.86}$$

Equations (2.83)-(2.86) show that Eq.(2.79) is true, thus we can make a conclusion that Eq.(2.78) is also true.

Now we can introduce the Lanczos matrix T_j [20]

$$T_j \equiv \begin{bmatrix} \alpha_1 & \beta_2 & 0 & \cdots & 0 & 0 & 0 \\ \beta_2 & \alpha_2 & \beta_3 & \cdots & 0 & 0 & 0 \\ 0 & \beta_3 & \alpha_3 & \cdots & 0 & 0 & 0 \\ \vdots & \vdots & \vdots & \ddots & \vdots & \vdots & \vdots \\ 0 & 0 & 0 & \cdots & \alpha_{j-2} & \beta_{j-1} & 0 \\ 0 & 0 & 0 & \cdots & \beta_{j-1} & \alpha_{j-1} & \beta_j \\ 0 & 0 & 0 & \cdots & 0 & \beta_j & \alpha_j \end{bmatrix}, \tag{2.87}$$

and a matrix

$$\Phi_j \equiv \{|\phi_1\rangle, |\phi_2\rangle, ..., |\phi_j\rangle\}, \tag{2.88}$$

which is a $D \times j$ matrix whose ith column is the ith Lanczos vector $|\phi_i\rangle$. It is clear that for any $j \leq D$ we have

$$\Phi_j^T \Phi_j = I_j. \tag{2.89}$$

Equation (2.77) can be rewritten in matrix form as

$$H\Phi_j = \Phi_j T_j + \beta_{j+1} |\phi_{j+1}\rangle \langle e_j|, \tag{2.90}$$

where $\langle e_j|$ is the coordinate vector whose jth component is 1 and the others are 0. By multiplying Φ_j^T on both sides of Eq.(2.90) and using Eq.(2.78), one can get

$$T_j = \Phi_j^T H \Phi_j, \tag{2.91}$$

which means that the Lanczos matrix T_j is the orthogonal projection of H onto the subspaces (Krylov subspace) spanned by Φ_j. It is easy to find a unitary matrix Ω to diagonalize the tri-diagonal matrix T_j ($\Omega_j^+ T_j \Omega_j = \widetilde{T}_j$). Then the Hamiltonian can be represented as

$$H = \Phi_j T_j \Phi_j^T = \Phi_j \Omega_j \widetilde{T}_j \Omega_j^+ \Phi_j^T, \tag{2.92}$$

and with the same procedure in the exact diagonalization algorithm, we can write the time evolution operator as

$$U(t) = \lim_{j \to D} U_j(t) = \lim_{j \to D} \Phi_j \Omega_j e^{-it\widetilde{T_j}} \Omega_j^+ \Phi_j^T. \tag{2.93}$$

The memory and CPU time of the Lanczos algorithm scale as D and $j^2 D$ respectively [3].

Having shown how to use the Lanczos algorithm to perform the time evolution operator, we now discuss about how to use this algorithm to find the algebraically-smallest or algebraically-largest of the Hamiltonian. In general, one can find these values by direct diagonalization of the Hamiltonian. But as we mentioned before, the exact diagonalization algorithm may need a huge memory and a lot of CPU time, and is therefore not suitable when D is large. It was already proved that the algebraically-smallest or algebraically-largest of the eigenvalue of H, are well approximated by the eigenvalues of the corresponding Lanczos matrix T_j ($j \ll D$) [20]. If we want to construct the ground state of the system only, that is, to find the algebraically-smallest of the eigenvalue and the corresponding eigenstate of the Hamiltonian, we can use the following algorithm:

1) Firstly select a unit vector $|\phi_1\rangle$ and a sequence of $\{k\}$, e.g., $\{k = 10, 20, 30, 40...\}$;

2) Follow the Lanczos procedure to generate the Lanczos matrix T_j, and when j reaches the value in $\{k\}$, diagonalize the matrix $T_{j=k}$ to get the corresponding algebraically-smallest of the eigenvalue E_k;

3) Increase the value of j, until $E_K - E_{K+1} \leq \varepsilon$ (ε is a very small positive number, for example, $\varepsilon = 10^{-10}$), which means that to increase the dimension of the Lanczos matrix has very small influence to the algebraically-smallest eigenvalue. Then we can regard E_{K+1} as a good approximation of the algebraically-smallest eigenvalue of H, and the ground state of H is $|Ground\rangle = |K+1\rangle$, where $|K+1\rangle$ is the eigenvector of T_{K+1} corresponding to the algebraically-smallest eigenvalue E_{K+1}.

References

[1] M. Abramowitz and I. Stegun, Handbook of Mathematical Functions, Dover, New York, 1964.

[2] W.H. Press, B.P. Flannery, S.A. Teukolsky, and W.T. Vetterling, Numerical Recipes, Cambridge, New York, 1986.

[3] H. De Raedt and K. Michielsen, "Computational Methods for Simulating Quantum Computers", Handbook of Theoretical and Computational Nanotechnology, Vol. 3: Quantum and molecular computing, quantum simulations, Chapter 1, pp. 2 – 48, M. Rieth and W. Schommers eds., American Scientific Publisher, Los Angeles (2006).

[4] H.F. Trotter, Proc. Am. Math. Soc. 10, 545 (1959).

[5] M. Suzuki, S. Miyashita, and A. Kuroda, Prog. Theor. Phys. 58, 1377 (1977)

[6] M. Suzuki, J. Math. Phys. 26, 601 (1985).

[7] H. De Raedt and B. De Raedt, Phys. Rev. A28, 3575 (1983).

[8] M. Suzuki, J. Math. Phys. 32, 400 (1991).

[9] H. De Raedt, Comp. Phys. Rep. 7, 1 (1987).

[10] M.D. Feit, J.A. Fleck, and A. Steiger, J. Comput. Phys 47, 412 (1982).

[11] H. De Raedt and P. de Vries, Z. Phys. B77, 243 (1989).

[12] M. Krech, A. Bunker, and D.P. Landau, Comp. Phys. Comm. 111, 1 (1998).

[13] K. Michielsen, H. De Raedt, J. Przeslawski, and N. García, Phys. Rep. 304, 89 (1998).

[14] H. De Raedt, A.H. Hams, K. Michielsen, and K. De Raedt, Comp. Phys. Comm. 132, 1 (2000).

[15] J.S. Kole, M.T. Figge, and H. De Raedt, Phys. Rev. E64, 066705 (2001).

[16] P. de Vries and H. De Raedt, Phys. Rev. B47, 7929 (1993).

[17] J.H. Wilkinson, The Algebraic Eigenvalue Problem, Clarendon Press, Oxford, 1965.

[18] G.H. Golub and C.F. Van Loan, Matrix Computations, John Hopkins University Press, Baltimore, 1996.

[19] B.N. Parlett, The Symmetric Eigenvalue Problem, Classics in Applied Mathematics, 20, Society for Industrial and Applied Mathematics, (SIAM), Philadelphia, PA, 1998.

[20] J. K. Cullum and R. A. Willoughby, Lanczos Algorithms for Large Symmetric Eigenvalue Computations, Vol.I Theory, Birkhäuser Boston, Inc., 1985.

Chapter 3

Giant Enhancement of Quantum Decoherence by Frustrated Environments

---

This chapter was previously published as
S. Yuan, M.I. Katsnelson, and H. De Raedt, JETP Lett. **84**, 99-103 (2006).

The interaction between a quantum system, called central system in what follows, and its environment affects the state of the former. Intuitively, we expect that by turning on the interaction with the environment, the fluctuations in the environment will lead to a reduction of the coherence in the central system. This process is called decoherence [1, 2]. In general, there are two different mechanisms that contribute to decoherence. If the environment is dissipative (or coupled to a dissipative system), the total energy is not conserved and the central system + environment relax to a stationary equilibrium state, for instance the thermal equilibrium state. In this chapter, we exclude this class of dissipative processes and restrict ourselves to closed quantum systems in

which a small, central system is brought in contact with a larger quantum system that is prepared in its ground state. Then, decoherence is solely due to fact that the initial product state (wave function of the central system times wave function of the environment) evolves into an entangled state of the whole system. The interaction with the environment causes the initial pure state of the central system to evolve into a mixed state, described by a reduced density matrix [3], obtained by tracing out all the degrees of freedom of the environment [1, 2, 4, 5].

Not all initial states are equally sensitive to decoherence. The class of states that is "robust" with respect to the interaction with the environment are called pointer states [2]. If the Hamiltonian of the central system is a perturbation, relative to the interaction Hamiltonian H_{int}, the pointer states are eigenstates of H_{int} [2, 6]. In this case, the pointer states are essentially "classical states", such as states with definite particle positions or with definite spin directions of individual particles for magnetic systems. In general, these states, being a product of states of individual particles forming the system, are not entangled. On the other hand, decoherence does not necessarily imply that the central system evolves to a classical-like state. If H_{int} is much smaller than the typical energy differences in the central system, the pointer states are eigenstates of the latter, that is, they may be "quantum" states such as standing waves, stationary electron states in atoms, tunnelling-split states for a particle distributed between several potential wells, singlet or triplet states for magnetic systems, etc. [6]. This may explain, for example, that one can observe linear atomic spectra - the initial states of an atom under the equilibrium conditions are eigenstates of its Hamiltonian and not arbitrary superpositions thereof.

Let us now consider a central system for which the ground state is a maximally entangled state, such as a singlet. In the absence of dissipation and for an environment that is in the ground state before we bring it in contact with this central system, the loss of phase coherence induces one of following qualitatively different types of behavior:

1. The interaction/bath dynamics is such that there is very little relaxation.

2. The system as a whole relaxes to some state (which may or may not be close to the ground state) and this state is a complicated superposition of the states of the central system and the environment.

3. The system as a whole relaxes to a state that is (to good approximation)

a direct product of the states of the central system and a superposition of states of the environment. In this case there are two possibilities:

(a) The central system does not relax to its ground state;

(b) The central system relaxes to its maximally entangled ground state.

Only case 3b is special: The environment and central system are not entangled (to a good approximation) but nevertheless the decoherence induces a very strong entanglement in the central system. In this chapter, we demonstrate that, under suitable conditions, dissipation free decoherence forces the central system to relax to a maximally entangled state which itself, shows very little entanglement with the state of the environment.

3.1 Model

Most theoretical investigations of decoherence have been carried out for oscillator models of the environment for which powerful path-integral techniques can be used to treat the environment analytically [4, 5]. On the other hand, it has been pointed out that a magnetic environment, described by quantum spins, is essentially different from the oscillator model in many aspects [7]. For the simplest model of a single spin in an external magnetic field, some analytical results are known [7]. For the generic case of two and more spins, numerical simulation [8, 9] is the main source of theoretical information. Not much is known now about which physical properties of the environment are important for the efficient selection of pointer states. Recent numerical simulations [9] confirm the hypothesis [10] on the relevance of the chaoticity of the environment but its effect is actually not drastic.

In this chapter, we report on the results of numerical simulations of quantum spin systems, demonstrating the crucial role of frustrations in the environment on decoherence. In particular, we show that, under appropriate conditions, decoherence can cause an initially classical state of the central system to evolve into the most extreme, maximally entangled state. We emphasize that we only consider systems in which the total energy is conserved such that the decoherence is not due to dissipation.

We study a model in which two antiferromagnetically coupled spins, called the central system, interact with an environment of spins. The model is defined

Table 3.1: Minimum value of the correlation of the central spins and the energy of the whole system (which is conserved), as observed during the time evolution corresponding to the curves listed in the first column. The correlations $\langle \mathbf{S}_1 \cdot \mathbf{S}_2 \rangle_0$ and the ground state energy E_0 of the whole system are obtained by numerical diagonalization of the Hamiltonian Eq.(3.1).

	$\langle \Psi(t)\|H\|\Psi(t)\rangle$	E_0	$\min_t \langle \mathbf{S}_1(t) \cdot \mathbf{S}_2(t)\rangle$	$\langle \mathbf{S}_1 \cdot \mathbf{S}_2 \rangle_0$
Fig. (3.1) (a)	-1.299	-1.829	-0.659	-0.723
Fig. (3.1) (b)	-1.532	-2.065	-0.695	-0.721
Fig. (3.1) (c)	-1.856	-2.407	-0.689	-0.696
Fig. (3.2)	-4.125	-4.627	-0.744	-0.749
Fig. (3.3) (a)	-1.490	-1.992	-0.746	-0.749
Fig. (3.3) (b)	-0.870	-1.379	-0.260	-0.741
Fig. (3.3) (c)	-1.490	-1.997	-0.737	-0.744
Fig. (3.3) (d)	-2.654	-3.160	-0.742	-0.745
Fig. (3.3) (e)	-7.791	-8.293	-0.716	-0.749
Fig. (3.3) (f)	-3.257	-3.803	-0.713	-0.718
Fig. (3.4) (b)	-0.884	-1.388	-0.424	-0.733
Fig. (3.3) (c)	-1.299	-1.829	-0.659	-0.723
Fig. (3.3) (d)	-1.299	-1.807	-0.741	-0.743
Fig. (3.3) (e)	-1.843	-2.365	-0.738	-0.735

by

$$\begin{aligned} H &= H_c + H_e + H_{int}, \\ H_c &= -J\mathbf{S}_1 \cdot \mathbf{S}_2, \\ H_e &= -\sum_{i=1}^{N-1} \sum_{j=i+1}^{N} \sum_{\alpha} \Omega_{i,j}^{(\alpha)} I_i^\alpha I_j^\alpha, \\ H_{int} &= -\sum_{i=1}^{2} \sum_{j=1}^{N} \sum_{\alpha} \Delta_{i,j}^{(\alpha)} S_i^\alpha I_j^\alpha, \end{aligned} \tag{3.1}$$

where the exchange integrals $J < 0$ and $\Omega_{i,j}^{(\alpha)}$ determine the strength of the interaction between spins $\mathbf{S}_n = (S_n^x, S_n^y, S_n^z)$ in the central system (H_c), and the spins $\mathbf{I}_n = (I_n^x, I_n^y, I_n^z)$ in the environment (H_e), respectively. The exchange

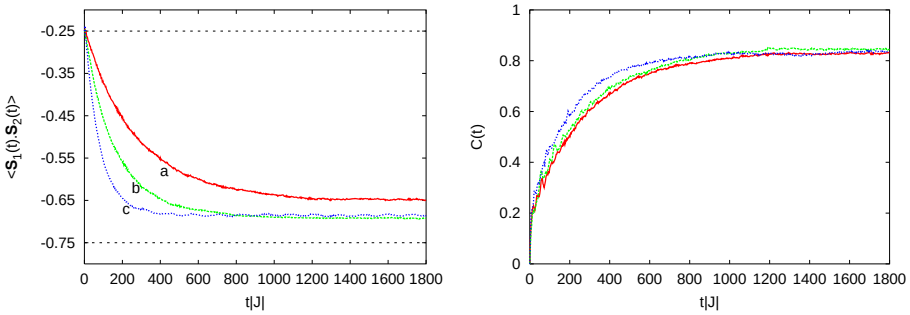

Figure 3.1: (color online) Left: Time evolution of the correlation $\langle\Psi(t)|\mathbf{S}_1 \cdot \mathbf{S}_2|\Psi(t)\rangle$ of the two spins in the central system. Dashed horizontal line at -1/4: Correlation in the initial state ($\langle\Psi(t=0)|\mathbf{S}_1 \cdot \mathbf{S}_2|\Psi(t=0)\rangle = -1/4$); Horizontal line at -3/4: Expectation value in the singlet state; (a) Environment containing $N = 14$ quantum spins; (b) $N = 16$; (c) $N = 18$. The parameters $\Omega_{i,j}^{(\alpha)}$ and $\Delta_{i,j}^{(\alpha)}$ are uniform random numbers in the range $[-0.15|J|, 0.15|J|]$. Right: Time evolution of the concurrence $C(t)$ for three different random realizations of a spin glass environment. The parameters are uniform random numbers in the range $-0.15|J| \leq \Omega_{i,j}^{(\alpha)}, \Delta_{i,j}^{(\alpha)} \leq 0.15|J|$ and the environment contains $N = 14$ quantum spins. The transition from an unentangled state ($C(t) = 0$) to a nearly fully entangled state ($C(t) = 1$) is clearly seen.

integrals $\Delta_{i,j}^{(\alpha)}$ control the interaction (H_{int}) of the central system with its environment. In Eq.(3.1), the sum over α runs over the x, y and z components of spin 1/2 operators. The number of spins in the environment is N.

Initially, the central system is in the spin-up - spin-down state and the environment is in its ground state. Thus, we write the initial state as $|\Psi(t = 0)\rangle = |\uparrow\downarrow\rangle|\Phi_0\rangle$. The time evolution of the system is obtained by solving the time-dependent Schrödinger equation for the many-body wave function $|\Psi(t)\rangle$, describing the central system plus the environment. The numerical method that we use is described in Ref. [11]. It conserves the energy of the whole system to machine precision.

By changing the parameters of model (3.1), we explore the conditions under which the central system clearly shows an evolution from the initial spin-up - spin-down state towards the maximally entangled singlet state. We consider systems that range from the rotationally invariant Heisenberg case to the extreme case in which H_e and H_{int} reduce to the Ising model, topologies for which the central system couples to two and to all spins of the environment, and values of parameters that are fixed or are allowed to fluctuate randomly. Illustrative results of these calculations are shown in Figs. 3.1, -

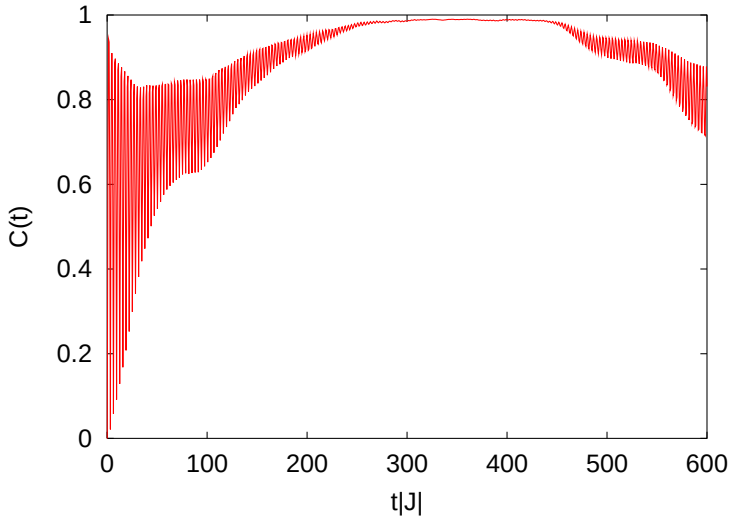

Figure 3.2: (color online) Time evolution of the concurrence $C(t)$ for the case of a frustrated antiferromagnetic environment. The interactions of the central system and the environment are uniform random numbers in the range $-0.15|J| \leq \Delta_{i,j}^{(\alpha)} \leq -0.05|J|$. The environment contains 14 quantum spins, arranged on a triangular lattice and interacting with nearest neighbors only. The nonzero exchange integrals are uniform random numbers in the range $-0.55|J| \leq \Omega_{i,j}^{(\alpha)} \leq -0.45|J|$. The transition from an unentangled state ($C(t) = 0$) to a nearly fully entangled state ($C(t) = 1$) is evident, as is the onset of recurrent behavior due to the finite size of the environment.

3.4,. In Table 3.1, we present the corresponding numerical data of the energy $\langle\Psi(0)|H|\Psi(0)\rangle = \langle\Psi(t)|H|\Psi(t)\rangle)$ and of the two-spin correlation $\langle \mathbf{S}_1(t) \cdot \mathbf{S}_2(t)\rangle = \langle\Psi(t)|\mathbf{S}_1 \cdot \mathbf{S}_2|\Psi(t)\rangle$. For comparison, Table 3.1. also contains the results of the energy E_0 and of the two-spin correlation $\langle \mathbf{S}_1 \cdot \mathbf{S}_2\rangle_0$. in the ground state of the whole system, as obtained by numerical diagonalization of the Hamiltonian Eq.(3.1).

We monitor the effects of decoherence by computing the expectation value $\langle\Psi(t)|\mathbf{S}_1 \cdot \mathbf{S}_2|\Psi(t)\rangle$. The central system is in the singlet state if $\langle \mathbf{S}_1(t) \cdot \mathbf{S}_2(t)\rangle = -3/4$, that is if $\langle \mathbf{S}_1(t) \cdot \mathbf{S}_2(t)\rangle$ reaches its minimum value. We also study the time evolution of the concurrence $C(t)$, which is a convenient measure for the entanglement of the spins in the central system [12]. The concurrence is equal to one if the central system is in the singlet state and is zero for an unentangled pure state such as the spin-up - spin-down state [12].

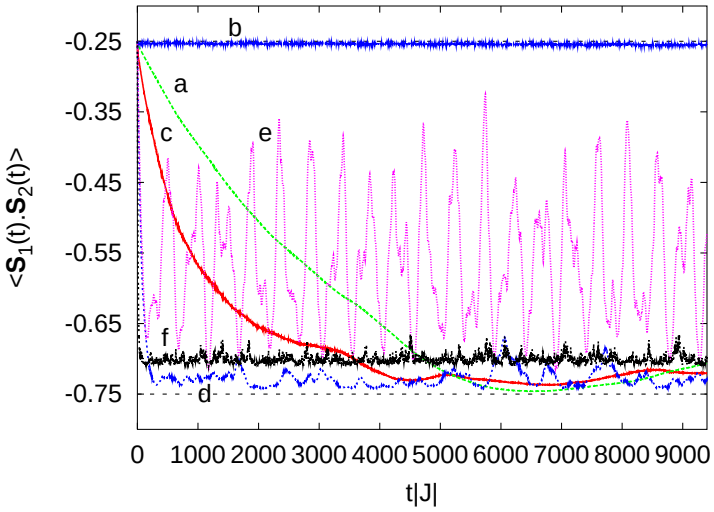

Figure 3.3: (color online) Time evolution of the correlation $\langle\Psi(t)|\mathbf{S}_1 \cdot \mathbf{S}_2|\Psi(t)\rangle$ of the two spins in the central system. Environment containing $N = 16$ quantum spins. Dashed horizontal line at -1/4: Correlation in the initial state ($\langle\Psi(t=0)|\mathbf{S}_1 \cdot \mathbf{S}_2|\Psi(t=0)\rangle = -1/4$); Horizontal line at -3/4: Expectation value in the singlet state. For all curves (a-f) $\Delta_{i,j}^{(x)} = \Delta_{i,j}^{(y)} = 0$, that is H_{int} is Ising like. The values of $\Delta_{i,j}^{(z)}$ are: (a) random $-0.0375\,|J|$ or $0.0375\,|J|$, (b-e) random $-0.075\,|J|$ or $0.075\,|J|$, (f) random $-0.15\,|J|$ or $0.15\,|J|$. The values of $\Omega_{i,j}^{(\alpha)}$ are uniform random numbers in the range: (b) $[-0.0375|J|, 0.0375|J|]$, (a,c) $[-0.15|J|, 0.15|J|]$, (d,f) $[-0.3|J|, 0.3|J|]$ and (e) $[-|J|, |J|]$.

3.2 Role of Frustrated Environments

A very extensive search through parameter space leads to the following conclusions:

- The maximum amount of entanglement strongly depends on the values of the model parameters $\Omega_{i,j}^{(\alpha)}$ and $\Delta_{i,j}^{(\alpha)}$. For the case in which there is strong decoherence, increasing the size of the environment will enhance the decoherence in the central system (compare the curves of Fig. 3.1. (a,b,c) and Fig. 3.4. (d,e)). Keeping the size of the environment fixed, different realizations of the random parameters do not significantly change the results for the correlation and concurrence (right panel of Fig. 3.1.). However, the range of random values $\Omega_{i,j}^{(\alpha)}$ and $\Delta_{i,j}^{(\alpha)}$ for which maximal entanglement can be achieved is narrow, as illustrated in Figs. 3.3. and 3.4. In Fig. 3.3. we compare results for the same type of H_{int} (Ising like) and the same type of H_e (anisotropic Heisenberg

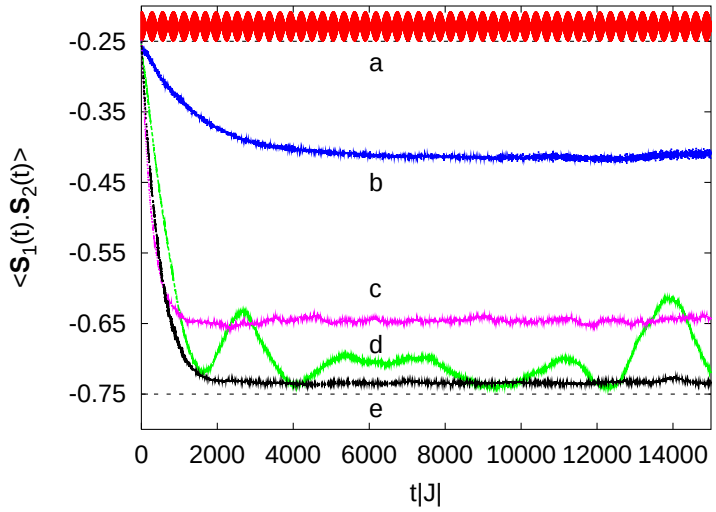

Figure 3.4: (color online) Effect of the symmetry of the exchange interactions $\Omega_{i,j}^{(\alpha)}$ and $\Delta_{i,j}^{(\alpha)}$ on the time evolution of the correlation $\langle\Psi(t)|\mathbf{S}_1\cdot\mathbf{S}_2|\Psi(t)\rangle$ of the two spins in the central system. Dashed horizontal line at -1/4: Correlation in the initial state ($\langle\Psi(t=0)|\mathbf{S}_1\cdot\mathbf{S}_2|\Psi(t=0)\rangle=-1/4$); Horizontal line at -3/4: Correlation in the singlet state; Other lines from top to bottom (at $t|J|=6000$): (a) Ising H_{int} with Ising H_e, $N=14$; (b) Heisenberg-like H_{int} with Ising H_e, $N=14$; (c) Heisenberg-like H_{int} with Heisenberg-like H_e, $N=14$; (d) Ising H_{int} with Heisenberg-like H_e, $N=14$; (e) Same as (d) except that $N=18$. We use the term Heisenberg-like H_{int} (H_e) to indicate that $\Delta_{i,j}^{(\alpha)}$ ($\Omega_{i,j}^{(\alpha)}$) are uniform random numbers in the range $[-0.15\,|J|\,,0.15\,|J|]$. Likewise, Ising H_{int} (H_e) means that $\Delta_{i,j}^{(x,y)}=0$ ($\Omega_{i,j}^{(x,y)}=0$), and $\Delta_{i,j}^{(z)}$ ($\Omega_{i,j}^{(z)}$) are random $-0.075\,|J|$ or $0.075\,|J|$.

like), but with different values of the model parameters. In Fig. 3.4. , we present results for different types of H_{int} and H_e. but for parameters within the same range.

- Environments that exhibit some form of frustration, such as spin glasses or frustrated antiferromagnets, may be very effective in producing a high degree of entanglement between the two central spins, see Figs. 3.1 -3.4.

- Decoherence is most effective if the exchange couplings between the system and the environment are random (in a limited range) and anisotropic, see Figs. 3.3. and 3.4.

- The details of the internal dynamics of the environment affects the maximum amount of entanglement that can be achieved [9], and also affects the speed of the initial relaxation (compare the curves of Fig. 3.3.

(b,c,d,e), Fig. 3.4. (a,d) and Fig. 3.4. (b,c)).

- For the case in which there is strong decoherence, for the same H_e and the same type of H_{int}, decreasing the strengh of H_{int} will reduce the relaxation to the finial state, and the final state comes closer to the singlet state (compare the curves of Fig. 3.3. (a,c) and Fig. 3.3. (d,f)).

Earlier simulations for the Ising model in a transverse field have shown that time-averaged distributions of the energies of the central system and environment agree with those of the canonical ensemble at some effective temperature [13, 14]. Our results do not contradict these findings but show that there are cases in which the central system relaxes from a high energy state to its ground state while the environment starts in the ground state and ends up in state with slightly higher energy. As shown in Fig.4(e), this state is extremely robust and shows very little fluctuations.

3.3 Summary

For the models under consideration, the efficiency of decoherence decreases drastically in the following order: Spin glass (random long-range interactions of both signs); Frustrated antiferromagnet (triangular lattice with the nearest-neighbour interactions); Bipartite antiferromagnet (square lattice with the nearest-neighbour interactions); One-dimensional ring with the nearest-neighbour antiferromagnetic interactions. This can be understood as follows. A change of the state of the central system affects a group of spins in the environment. The suppression of off-diagonal elements of the reduced density matrix can be much more effective if the group of disturbed spins is larger. The state of the central system is the most flexible in the case of a coupling to a spin glass for which, in the thermodynamic limit, an infinite number of infinitely closed quasi-equilibrium configurations exist [15, 16]. As a result, a very small perturbation leads to the change of the system *as a whole*. This may be considered as a quantum analog of the phenomenon of "structural relaxation" in glasses. This suggests that frustrated spin systems that are close to the glassy state should provide extremely efficient decoherence.

To conclude, we have demonstrated that frustrations and, especially, glassiness of the spin environment result in a very strong enhancement of its decohering action on the central spin system. Our results convincingly show that this

enhancement can be so strong that solely due to decoherence, a fully disentangled state may evolve into a fully entangled state, even if the environment contains a relatively small numbers of spins.

References

[1] D. Giulini, E. Joos, C. Kiefer, J. Kupsch, I.-O. Stamatescu, and H.D. Zeh, *Decoherence and the Appearance of a Classical World in Quantum Theory* (Springer, Berlin, 1996).

[2] W.H. Zurek, Rev. Mod. Phys. **75**, 715 (2003).

[3] J. von Neumann, Mathematical Foundations of Quantum Mechanics (Princeton University Press, Princeton) 1955.

[4] R.P. Feynman and F.L Vernon, Ann. Phys. (N.Y.), **24**, 118 (1963).

[5] A.J. Leggett, S. Chakravarty, A.T. Dorsey, et al., Rev. Mod. Phys., **59**, 1 (1987).

[6] J.-P. Paz and W.H. Zurek, Phys. Rev. Lett., **82**, 5181 (1999).

[7] N.V. Prokof'ev and P.C.E. Stamp, Rep. Prog. Phys., **63**, 669 (2000)

[8] V.V. Dobrovitski, H.A. De Raedt, M.I. Katsnelson, et al., Phys. Rev. Lett., **90**, 210401 (2003).

[9] J. Lages, V.V. Dobrovitski, M.I. Katsnelson, et al., Phys. Rev. E, **72**, 026225 (2005).

[10] W.H. Zurek, Nature **412**, 712 (2001).

[11] V.V. Dobrovitski and H.A. De Raedt, Phys. Rev. E, **67**, 056702 (2003).

[12] W.K. Wootters, Phys. Rev. Lett., **80**, 2245 (1998).

[13] R.V. Jensen and R. Shankar, Phys. Rev. Lett., **54**, 1879 (1985).

[14] K. Saito, S. Takasue, and S. Miyashita, Phys. Rev. Lett., **65**, 1243 (1996).

[15] K. Binder and A.P. Young, Rev. Mod. Phys., **58** 801(1986).

[16] M. Mezard, G. Parisi, and M.A. Virasoro, Spin Glass Theory and Beyond (World Scientific, Singapore) 1987.

Chapter 4

Evolution of a Quantum Spin System to its Ground State: Role of Entanglement and Interaction Symmetry

---

This chapter was previously published as
S. Yuan, M.I. Katsnelson, and H. De Raedt, Phys. Rev. A **75**, 052109 (2007).

The foundations of non-equilibrium statistical mechanics are still under debate (for a general introduction to the problem, see, e.g., Ref. [1]; see also a very recent discussion [2] and Refs. therein). There is a common believe that a generic "central system" that interacts with a generic environment evolves into a state described by the canonical ensemble (in the limit of low temperatures, this means the evolution to the ground state). Experience shows that this is true but a detailed understanding of this process, which is crucial for a

rigorous justification of statistical physics and thermodynamics, is still lacking. In particular, in this context the meaning of "generic" is not clear. The key question is how the evolution to the equilibrium state depends on the details of the dynamics of the central system itself, on the environment, and on the interaction between the central system and the environment.

In one of the first applications of computers to a basic physics problem Fermi, Pasta, and Ulam attempted to simulate the relaxation to thermal equilibrium of a system of interacting anharmonic oscillators [3]. The results obtained appeared to be counterintuitive, as we know now, due to complete integrability (in the continuum medium limit) of the model they simulated [4].

Bogoliubov [5] has considered in a mathematically rigorous way the evolution to thermal equilibrium of a classical harmonic oscillator (central system) connected to an environment of classical harmonic oscillators which are already thermalized (for a generalization to a nonlinear Hamiltonian central system with one degree of freedom, see in Ref. [6]). Also, for quantum systems this "bosonic bath" is the bath of choice, starting with the seminal works by Feynman and Vernon [7] and Caldeira and Leggett [8] (for a review, see Ref. [9]). On the other hand, as we know now, the bosonic environment differs in many ways from, say, a spin-bath environment (such as nuclear spins) that dominate the decoherence processes of magnetic systems at low enough temperatures [10]. The evolution of quantum spin systems to the equilibrium state has been investigated in Refs. [11–13], for a very special class of spin Hamiltonians.

In terms of the modern "decoherence program" quantum systems interacting with an environment evolve to one of the robust "pointer states", the superposition of the pointer states being, in general, not a pointer state [14, 15]. The decoherence program is supposed to explain the macroscopic quantum superpostion ("Schrödinger cat") paradox, that is, the inapplicability of the superposition principle to the macroworld. Indeed, it is confirmed in many ways that, for the case where the interaction with environment is strong in comparison with typical energy differences for the central system, the classical "Schrödinger cat states" are the pointer states. At the same time, some less trivial pointer states have been found in computer simulations of quantum spin systems for some range of the model parameters [16–18]. In fact, the evolution of quantum spin systems to equilibrium is still an open issue (see also Refs. [19–21]). Recently, the effect of an environment of $N \gg 1$ spins on the entanglement of the two spins of the central system has attracted much

attention [16–18, 22–30].

The relationship between the pointer states and the eigenstates of the Hamiltonian of central system is of special interest for the foundations of quantum statistical mechanics: The standard scenario assumes that the density matrix of the system at the equilibrium is diagonal in the basis of these eigenstates. Paz and Zurek [31] have conjectured that pointer states are the eigenstates of the central system if the interaction of the central system with each degree of freedom of the environment is a perturbation, relative to the Hamiltonian of the central system. In view of the foregoing, it is important to establish the conditions under which this conjecture holds and to explore situations in which the interaction with environment can no longer be regarded as a perturbation with respect to the Hamiltonian of the central system.

In previous chapter, we reported a first collection of results for an antiferromagnetic Heisenberg system coupled to a variety of different environments. Our primary goal was to establish the conditions under which the central system relaxes from the initial spin-up - spin-down state towards its ground state, that is the maximally entangled singlet state. We found that environments that exhibit some form of frustration, such as spin glasses or frustrated antiferromagnets, may be very effective in producing a final state with a high degree of entanglement between the two central spins. We demonstrated that the efficiency of the decoherence process decreases drastically with the type of environment in the following order: Spin glass and random coupling of all spins to the central system; Frustrated antiferromagnet (triangular lattice with the nearest-neighbors interactions); Bipartite antiferromagnet (square lattice with the nearest-neighbors interactions); One-dimensional ring with the nearest-neighbors antiferromagnetic interactions [22].

Competing interactions, frustration and glassiness provide a very efficient mechanism for decoherence whereas the difference between integrable and chaotic systems is less important [18]. Furthermore, we observed that for a fixed system size of the environment and in those cases for the decoherence is effective, different realizations of the random parameters do not significantly change the results. However, maximal entanglement in the central system was found for a relatively narrow range of the couplings between the environment spins and the interaction between the central spins and those of the environment.

Having established that the decoherence caused by a coupling to a frustrated, spin-glass-like environment can be a very effective, it is of interest to study in

Table 4.1: The values of the correlation functions $\langle \mathbf{S}_1 \cdot \mathbf{S}_2 \rangle$, $\langle S_1^z S_2^z \rangle$, $\langle S_1^x S_2^x \rangle$, the total magnetization M, the concurrence C and the magnetization $\langle S_1^z \rangle$ for different states of the central system.

$\lvert\varphi\rangle$	$\langle \mathbf{S}_1 \cdot \mathbf{S}_2 \rangle$	$\langle S_1^z S_2^z \rangle$	$\langle S_1^x S_2^x \rangle$	M	C	$\langle S_1^x \rangle$
$\frac{1}{\sqrt{2}}(\lvert\uparrow\downarrow\rangle - \lvert\downarrow\uparrow\rangle)$	$-3/4$	$-1/4$	$-1/4$	0	1	0
$\frac{1}{\sqrt{2}}(\lvert\uparrow\downarrow\rangle + \lvert\downarrow\uparrow\rangle)$	$1/4$	$-1/4$	$1/4$	0	1	0
$\frac{1}{\sqrt{2}}(\lvert\uparrow\uparrow\rangle - \lvert\downarrow\downarrow\rangle)$	$1/4$	$1/4$	$-1/4$	0	1	0
$\frac{1}{\sqrt{2}}(\lvert\uparrow\uparrow\rangle + \lvert\downarrow\downarrow\rangle)$	$1/4$	$1/4$	$1/4$	0	1	0
$\lvert\uparrow\downarrow\rangle$	$-1/4$	$-1/4$	0	0	0	$1/2$
$\lvert\downarrow\uparrow\rangle$	$-1/4$	$-1/4$	0	0	0	$-1/2$
$\lvert\uparrow\uparrow\rangle$	$1/4$	$1/4$	0	1	0	$1/2$
$\lvert\downarrow\downarrow\rangle$	$1/4$	$1/4$	0	-1	0	$-1/2$

detail, the time evolution of the central system coupled to such an environment. In this chapter, we consider as a central system, two ferro- or antiferromagnetically coupled spins that interact with a spin-glass environment. The interactions between each of the spin components of the latter are chosen randomly and uniformly from a specified interval centered around zero, making it very unlikely that there are conserved quantities in this three-component spin-glass. For the interaction of the central system with each of the spins of the environment we consider two cases.

In the first case, the couplings between the three components are generated using the same procedure as used for the environment. In the second case, the central system interacts with the environment via the z-components of the spins only. This implies that both the Hamiltonians that describe the central system (isotropic Heisenberg model) and the interaction between the central system and the environment commute with the total magnetization of the central system; hence the latter is conserved during the time evolution. In contrast to the naive picture in which the presence of conserved quantities reduces the decoherence, we find that the presence of a conserved quantity may affect significantly the nature of the stationary state to which the central system relaxes.

4.1 Model

The model Hamiltonian that we study is defined by

$$\begin{aligned} H &= H_c + H_e + H_{ce}, \\ H_c &= -J\mathbf{S}_1 \cdot \mathbf{S}_2, \\ H_e &= -\sum_{i=1}^{N-1}\sum_{j=i+1}^{N}\sum_{\alpha}\Omega_{i,j}^{(\alpha)} I_i^{\alpha} I_j^{\alpha}, \\ H_{ce} &= -\sum_{i=1}^{2}\sum_{j=1}^{N}\sum_{\alpha}\Delta_{i,j}^{(\alpha)} S_i^{\alpha} I_j^{\alpha}, \end{aligned} \tag{4.1}$$

where the exchange integrals J and $\Omega_{i,j}^{(\alpha)}$ determine the strength of the interaction between spins $\mathbf{S}_n = (S_n^x, S_n^y, S_n^z)$ in the central system (H_c), and the spins $\mathbf{I}_n = (I_n^x, I_n^y, I_n^z)$ in the environment (H_e), respectively. The exchange integrals $\Delta_{i,j}^{(\alpha)}$ control the interaction (H_{ce}) of the central system with its environment. In Eq.(4.1), the sum over α runs over the x, y and z components of spin-1/2 operators $\mathbf{S}$ and $\mathbf{I}$. The exchange integral J of the central system can be positive or negative, the corresponding ground state of the central system being ferromagnetic or antiferromagnetic, respectively.

In the sequel, we will use the term "Heisenberg-like" H_{ce} (H_e) to indicate that $\Delta_{i,j}^{(\alpha)}$ ($\Omega_{i,j}^{(\alpha)}$) are uniform random numbers in the range $[-\Delta|J|, \Delta|J|]$ ($[-\Omega|J|, \Omega|J|]$) for all α's and use the expression "Ising-like" H_{ce} (H_e) to indicate that $\Delta_{i,j}^{(x,y)} = 0$ ($\Omega_{i,j}^{(x,y)} = 0$), and that $\Delta_{i,j}^{(z)}$ ($\Omega_{i,j}^{(z)}$) are dichotomic random variables taking the values $\pm\Delta$ ($\pm\Omega$). The parameters Δ and Ω determine the maximum strength of the interactions.

The quantum state of central system is completely determined by its reduced density matrix, the 4×4 matrix that is obtained by computing the trace of the full density matrix over all but the four states of the central system. In our simulation work, the whole system is assumed to be in a pure state, denoted by $|\Psi(t)\rangle$. Although the reduced density matrix contains all the information about the central system, it is often convenient to characterize the state of the central system by other quantities, such as the correlation functions $\langle\Psi(t)|\mathbf{S}_1 \cdot \mathbf{S}_2|\Psi(t)\rangle$, $\langle\Psi(t)|S_1^z S_2^z|\Psi(t)\rangle$, and $\langle\Psi(t)|S_1^x S_2^x|\Psi(t)\rangle$, the single-spin magnetizations $\langle\Psi(t)|S_1^x|\Psi(t)\rangle$, $\langle\Psi(t)|S_2^x|\Psi(t)\rangle$, the total magnetization $M \equiv \langle\Psi(t)|\,(S_1^z + S_2^z)\,|\Psi(t)\rangle$, and the concurrence $C(t)$ [33, 34]. The concurrence, which is a convenient measure for the entanglement of the spins in the central system, is equal to one if the state of central system is unchanged under

a flip of the two spins, and is zero for an unentangled pure state such as the spin-up - spin-down state. In Table 4.1, we show the values of these quantities for to different states of the central system.

As the energy of central system is given by $-J\langle\Psi(t)|\mathbf{S}_1\cdot\mathbf{S}_2|\Psi(t)\rangle$, it follows from Table 4.1 that the four eigenstates of the central system H_c are given by

$$\begin{aligned} |S\rangle &= \frac{|\uparrow\downarrow\rangle - |\downarrow\uparrow\rangle}{\sqrt{2}}, \\ |T_0\rangle &= \frac{|\uparrow\downarrow\rangle + |\downarrow\uparrow\rangle}{\sqrt{2}}, \\ |T_1\rangle &= |\uparrow\uparrow\rangle, \\ |T_{-1}\rangle &= |\downarrow\downarrow\rangle, \end{aligned} \tag{4.2}$$

satisfying

$$H_c\,|S\rangle = E_S\,|S\rangle\,,\ H_c\,|T_{1,0,-1}\rangle = E_T\,|T_{1,0,-1}\rangle\,, \tag{4.3}$$

where $E_S = 3J/4$ and $E_T = -J/4$.

From Table 4.1, it is clear that the singlet state $|S\rangle$ is most easily distinguished from the others as the central system is in the singlet state if and only if $\langle\mathbf{S}_1\cdot\mathbf{S}_2\rangle = -3/4$. To identify other states, we usually need to know at least two of the quantities listed in Table 4.1. For example, to make sure that the system is the triplet state $|T_0\rangle$, the values of $\langle\mathbf{S}_1\cdot\mathbf{S}_2\rangle$ and $\langle S_1^z S_2^z\rangle$ should match with the corresponding entries of Table 4.1. Likewise, the central system will be in the state $|\uparrow\uparrow\rangle$ if $\langle\mathbf{S}_1\cdot\mathbf{S}_2\rangle$ and M agree with the corresponding entries of Table 4.1.

In general, we monitor the effects of the decoherence by plotting the time dependence of the two-spin correlation function $\langle\mathbf{S}_1\cdot\mathbf{S}_2\rangle$ and the matrix elements of the density matrix. We compute the matrix elements of the density matrix in the basis of eigenvectors of the central system (see Eq.(4.2)). If necessary to determine the nature of the state, we consider all the quantities listed in Table 4.1.

The simulation procedure is as follows. First, we select a set of model parameters. Next, we compute the ground state $|\phi_0\rangle$ of the environment and, for reference, the ground state of the whole system also. The spin-up – spin-down state ($|\uparrow\downarrow\rangle$) is taken as the initial state of the central system. Thus, the initial state of the system reads $|\Psi(t=0)\rangle\rangle = |\uparrow\downarrow\rangle\,|\phi_0\rangle$ and is a product state of the state of the central system and the ground state of the environment which, in general is a (very complicated) linear combination of the 2^N basis states of the environment.

The time evolution of the whole system is obtained by solving the time-dependent Schrödinger equation for the many-body wave function $|\Psi(t)\rangle$, describing the central system plus the environment. The numerical method that we use is described in Ref. [32]. It conserves the energy of the whole system to machine precision.

In our model, decoherence is solely due to fact that the initial product state $|\Psi(0)\rangle = |\uparrow\downarrow\rangle$ evolves into an entangled state of the whole system. The interaction with the environment causes the initial pure state of the central system to evolve into a mixed state, described by a reduced density matrix [35], obtained by tracing out all the degrees of freedom of the environment [7, 9, 14, 15]. If the Hamiltonian of the central system H_c is a perturbation, relative to the interaction Hamiltonian H_{ce}, the pointer states are eigenstates of H_{ce} [15, 31]. On the other hand, if H_{ce} is much smaller than the typical energy differences in the central system, the pointer states are eigenstates of H_c, that is, they may be singlet or triplet states. In fact, as we will show, the selection of the eigenstate as the pointer state is also determined by the state and the dynamics of the environment.

In the simulations that we discuss in this chapterchapter, the interactions between the central system and the environment are either Ising or Heisenberg-like. The interesting regime for decoherence occurs when each coupling of the central system with the environment is weak, that is, $\Delta \ll |J|$, but there is of course nothing that prevents us from performing simulations outside this regime. The interaction within the environment are taken to be Heisenberg-like, Ω being a parameter that we change.

4.2 Heisenberg-like H_{ce}

4.2.1 Ferromagnetic Central System

In this section, we consider a ferromagnetic ($J = 1$) central system that interacts with the environment via a Heisenberg-like interaction (recall that throughout this chapter the environment itself is always Heisenberg-like).

In Fig. 4.1, we present simulation results for the two-spin correlation function for different values of the parameter Ω that determines the maximum strength of the coupling between the $N(N-1)/2$ pairs of spins in the environment. Clearly, in case (a), the relaxation is rather slow and confirming that there is relaxation to the ground state requires a prohibitively long simulation. For

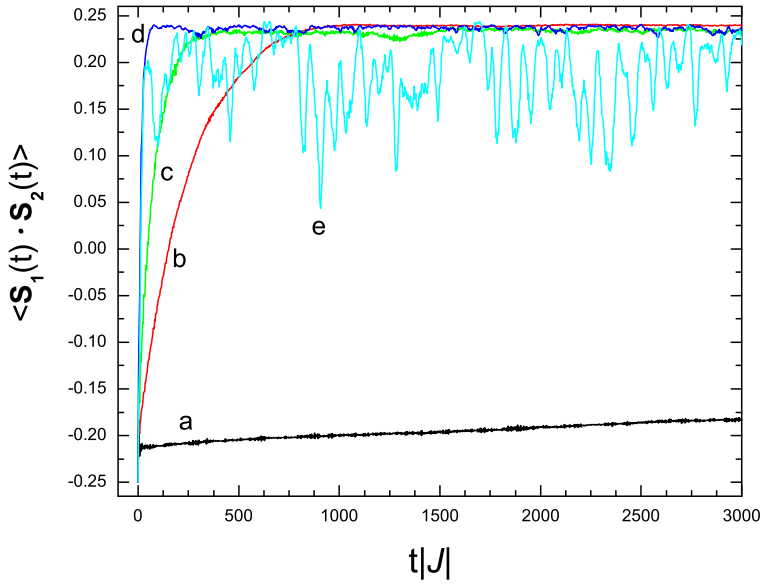

Figure 4.1: (Color online) The time evolution of the correlation $\langle\Psi(t)|\mathbf{S}_1 \cdot \mathbf{S}_2|\Psi(t)\rangle$ of the ferromagnetic central system with Heisenberg-like H_{ce} and H_e. The model parameters are $\Delta = 0.15$ and a: $\Omega = 0.075$; b: $\Omega = 0.15$; c: $\Omega = 0.20$; d: $\Omega = 0.30$; e: $\Omega = 1$. The number of spins in the environment is $N = 14$.

cases (b) – (d), the results are in concert with the intuitive picture of relaxation due to decoherence: The correlation shows the relaxation from the up-down initial state of the central system to the fully polarized state in which the two spins point in the same direction.

An important observation is that our data convincingly shows that it is not necessary to have a macroscopically large environment for decoherence to cause relaxation to the ground state: A spin-glass with $N = 14$ spins seems to be more than enough to mimic such an environment. This observation is essential for numerical simulations of relatively small systems to yield the correct qualitative behavior.

Qualitative arguments for the high efficiency of the spin-glass bath were given in Ref. [22]. Since the spin-glasses possess a huge amount of the states that have an energy close to the ground state energy but have wave functions that are very different from the ground state, the orthogonality catastrophe, blocking the quantum interference in the central system [9, 14] is very strongly pronounced in this case.

This conclusion is further supported by Fig. 4.2 where we show the diagonal

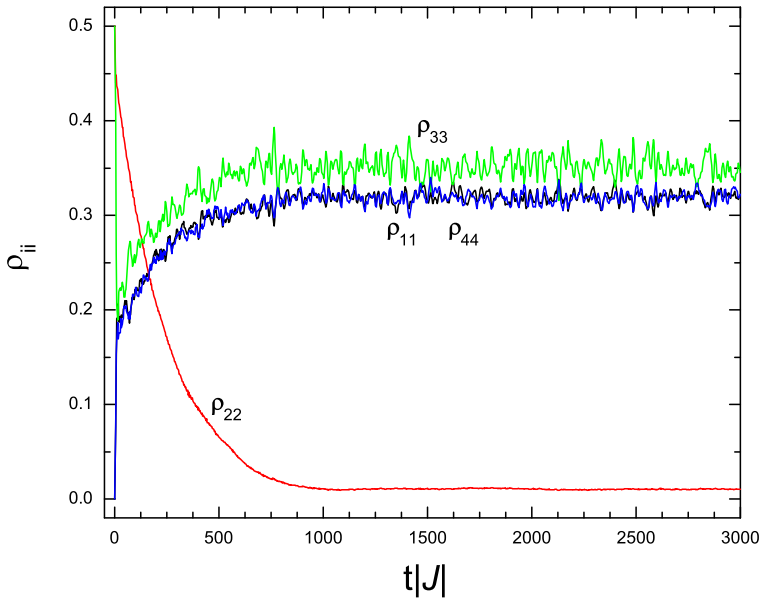

Figure 4.2: (Color online) The time evolution of the diagonal matrix elements of the reduced density matrix of the central system for $\Delta = 0.15$ and $\Omega = 0.15$ (case (b) of Fig. 4.1). The number of spins in the environment is $N = 14$.

elements of the reduced density matrix for case (b). After reaching the steady state, the nondiagonal elements exhibit minute fluctuations about zero and are therefore not shown. From Fig. 4.2, it is then clear that central system relaxes to a mixture of the (spin-up, spin-up), (spin-down, spin-down), and triplet state, as expected of intuitive grounds. In case (e), the characteristic strength of the interactions between the spins in the environment is of the same order as the exchange coupling in the central system ($\Omega \approx J$), a regime in which there clearly is significant transfer of energy, back-and-forth, between the central system and the environment.

From the data for (b) – (d), shown in Fig. 4.1, we conclude that the time required to let the central system relax to a state that is close to the ground state depends on the energy scale (Ω) of the random interactions between the spins in the environment. As it is difficult to define the point in time at which the central system has reached its stationary state, we have not made an attempt to characterize the dependence of the relaxation time on Ω.

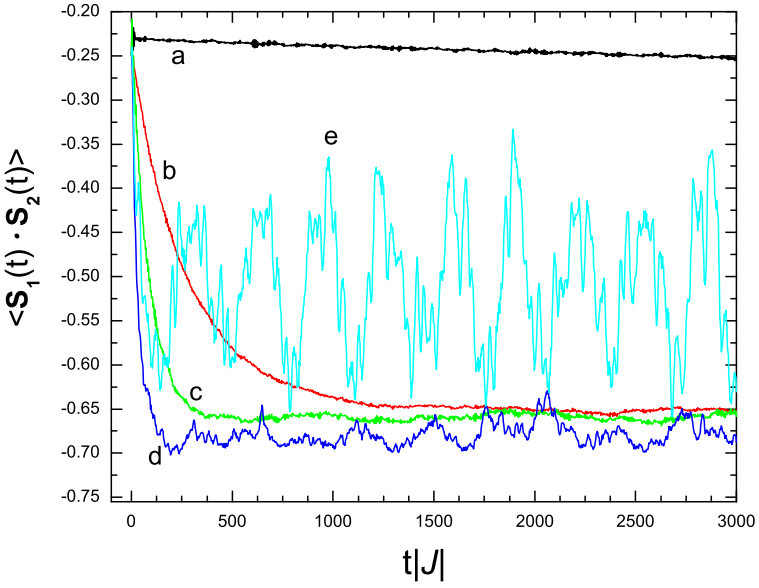

Figure 4.3: (Color online) The time evolution of the correlation $\langle\Psi(t)|\mathbf{S}_1 \cdot \mathbf{S}_2|\Psi(t)\rangle$ of the antiferromagnetic central system with Heisenberg-like H_{ce} and H_e. The model parameters are $\Delta = 0.15$ and a: $\Omega = 0.075$; b: $\Omega = 0.15$; c: $\Omega = 0.20$; d: $\Omega = 0.30$; e: $\Omega = 1$. The number of spins in the environment is $N = 14$.

4.2.2 Antiferromagnetic Central System

We now consider what happens if we replace the ferromagnetic central system by an antiferromagnetic one.

The main difference between the antiferromagnetic and the ferromagnetic central system is that the ground state of the former is maximally entangled (a singlet) whereas the latter is a fully polarized product state.

In Fig. 4.3, we present simulation results for the two-spin correlation function for different values of the parameter Ω. In passing, we mention that in our simulations, we change the sign of J only, that is we use the same parameters for H_{ce} and H_e as in the corresponding simulations of the ferromagnetic case. Apart from the change is sign, the curves for all cases (a–e) in Fig. 4.1 and Fig. 4.3 are qualitatively similar. However, this is a little deceptive.

As for the ferromagnetic central system, in case (a), the relaxation is rather slow and confirming that there is relaxation to the ground state requires a prohibitively long simulation. In case (e), we have $\Omega \approx |J|$ and as already explained earlier, this case is not of immediate relevance to the question ad-

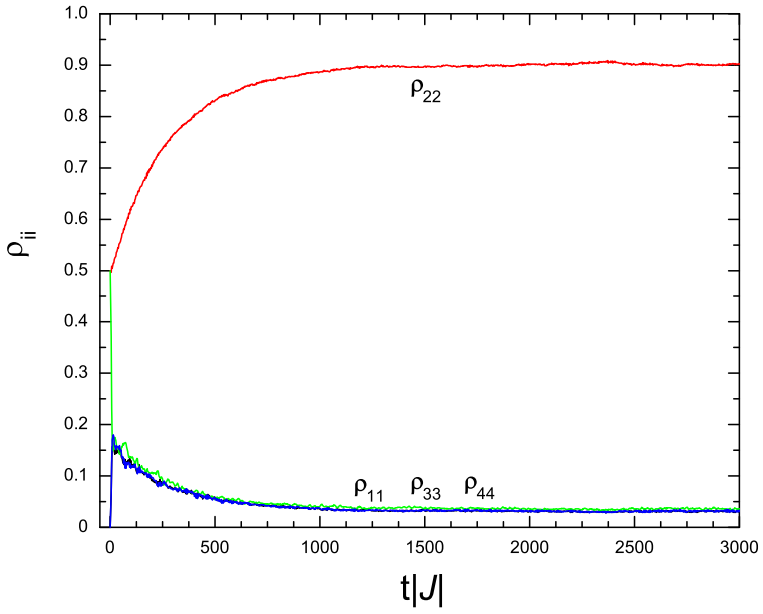

Figure 4.4: (Color online) The time evolution of the diagonal matrix elements of the reduced density matrix of the central system for $\Delta = 0.15$ and $\Omega = 0.15$ (case (b) of Fig. 4.3). The number of spins in the environment is $N = 14$.

dressed in this chapter. For cases (b) – (d), the results are in concert with the intuitive picture of relaxation due to decoherence except that the central system does not seem to relax to its true ground state. Indeed, the two-spin correlation relaxes to a value of about 0.65 – 0.70, which is much further away from the ground state value $-3/4$ than we would have expected on the basis of the results of the ferromagnetic central system. In the true ground state of the whole system, the value of the two-spin correlation in case (b) is -0.7232, and hence significantly lower than the typical values, reached after relaxation. On the one hand, it is clear (and to be expected) that the coupling to the environment changes the ground state of the central system, but on the other hand, our numerical calculations show that this change is too little to explain the apparent difference from the results obtained from the time-dependent solution.

In Fig. 4.4, we plot the diagonal matrix elements of the density matrix (calculated in the basis for which the Hamiltonian of the central system is diagonal) for case (b). From these data and the fact that the nondiagonal elements are negligibly small (data not shown), we conclude that the central system relaxes

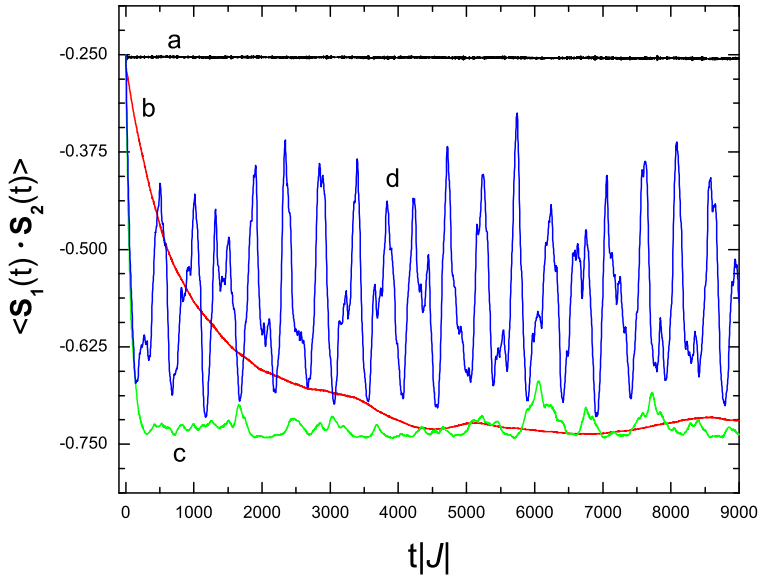

Figure 4.5: (Color online) The time evolution of the correlation $\langle\Psi(t)|\mathbf{S}_1 \cdot \mathbf{S}_2|\Psi(t)\rangle$ of the antiferromagnetic central system with Ising-like H_{ce} and Heisenberg-like H_e. The model parameters are $\Delta = 0.075$ and a: $\Omega = 0.075$; b: $\Omega = 0.15$; c: $\Omega = 0.30$; d: $\Omega = 1$. The number of spins in the environment is $N = 16$.

to a mixture of the singlet state and the (spin-up, spin-up) and (spin-down, spin-down) states, the former having much more weight (0.9 to 0.05) than the two latter states. Thus, at this point, we conclude that our results suggest that decoherence is less effective for letting a central system relax to its ground state if this ground state is entangled than if it is a product state. Remarkably, this conclusion changes drastically when we replace the Heisenberg-like H_{ce} by an Ising-like H_{ce}, as we demonstrate next.

4.3 Ising-like H_{ce}

In our simulation, the initial state of the central system is $|\uparrow\downarrow\rangle$ and this state has total magnetization $M = 0$. For an Ising-like H_{ce} with Heisenberg-like H_e coupling, the magnetization M of the central system commutes with the Hamiltonian (4.1) of the whole system. Therefore, the magnetization of the central system is conserved during the time evolution, and the central system will always stay in the subspace with $M = 0$. In this subspace, the ground state for antiferromagnetic central system is the singlet state $|S\rangle$ while for the

ferromagnetic central system the ground state (in the $M = 0$ subspace) is the entangled state $|T_0\rangle$. Thus, in the Ising-like H_{ce}, starting from the initial state $|\uparrow\downarrow\rangle$, the central system should relax to an entangled state, for both a ferro- or antiferromagnetic central system.

If the initial state of the central system is $|\uparrow\downarrow\rangle$, it can be proven (see Appendix) that

$$\langle\Psi(t)|\mathbf{S}_1 \cdot \mathbf{S}_2|\Psi(t)\rangle_F + \langle\Psi(t)|\mathbf{S}_1 \cdot \mathbf{S}_2|\Psi(t)\rangle_A = -\frac{1}{2}, \tag{4.4}$$

where the subscript F and A refer to the ferro- antiferromagnetic central system, respectively. Likewise, for the concurrence we find $C_F(t) = C_A(t)$ and similar symmetry relations hold for the other quantities of interest. Of course, this symmetry is reflected in our numerical data also, hence we can limit ourselves to presenting data for the antiferromagnetic central system with Ising-like H_{ce} and Heisenberg-like H_e.

In Fig. 4.5, we present simulation results for the two-spin correlation function for different values of the parameter Ω. Notice that compared to Figs. 4.1– 4.4, we show data for a time interval that is three times larger. For the cases (b,c), the main difference between Fig. 4.3 and Fig. 4.5 is that for the latter and unlike for the former, the central system relaxes to a state that is very close to the ground state. Thus, we conclude that the presence of a conserved quantity (the magnetization of the central system) acts as a catalyzer for relaxing to the ground state. Although it is quite obvious that by restricting the time evolution of the system to the $M = 0$ subspace, we can somehow force the system to relax to the entangled state, it is by no means obvious why the central system actually does relax to a state that is very close to the ground state.

Intuitively, we would expect that the presence of a conserved quantity hinders the relaxation and indeed, that is what we observe in cases (a,b) where the relaxation is much slower than in cases (a,b) of Fig. 4.1 or of Fig. 4.3. Notwithstanding this, in the presence of a conserved quantity, the central system relaxes to a state that is much closer to the true ground state than the one it would relax to in the absence of this conserved quantity.

4.4 Role of Δ

Now, we study the effect of changing the strength Δ of the coupling between the central system and the environment. For a qualitative discussion of this

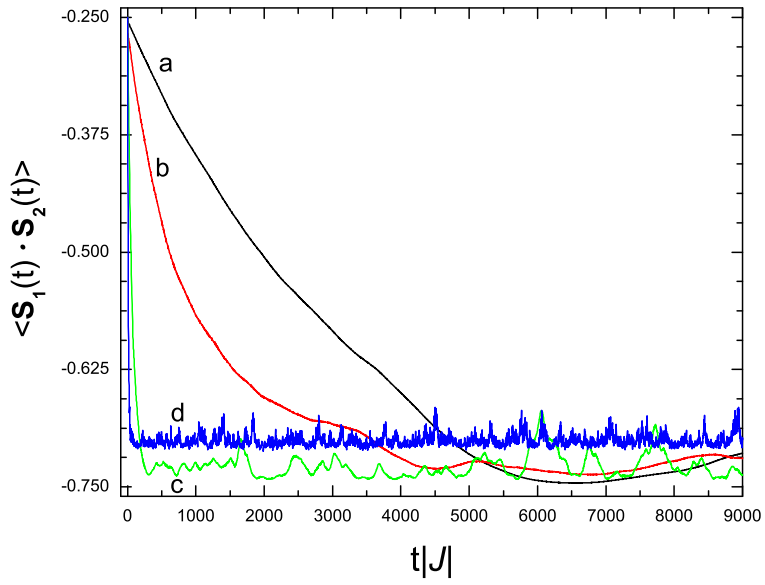

Figure 4.6: (Color online) The time evolution of the correlation $\langle\Psi(t)|\mathbf{S}_1 \cdot \mathbf{S}_2|\Psi(t)\rangle$ of the antiferromagnetic central system with Ising-like H_{ce} and Heisenberg-like H_e. a: $\Delta = 0.0375$ and $\Omega = 0.15$; b: $\Delta = 0.075$ and $\Omega = 0.15$; c: $\Delta = 0.075$ and $\Omega = 0.3$; d: $\Delta = 0.15$ and $\Omega = 0.3$. The number of spins in the environment is $N = 16$.

aspect, it suffices to consider the case of Ising-like H_{ce}, as we have seen that then, the central system most easily relaxes to its ground state.

In Fig. 4.6, we present some representative simulation results for the two-spin correlation function for different values of the parameters Δ and Ω. By simply comparing the time intervals of the plots for cases (a,b) and (c,d), it is immediately clear that the speed of relaxation changes drastically with Δ. For a "slow" environment (small enough Ω) the effect is rather trivial, namely, the larger Δ the faster the relaxation. In the case (c) the system comes close to the triplet state in comparison with (d), probably, since the perturbation of the ground state of the central system is smaller.

4.5 Sensitivity of the Results to Characteristics of the Environment

Finally, we study the effect of small changes to the initial state of the environment and of the number of spins in the environment.

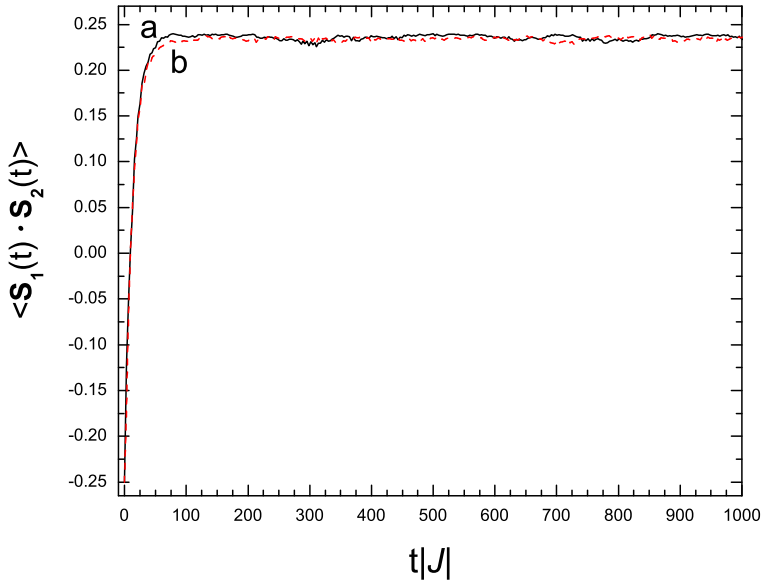

Figure 4.7: (Color online) The time evolution of the correlation $\langle\Psi(t)|\mathbf{S}_1 \cdot \mathbf{S}_2|\Psi(t)\rangle$ of a ferromagnetic central system with Heisenberg-like H_{ce} and Heisenberg-like H_e with $\Delta = 0.15$ and $\Omega = 0.3$. Initial state of the environment is solid line (a): ground state; dashed line (b): close to but not the same as the ground state. The number of spins in the environment is $N = 14$.

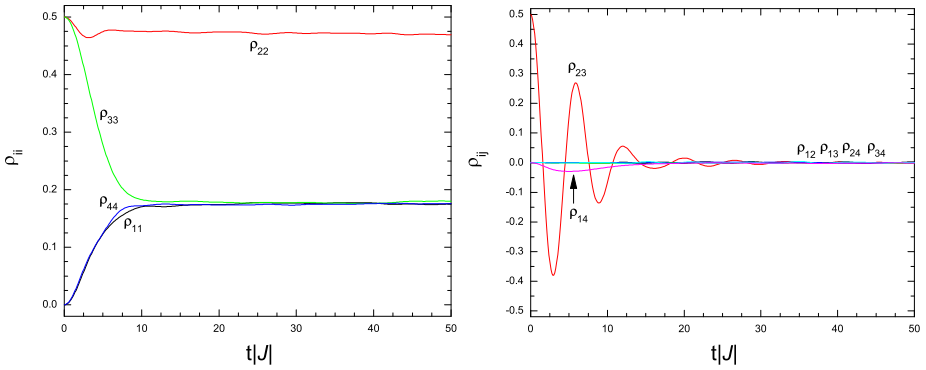

Figure 4.8: (Color online) The time evolution of the diagonal elements (left panel) and the real parts of the off-digonal elements (right panel) of the reduced density matrix in the antiferromagnetic central system, with Heisenberg-like H_{ce} and Heisenberg-like H_e ($\Delta = 0.15$ and $\Omega = 0.15$). The initial state of the central two spins is the up-down state, and the environment is initially in a random state. The number of spins in the environment is $N = 14$.

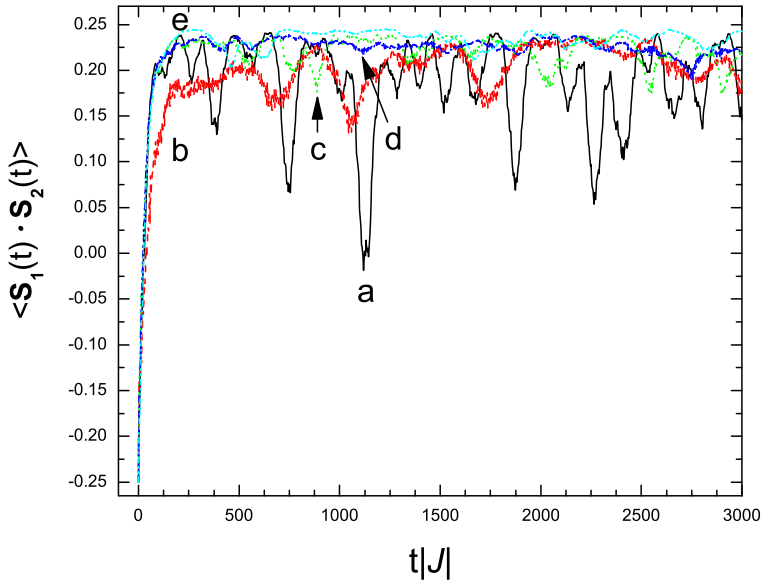

Figure 4.9: (Color online) The time evolution of the correlation $\langle\Psi(t)|\mathbf{S}_1 \cdot \mathbf{S}_2|\Psi(t)\rangle$ of a ferromagnetic central system with Heisenberg-like H_{ce} and Heisenberg-like H_e with $\Delta = 0.15$ and $\Omega = 0.3$. The number of spins in the environment is a: $N = 8$; b: $N = 9$; c: $N = 10$; d: $N = 11$; e: $N = 12$.

For the spin glasses, the true ground state is rather difficult to reach, and there are a lot of states with a very close energy but essentially different characteristics. To check how relevant it can be for our observations, we replace the environment ground state by one of these states and study the time evolution of the central system as we did before. In Fig. 4.7, we show typical results for a ferromagnetic central system with Heisenberg-like H_{ce} and Heisenberg-like H_e. In the initial state, the energy of the environment $E_b = -2.247$, which is a little bit higher than the ground-state energy of the environment $E_a = -2.321$. The time evolution of the correlation function of the two central spins for the cases (a) and (b) (see Fig. 4.7) clearly demonstrates that in both cases, the central system evolves to the ground state, and that the dynamics of this evolution is also very similar. This confirms that as long as the energy of the initial state of the environment is close to its ground state energy, the qualitative features of the decoherence process remain the same. If, on the other hand, we prepare the environment in a random state (which, roughly speaking, corresponds to a very high temperature), the central system does not relax to its ground state but to a mixed state with a diagonal density

matrix, as expected (see Fig. 4.8).

Second, we study the effect of finite size of the environment on the decoherence process. Some typical results for a ferromagnetic central system with Heisenberg-like H_{ce} and Heisenberg-like H_e with different numbers N of the environment spins are shown in Fig. 4.9. It looks reasonable to define the border between a mesoscopic and a macroscopic environment as the value of N for which the oscillations in the two-particle correlation are no longer well-defined. Thus, on the basis of the data displayed in Fig. 4.9 one can say that $N \approx 11$ is large enough for the spin-glass environment to mimic the macroscopic system. Needless to say, this statement is very qualitative but, in any case, the N dependence of the results shown in Fig. 4.9 demonstrates the effectiveness of the spinglass as a model environment to study decoherence processes with rather modest requirements as to the environment size.

4.6 Summary

We have presented the results of simulations that address the question of how a small quantum system evolves to its ground state when it is brought into contact with an environment consisting of quantum spins. Our systematic study confirms the suggestion of Ref. [22] that the use of a spin-glass thermal bath is indeed a very efficient way to simulate decoherence processes. Environments containing 14 – 16 spins are sufficiently large to induce a complete decay of the Rabi oscillations; this is in sharp contrast to environments that have a more simple structure, such as spin-chains or square lattices [22].

In general, it turns out that the relaxation to the ground state is a more complicated process than one would naively expect, depending essentially on the ratio between parameters of the interaction and environment Hamiltonians. Two general conclusions are: (i) the central system more easily evolves to its ground state when the latter is less entangled (e.g., up-down state compared to the singlet) and (ii) constraints on the system such as existence of additional integrals of motion can make the evolution to the ground state more efficient.

At first sight, the latter statement looks a bit counterintuitive since it means that it may happen that a more regular system exhibits stronger relaxation than a chaotic one. The reason that it may happen is that the larger is the dimensionality of available Hilbert space for the central system, the more complicated is the decoherence process due to the appearance of the whole

hierarchy of decoherence times for different elements of the reduced density matrix. A manifestation of this phenomenon has been observed earlier [16]: Under certain conditions, the same central system as studied here (four by four reduced density matrix) displays "quantum oscillations without quantum coherence" whereas for a single spin in magnetic field (two by two reduced density matrix) decoherence can, relatively easily, suppress the Rabi oscillations completely.

We believe that these results can stimulate further development and clarification of the "decoherence program" [15, 36]. Assuming that the interaction with an environment is weak enough, a hypothesis that the pointer states should be the eigenstates of the Hamiltonian of the central system was proposed [31], with the very ambitious aim of explaining the basic phenomenon of "quantum jumps".

In this chapter, we demonstrate that, apart from just the strength of different interactions, also their symmetry and the amount of entanglement of the ground state of the central system may play an essential role. Among the cases that we consider in this chapter, there are two situations where the standard decoherence scenario works as envisaged [31]. If the ground state is not entangled (as in the case of the up-down state for the case of ferromagnetic interactions) or if the Hilbert space is restricted due to some conservation laws (as for the singlet ground state in the Ising-type interaction Hamiltonian), the central system clearly evolves to its ground state, supposed to be the pointer state according to Ref. [31]. However, if the ground state of the central system is the fully entangled singlet state, and the interaction Hamiltonian is generic, without symmetries, the system evolves to some mixture of the ground state and excited states. Of course, the data presented here are not sufficient to make strong, general statements about the character of the pointer states, but we hope that, at least, our work will stimulate further research to establish the conditions under which the conjecture holds that the pointer states are the eigenstates of the central system.

Appendix

For the Hamiltonian Eq.(4.1), if $\Delta_{i,j}^{(x)} = \Delta_{i,j}^{(y)} = 0$, H_{ce} is Ising-like and it is easy to prove that $[M, H] = 0$, implying that the magnetization of the central two spins is a conserved quantity. In our simulations, we take as the initial state of the central system the spin-up - spin-down state ($|\uparrow\downarrow\rangle = (|S\rangle + |T_0\rangle)/\sqrt{2}$).

Hence, because $[M, H] = 0$, the central spin system will always stay in the subspace of $M = 0$. Thus, at any time t, the state of the whole system can be written as

$$|\Psi(t)\rangle = |S\rangle|\phi_S(t)\rangle + |T_0\rangle|\phi_{T_0}(t)\rangle, \tag{4.5}$$

where $|\phi_S\rangle$ and $|\phi_{T_0}\rangle$ denote the states of the environment.

Let us denote by $\{|\psi_i\rangle\}$ a complete set of states of the environment. Within the subspace spanned by the states $\{|S\rangle|\psi_i\rangle, |T_0\rangle|\psi_i\rangle\}$, the Hamiltonian Eq.(4.1) can be written as

$$\begin{aligned} H &= E_S|S\rangle\langle S| + E_T|T_0\rangle\langle T_0| + H_e \\ &\quad -\frac{1}{2}\sum_{j=1}^{N}(\Delta_{1,j}^{(z)} - \Delta_{2,j}^{(z)})\,(|S\rangle\langle T_0| + |T_0\rangle\langle S|)\,I_j^z, \end{aligned} \tag{4.6}$$

where we used $\langle S|S_1^z|S\rangle = \langle T_0|S_1^z|T_0\rangle = \langle S|S_2^z|S\rangle = \langle T_0|S_2^z|T_0\rangle = 0$, $\langle T_0|S_1^z|S\rangle = 1/2$, and $\langle T_0|S_2^z|S\rangle = -1/2$.

Introducing a pseudo-spin $\sigma = (\sigma^x, \sigma^y, \sigma^z)$ such that the eigenvalues $+1$ and -1 of σ^z correspond to the states $|S\rangle$ and $|T_0\rangle$, respectively, Eq.(4.6) can be written as

$$\begin{aligned} H &= \frac{E_S - E_T}{2} + \frac{E_S + E_T}{2}\sigma^z + H_e \\ &\quad -\frac{1}{2}\sum_{j=1}^{N}(\Delta_{1,j}^{(z)} - \Delta_{2,j}^{(z)})I_j^z\sigma^x, \end{aligned} \tag{4.7}$$

showing that in the case of Ising-like H_{ce}, the model Eq.(4.1) with two central spins is equivalent to the model Eq.(4.7) with one central spin.

From Eq.(4.7), it follows immediately that the Hamiltonian is invariant under the transformation $\{J, \sigma^z\} \to \{-J, -\sigma^z\}$. Indeed, the first, constant term in Eq.(4.7) is irrelevant and we can change the sign of the second term by rotating the speudo-spin by 180 degrees about the x-axis. Therefore, if the initial state is invariant under this transformation also, the time-dependent physical properties will not depend on the choice of the sign of J, hence the ferro- and antiferromagnetic system will behave in exactly the same manner.

For the case at hand, the initial state can be written as $(|S\rangle + |T_0\rangle)|\phi_0\rangle/\sqrt{2}$, which is trivially invariant under the transformation $\sigma^z \to -\sigma^z$. Summarizing: For Ising-like H_{ce} ($\Delta_{i,j}^{(x)} = \Delta_{i,j}^{(y)} = 0$), and an initial state that is invariant for

the transformation $|S\rangle \leftrightarrow |T_0\rangle$), $\langle\Psi(t)|A|\Psi(t)\rangle$ does not depend on the sign of J, for any observable A of the central system that is invariant for this transformation. Under these conditions, it is easy to prove that Eq.(4.4) holds and that the concurrence does not depend on the sign of J.

References

[1] R. Balescu, *Equilibrium and Nonequilibrium Statistical Mechanics* (Wiley, New York, 1975).

[2] S. Popescu, A. J. Short, and A. Winter, Nature Phys. **2**, 754 (2006).

[3] E. Fermi, J. Pasta, and S. Ulam, *Studies of the Nonlinear Problems I*, Los Alamos Report LA-1940 (1955), later published in *Collected Papers of Enrico Fermi*, ed. E. Segre, Vol. II (University of Chicago Press, 1965) p. 978.

[4] G. M. Zaslavsky, *Stochasticity of Dynamical Systems* (Nauka, Moscow, 1984)

[5] N. N. Bogoliubov, *Collection of Papers* (Naukova Dumka, Kiev, 1970), Vol. II, p. 77.

[6] M. I. Katsnelson and A. V. Trefilov, Fizika Metal. Metalloved. **64**, 629 (1987) [Engl. transl.: Phys. Met. Metallogr. **64** (4), 1 (1987)].

[7] R. P. Feynman and F. L. Vernon, Ann. Phys. (N. Y.) **24**, 118 (1963).

[8] A. O. Caldeira and A. J. Leggett, Ann. Phys. (N. Y.) **149**, 374 (1983).

[9] A. J. Leggett, S. Chakravarty, A. T. Dorsey, M. P. A. Fisher, A. Garg, and W. Zwerger, Rev. Mod. Phys. **59**, 1 (1987).

[10] N. V. Prokof'ev and P. C. E. Stamp, Rep. Prog. Phys. **63**, 669 (2000).

[11] R. V. Jensen and R. Shankar, Phys. Rev. Lett., **54**, 1879 (1985).

[12] K. Saito, S. Takesue, and S. Miyashita, Phys. Rev. E **54**, 2404 (1996).

[13] S. O. Skrøvseth, Europhys. Lett. **76**, 1178 (2006).

[14] D. Giulini, E. Joos, C. Kiefer, J. Kupsch, I.-O. Stamatescu, and H.D. Zeh, *Decoherence and the Appearance of a Classical World in Quantum Theory* (Springer, Berlin, 1996).

[15] W. H. Zurek, Rev. Mod. Phys. **75**, 715 (2003).

[16] V. V. Dobrovitski, H. A. De Raedt, M. I. Katsnelson, and B. N. Harmon, Phys. Rev. Lett. **90**, 210401 (2003).

[17] M. I. Katsnelson, V. V. Dobrovitski, H. A. De Raedt, and B. N. Harmon, Phys. Lett. A **318**, 445 (2003).

[18] J. Lages, V. V. Dobrovitski, M. I. Katsnelson, H. A. De Raedt, and B. N. Harmon, Phys. Rev. E **72**, 026225 (2005).

[19] F. M. Cucchietti, J. P. Paz, and W. H. Zurek, Phys. Rev. A **72**, 052113 (2005).

[20] Z. Gedik, Sol. State Commun. **138**, 82 (2006).

[21] W. H. Zurek, F. M. Cucchietti, and J. P. Paz, Acta Physica Polonica B, 38, No. 5, 1685 (2007).

[22] S. Yuan, M. I. Katsnelson, and H. De Raedt, JETP Lett. **84**, 99 (2006).

[23] A. Melikidze, V. V. Dobrovitski, H. A. De Raedt, M. I. Katsnelson, and B. N. Harmon, Phys. Rev. B **70**, 014435 (2004).

[24] M. Lucamarini, S. Paganelli, S. Mancini, Phys. Rev. A 69, 062308 (2004)

[25] J. van Wezel, J. van den Brink, and J. Zaanen, Phys. Rev. Lett. 94, 230401 (2005).

[26] Y. Gao and S. J. Xiong, Phys. Rev. A 71, 034102 (2005).

[27] X.-Z. Yuan, K.-D. Zhu, and Z.-J. Wu, Eur. Phys. J. **D** 33, 129 (2005).

[28] G.-F. Zhang, J.-Q. Liang, G.-E. Zhang, and Q.-W. Yan, Eur. Phys. J. **D** 32, 409 (2005).

[29] Y. Hamdouni, M. Fannes, and F. Petruccione, Phys. Rev. B **73**, 245323 (2006).

[30] W. Zhang, N. Konstantinidis, K. A. Al-Hassanieh, and V. V. Dobrovitski, J. Phys.: Cond. Matter **19**, 083202 (2007) .

[31] J.-P. Paz and W.H. Zurek, Phys. Rev. Lett. **82**, 5181 (1999).

[32] V. V. Dobrovitski and H. A. De Raedt, Phys. Rev. E **67**, 056702 (2003).

[33] S. Hill and W. K. Wootters, Phys. Rev. Lett. **78**, 5022 (1997)

[34] W. K. Wootters, Phys. Rev. Lett. **80**, 2245 (1998).

[35] J. von Neumann, *Mathematical Foundations of Quantum Mechanics* (Princeton University Press, Princeton, 1955).

[36] W. Zurek, Phil. Trans. R. Soc. Lond. A **356**, 1793 (1998).

Chapter 5

Importance of Bath Dynamics for Decoherence in Spin Systems

This chapter was previously published as
S. Yuan, M.I. Katsnelson, and H. De Raedt, arXiv:0707.2372.

It is commonly accepted that decoherence by nuclear spins is the main obstacle for realization of quantum computations in magnetic systems; see, e.g., discussions of specific silicon [1] and carbon [2] based quantum computers. Therefore, understanding the decoherence in quantum spin systems is a subject of numerous works (for review, see Refs. [3, 4]). The issue seems to be very complicated and despite many efforts, even some basic questions about character of the decoherence process are unsolved yet. Most of the problems cannot be solved analytically, in particular if there is more than one spin in the central system, but we can use the computer to simulate the dynamics and find useful information.

An unusual two-step decoherence was reported in Ref. [5]. This is an important phenomenon since it implies that, generally speaking, the observation of the Rabi oscillations does not guarantee access to sectors of the Hilbert space that may be essential for efficient quantum computation. Its origin is still poorly understood; it was described analytically in a framework of an exactly solvable model of noninteracting spins in the bath [6] but it is not clear how sensitive it is to the details of spin-spin interactions. In the real world, the environment has its own dynamics, which could be much slower or comparable to the central dynamics. First attempts to investigate numerically the effects of the environment dynamics [7] did not lead to definite conclusions.

The behavior of an open quantum system crucially depends on the ratio of typical energy differences of the central system δE_c and the energy E_{ce} which characterizes the interaction of the central system with the environment. The case $\delta E_c \ll E_{ce}$ has been studied extensively in relation to the "Schrödinger cat" problem and the physics is quite clear [8, 9]: As a result of time evolution, the central system passes to one of the "pointer states" [9] which, in this case, are the eigenstates of the interaction Hamiltonian. The opposite case, $\delta E_c \gg E_{ce}$ is less well understood. There is a conjecture that in this case the pointer states should be eigenstates of the Hamiltonian of the central system, but this is proven only for a very simple model [10]. On the other hand, this case is of primary interest if, say, the central system consists of electron spins whereas the environment are nuclear spins (e.g., if one considers the possibility of quantum computation using molecular magnets [11, 12]).

In fact, as we will show, the selection of an eigenstate as the pointer state is also determined by the state and the dynamics of the environment. Elsewhere [13, 14], we have already shown that if the environment is a spin glass and initially in the ground state, then independent of the initial state of the central system, the central system relaxes to a state that is very close to its ground state: The ground state is selected as the point state of the central system. In this chapter, we consider a realistic model of decoherence of a system of two spins by an environment of nuclear spins at elevated temperatures. We will demonstrate that the decoherence of the central system depends in a significant, nonintuitive manner on the details of the dynamics of the environment.

5.1 Model

We consider a generic quantum spin model described by the Hamiltonian $H = H_c + H_{ce} + H_e$ where

$$H_c = -J\mathbf{S}_1 \cdot \mathbf{S}_2,$$
$$H_e = -\sum_{i=1}^{N-1}\sum_{j=i+1}^{N}\sum_{\alpha}\Omega_{i,j}^{(\alpha)} I_i^\alpha I_j^\alpha,$$

and

$$H_{ce} = -\sum_{i=1}^{2}\sum_{j=1}^{N}\sum_{\alpha}\Delta_{i,j}^{(\alpha)} S_i^\alpha I_j^\alpha, \tag{5.1}$$

are the Hamiltonians of the central system, the environment, and the interaction of the central system and the environment, respectively. In Eq.(5.1), the exchange integrals J and $\Omega_{i,j}^{(\alpha)}$ determine the strength of the interaction between spins $\mathbf{S}_n = (S_n^x, S_n^y, S_n^z)$ of the central system H_c, and the spins $\mathbf{I}_n = (I_n^x, I_n^y, I_n^z)$ in the environment H_e, respectively. The exchange integrals $\Delta_{i,j}^{(\alpha)}$ control the interaction H_{ce} of the central system with its environment. In Eq.(5.1), the sum over α runs over the x, y and z components of spin-1/2 operators $\mathbf{S}$ and $\mathbf{I}$.

In the sequel, we will use the term "Heisenberg-like" H_e to indicate that each $\Omega_{i,j}^{(\alpha)}$ is a uniform random number in the range $[-\Omega|J|, \Omega|J|]$, Ω being a free parameter. We will consider two different kinds of H_{ce}, namely rotational invariant Heisenberg interactions $\Delta_{i,j}^{(\alpha)} \equiv \Delta$ and "Ising-like" interactions for which $\Delta_{i,j}^{(x)} = \Delta_{i,j}^{(y)} = 0$ and $\Delta_{i,j}^{(z)}$ are dichotomic random variables, taking the values $\pm\Delta$. Obviously, if H_{ce} is "Ising like", the total magnetization of the central system ($M = S_1^z + S_2^z$) is a conserved quantity.

As we demonstrate in this chapter, the connectivity of the spins in the environment affects the decoherence in a nontrivial manner. We characterize this connectivity by the number K, the number of environment spins with which a spin in the environment interacts. If $K = 0$, each spin in the environment interacts with the central system only. If $K = 2$, the structure of the environment is assumed to be that of a ring, that is each spin in the environment interacts with two other spins only. Likewise, $K = 4$ and $K = 6$ correspond environments in which the spins are placed on a square or triangular lattice, respectively and interact with nearest-neighbors only. If $K = N - 1$, each spin

in the environment interacts with all the other spins in the environment and, to give this case a name, we will refer to this case as "spin glass".

If the Hamiltonian of the central system H_c is a perturbation, relative to the interaction Hamiltonian H_{ce}, the pointer states are eigenstates of H_{ce} [9]. In the opposite case, that is the regime $|\Delta| \ll |J|$ that we explore in this chapter, the pointer states are supposed to be eigenstates of H_c [10]. The latter are given by $|1\rangle \equiv |T_1\rangle = |\uparrow\uparrow\rangle$, $|2\rangle \equiv |S\rangle = (|\uparrow\downarrow\rangle - |\downarrow\uparrow\rangle)/\sqrt{2}$, $|3\rangle \equiv |T_0\rangle = (|\uparrow\downarrow\rangle + |\downarrow\uparrow\rangle)/\sqrt{2}$, and $|4\rangle \equiv |T_{-1}\rangle = |\downarrow\downarrow\rangle$, satisfying $H_c|S\rangle = (3J/4)|S\rangle$ and $H_c|T_i\rangle = (-J/4)|T_i\rangle$ for $i = -1, 0, 1$.To check this conjecture is one of the main aims of our simulations.

The simulation procedure is as follows. We generate a random superposition $|\phi\rangle$ of all the basis states of the environment. This state corresponds to the equilibrium density matrix of the environment at infinite temperature. The spin-up – spin-down state ($|\uparrow\downarrow\rangle$) is taken as the initial state of the central system. Thus, the initial state of the whole system reads $|\Psi(t=0)\rangle\rangle = |\uparrow\downarrow\rangle\,|\phi\rangle$ and is a product state of the state of the central system and the random state of the environment which, in general is a (very complicated) linear combination of the 2^N basis states of the environment. In our simulations we take $N = 16$ which, from earlier work [13, 14], we know is sufficiently large for the environment to behave as a "large" system. For a given, fixed set of model parameters, the time evolution of the whole system is obtained by solving the time-dependent Schrödinger equation for the many-body wave function $|\Psi(t)\rangle\rangle$, describing the central system plus the environment. The numerical method that we use is described in Ref. [15]. It conserves the energy of the whole system to machine precision. We monitor the effects of the decoherence by plotting the time dependence of the matrix elements of the reduced density matrix of the central system. As explained earlier, in the regime of interest $|\Delta| \ll |J|$, the pointer states are the eigenstates of the central systems, hence we compute the matrix elements of the density matrix in the basis of eigenvectors of the central system.

5.2 Isotropic Heisenberg Coupling

In Fig. 5.1, we show the time evolution of the elements of the reduced density matrix of the central system for different connectivity numbers K and Heisenberg or Heisenberg-like interactions between central system and the spins in the environment. We conclude that:

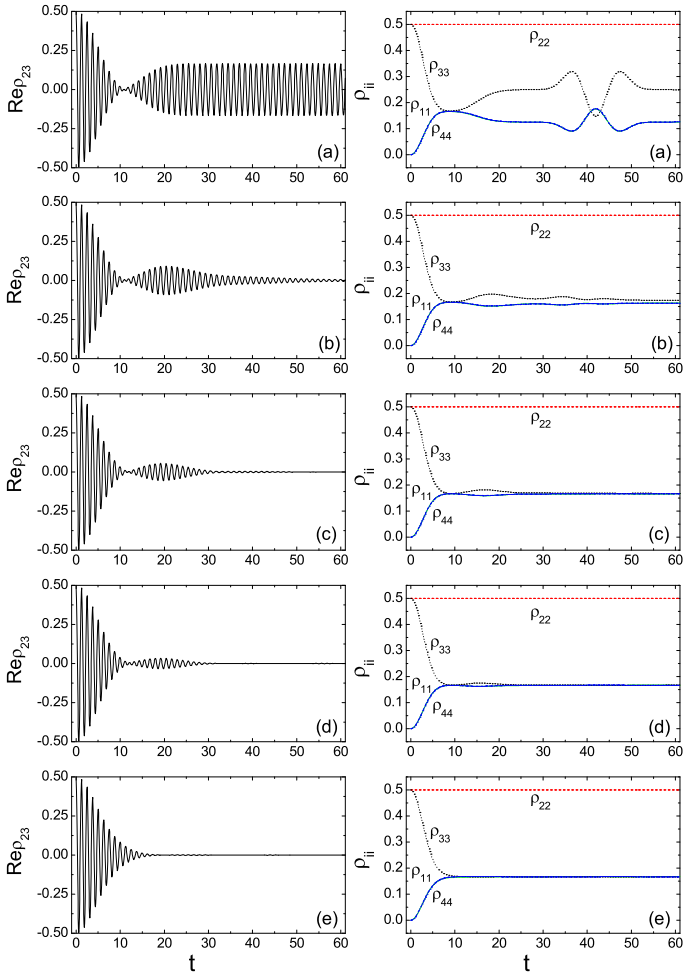

Figure 5.1: (Color online) The time evolution of the real part of the off-diagonal element ρ_{23} (right panel) and the diagonal elements $\rho_{11}, \ldots, \rho_{44}$ (left panel) of the reduced density matrix of a central system (with $J = -5$), interacting with a Heisenberg-like environment H_e (with $\Omega = 0.15$) via an isotropic Heisenberg Hamiltonian H_{ce} (with $\Delta = -0.075$) for different connectivity numbers K of the spins in the environment: (a) $K = 0$; (b) $K = 2$; (c) $K = 4$; (d) $K = 6$; (e) $K = N - 1$.

1. In agreement with earlier work [5, 6], we find that in the absence of interactions between the environment spins ($K = 0$) and after the initial fast decay, the central system exhibits long-time oscillations (see Fig. 5.1(a)(left)). In this case and in the limit of a large environment,

we have [6]

$$\text{Re } \rho_{23}(t) = \left[\frac{1}{6} + \frac{(1-bt^2)e^{-ct^2}}{3}\right]\cos\omega t, \tag{5.2}$$

where $b = N\Delta^2/4$, $c = b/2$ and $\omega = J - \Delta$. Equation (5.2) clearly shows the two-step process, that is, after the initial Gaussian decay of the amplitude of the oscillations, the oscillations revive and their amplitude levels of [6]. Notice that because of conservation laws, this behavior does not change if the environment is described by an isotropic Heisenberg Hamiltonian ($\Omega_{i,j}^{(\alpha)} \equiv \Omega$ for all α, i and j), whatever the value of K. If, as in Ref. [5], we take $\Delta_{i,j}^{(x)} = \Delta_{i,j}^{(y)} = \Delta_{i,j}^{(z)} \in [0, \Delta]$ random instead of the same, the amplitude of the long-living oscillations is no longer constant but decays very slowly [5].

2. The presence of Heisenberg-like (non-isotropic, random) interactions between the spins of the environment leads to a reduction and a decay of the amplitude of the long-living oscillations (see Fig. 5.1(b-e)(left)). The larger the connectivity number K, the faster is the decay of the amplitude. When K reaches its maximum $K = N - 1$ (spin glass), the second step in the decoherence process is no longer separated from the initial decay. In fact, it seems as if it has merged with the final stage of the first step (see Fig. 5.1(e)(left)). For $K = N - 1$, the time evolution of $\rho_{23}(t)$ can be fitted well by the function

$$\text{Re } \rho_{23}(t) = \left[\frac{e^{-a't}}{6} + \frac{(1-b't^2)e^{-c't^2}}{3}\right]\cos\omega' t, \tag{5.3}$$

with $a' = 0.13403$, $b' = 0.00659$, $c' = 0.01085$ and $\omega' = 5.01037$. For comparison, the values that enter Eq.(5.2) are $b = 0.0225$, $c = 0.01125$ and $\omega = 4.925$. It is of interest to note that if the dynamics of the environment is sufficiently slow ($\Omega \approx 0.01$ in Ref. [5]), this dynamics apparently does not affect the decoherence of the central spins [5]. Thus, the effectiveness of the decoherence process not only depends on K but also on the details of the interactions within the environment.

3. According to the general picture of decoherence [9], for an environment with nontrivial internal dynamics that initially is in a random superposition of all its eigenstates, we expect that the central system will evolve to a stable mixture of its eigenstates. In other words, the decoherence

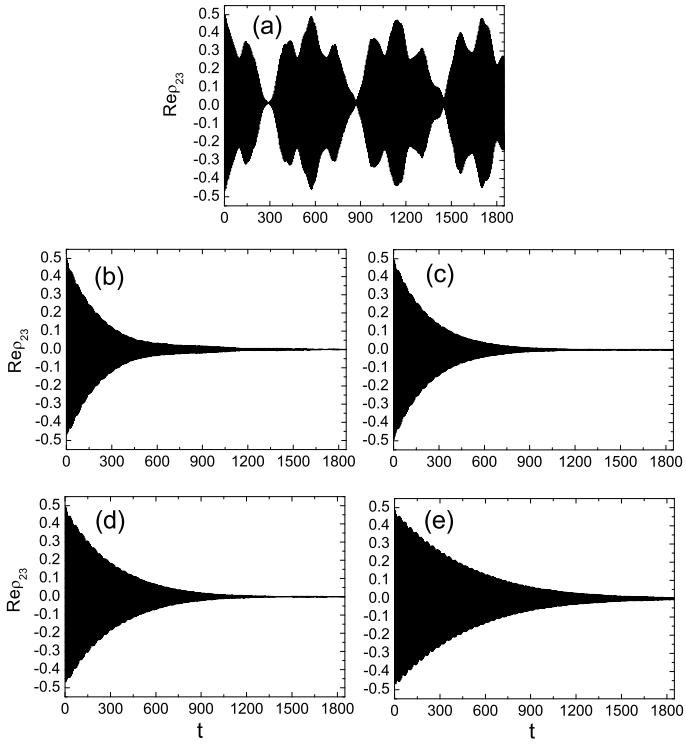

Figure 5.2: (Color online) The time evolution of the real part of the off-diagonal element ρ_{23} of the reduced density matrix of a central system (with $J = -1$), interacting with a Heisenberg-like environment H_e (with $\Omega = 0.15$) via an Ising-like Hamiltonian H_{ce} (with $\Delta = 0.075$) for different connectivity numbers K of the spins in the environment: (a) $K = 0$; (b) $K = 2$; (c) $K = 4$; (d) $K = 6$; (e) $K = N - 1$.

will cause all the off-diagonal elements of the reduced density matrix to vanish with time. Moreover, the weight of the degenerate eigenstates $|T_0\rangle$, $|T_{-1}\rangle$, and $|T_1\rangle$ in this mixed state are expected to be the same. As shown in Fig. 5.1(b-e)(right), our simulations confirm that this picture is correct in all respects. Furthermore, the results depicted in Fig. 5.1(b-e)(right) demonstrate that the connectivity number K has no effect on the value of ρ_{11}, ρ_{22}, ρ_{33} and ρ_{44} for long times.

Table 5.1: Frequency of oscillation ω'' and decoherence time τ for different connectivity K. In case 1 and case 2, for each K, the values of $\Omega_{i,j}^{(\alpha)}$ are the same but the values of $\Delta_{i,j}^{(\alpha)}$ are different. In case 2 and case 3, for each K, the values of $\Delta_{i,j}^{(\alpha)}$ are the same but the values of $\Omega_{i,j}^{(\alpha)}$ are different.

Case		$K=2$	$K=4$	$K=6$	$K=N-1$
1	ω''	1.015	1.015	1.016	1.017
	τ''	212.9	235.3	302.9	447.4
2	ω''	1.017	1.021	1.022	1.027
	τ''	93.07	105.0	110.4	182.1
3	ω''	1.021	1.022	1.022	1.027
	τ''	106.3	110.0	111.7	173.2

5.3 Anisotropic Ising-like Coupling

Next, we change the interactions between central system and the spins in the environment from Heisenberg-like to Ising-like but keep the interactions between different spins in the environment Heisenberg-like. In fact, in our simulations, the Hamiltonian H_e is the same for both cases. As explained earlier, in the Ising-like case, the total magnetization of the central system is conserved during the time evolution. Thus, as the initial state of the central system is $(|S\rangle + |T_0\rangle)/\sqrt{2}$, at any time t the state of the whole system can be written as

$$|\Psi(t)\rangle = |2\rangle|\phi_2(t)\rangle + |3\rangle|\phi_3(t)\rangle, \tag{5.4}$$

where $|\phi_2(t)\rangle$ and $|\phi_3(t)\rangle$ denote the states of the environment. In other words, only $\rho_{22}(t)$, $\rho_{23}(t)$, $\rho_{32}(t)$, and $\rho_{33}(t)$ can be nonzero.

On general grounds, we may expect that the presence of an additional conservation law slows down the decoherence and indeed, as shown in Fig. 5.2, this is the case. Note that the results of Fig. 5.2 have been obtained for $J=-1$ instead of for $J=-5$, the value used to compute the results shown in Fig. 5.1 (the latter value was chosen to facilitate the comparison with the results of Ref. [5]), but this factor of five in the value of J cannot account for the large difference in the observed decoherence times.

From Fig. 5.2, we conclude that

1. We never observe the two-step process that we find in the case of Heisenberg-like H_{ce}. For $K = 0$ (Fig. 5.2(a), there is no decoherence.

2. For $K > 0$, Re $\rho_{23}(t)$ vanishes with time, in agreement with the general picture of decoherence [9]. However, quite unexpectedly, the rate of decoherence *increases* with K, in contrast to the case of Heisenberg-like H_{ce} in which the rate of decoherence decreases with K. The data presented in Figs. 5.2(b-d) can all be fitted very well by

$$\text{Re } \rho_{23}(t) = \frac{1}{2} e^{-t/\tau''} \cos \omega'' t, \tag{5.5}$$

where $\omega'' \approx |J|$ and the values of τ'' depend on K. In Table 5.1, we give some typical results for these parameters. Cases 1 and 2 illustrate that (random) changes in H_{ce} may affect the value of the decoherence time τ'' significantly but the general trend, the increase of τ'' with K seems generic.

5.4 Summary

In conclusion, we have shown that (1) the pure quantum state of the central spin system evolves into the classical, mixed state, and (2) if the interaction between the central system and environment is much smaller than the coupling between the spins in the central system, the pointer states are the eigenstates of the central system. Both these observations are in concert with the general picture of decoherence [9].

Furthermore, we have demonstrated that, in the case that the environment is a spin system, the details of this spin system are important for the decoherence of the central system. In particular, we have shown that (1) changing the internal dynamics of the environment may change the qualitative features of the decoherence of the central spin system, and that (2) the dependence of the decoherence time of the central spin system on the connectivity of the interactions between spins of the environment is counterintuitive.

References

[1] B.E. Kane, Nature **393**, 133 (1998).

[2] B. Trauzettel, D.V. Bulaev, D. Loss and G. Burkard, Nature Phys. **3**, 192 (2007).

[3] N.V. Prokof'ev and P.C.E. Stamp, Rep. Prog. Phys. **63**, 669 (2000).

[4] W. Zhang, N. Konstantinidis, K.A. Al-Hassanieh and V.V. Dobrovitski, J. Phys.: Cond. Matter **19**, 083202 (2007).

[5] V.V. Dobrovitski, H.A. De Raedt, M.I. Katsnelson and B.N. Harmon, Phys. Rev. Lett. **90**, 210401 (2003).

[6] A. Melikidze, V. V. Dobrovitski, H. A. De Raedt, M.I. Katsnelson and B.N. Harmon, Phys. Rev. B **70**, 014435 (2004).

[7] J. Lages, V.V. Dobrovitski, M.I. Katsnelson, H.A. De Raedt and B.N. Harmon, Phys. Rev. E **72**, 026225 (2005).

[8] D. Giulini, E. Joos, C. Kiefer, J. Kupsch, I.-O. Stamatescu, and H.D. Zeh, *Decoherence and the Appearance of a Classical World in Quantum Theory* (Springer, Berlin, 1996).

[9] W.H. Zurek, Rev. Mod. Phys. **75**, 715 (2003).

[10] J.-P. Paz and W.H. Zurek, Phys. Rev. Lett. **82**, 5181 (1999).

[11] V.V. Dobrovitski , M.I. Katsnelson and B.N. Harmon, Phys. Rev. Lett. **84**, 3458 (2000).

[12] M.N. Leuenberger and D. Loss, Nature **410**, 789 (2001).

[13] S. Yuan, M.I. Katsnelson and H. De Raedt, JETP Lett. **84**, 99 (2006).

[14] S. Yuan, M.I. Katsnelson and H. De Raedt, Phys. Rev. A **75**, 052109 (2007).

[15] V.V. Dobrovitski and H.A. De Raedt, Phys. Rev. E **67**, 056702 (2003).

Chapter 6

Quantum Dynamics of Spin Wave Propagation Through Domain Walls

---

This chapter was previously published as
S. Yuan, H. De Raedt, and S. Miyashita, J. Phys. Soc. Jpn. **75**, 084703 (2006).

Wave propagation in one-dimensional magnets through a magnetic domain wall (DW) is an interesting topic in quantum many-body physics. A DW separates two regions with opposite magnetization. The DW in mesoscopic wire can be considered to be self-assembled stable nanostructures which is treated as a kind of soliton in a continuous medium. Such structure can be created or annihilated by some external action [1]. The manipulation of DW in stripes has already been proposed as a way of storing information or even performing logic functions, and to offer new types of electronics devices [1] in which the DW motion carries the information along a magnetic wire of submi-

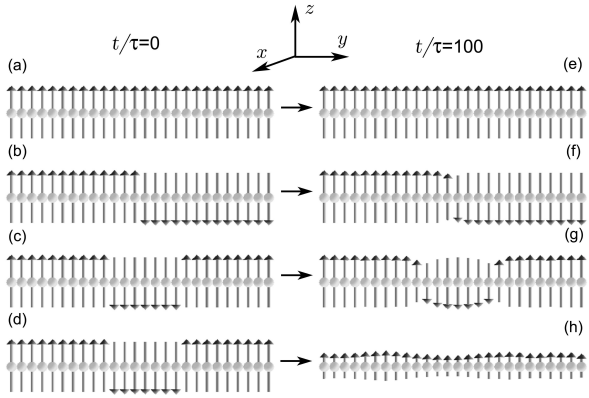

Figure 6.1: Left pictures (a,b,c,d): Spin configurations at time $t/\tau = 0$; Right pictures (e,f,g): Dynamically stable spin configurations for the Heisenberg-Ising model ($\lambda = 2$), at time $t/\tau = 100$. (e): Ferromagnetic state of the spin chain; (f): State containing a DW at the center of the chain; (g): State containing two DWs. Right picture (h): Spin configuration at time $t/\tau = 100$ for the Heisenberg model ($\lambda = 1$), illustrating the instability of the initial domain wall state (d).

crometer width, with DW velocities up to thousand kilometers per second [2]. Recently, a direct observation of the pendulum dynamics of a DW has been reported [3]. The DW as a topological particle has a very small but finite mass of 6.6×10^{-23}kg [3, 4].

The structure of DWs and also wave propagation in one-dimensional classical spin systems has been studied in Refs. [5, 6]. Recently, the interaction between DWs and spin waves has attracted a lot of interest. Hertel *et al* showed that the DW induced phase shift of spin waves in the Landau-Lifshitz-Gilbert (LLG) model of thin, narrow strips, is a characteristic property of such systems [8]. The value of the phase shift of spin waves passing through a DW was found to be proportional to the angle by which the magnetization of DW rotates in the film plane [8]. This effect might be used as a concept for a new generation of nonvolatile memory storage and logical devices [8].

On the other hand, recent progress in synthesizing materials containing ferromagnetic chains [9–12] opens new possibilities to study the interaction between a spin wave and a DW in a microscopic spin chain. Furthermore, quantum spin models provide a playground to investigate how quantum information can be transferred in quantum spin networks [13–15]. But, in contrast to the nanoscale phenomena mentioned earlier, on the atomic level, the spin dynamics is purely quantum mechanical and in such strongly quantum fluctuating

systems it must be described by the time-dependent Schrödinger equation (TDSE). Then, it is of considerable interest to compare the properties of spin wave propagation through a magnetic domain boundary in a single spin chain with the dynamics obtained in mesoscopic system, in which the magnetization is regarded as a classical, continuous variable. In the nanoscale regime, the DW is defined as the boundary of regions with opposite magnetization. On the atomic level, a DW may be defined as a structure that is dynamically stable under quantum mechanical motion, the existence of which has to be confirmed.

6.1 Model

In this chapter, we study the stability of DWs and the effects of DWs on the spin wave propagation in a chain of N sites on which we place $S = 1/2$ spins. We solve the TDSE to compute the time-evolution of the magnetization at each lattice site. The Hamiltonian of the spin chain is given by [16]

$$H = -J \sum_{n=1}^{N-1} (S_n^x S_{n+1}^x + S_n^y S_{n+1}^y + \lambda S_n^z S_{n+1}^z), \tag{6.1}$$

where the exchange integrals $J > 0$ and λJ determine the strength of the interaction between the x, y and z components of spin 1/2 operators $\mathbf{S}_n = (S_n^x, S_n^y, S_n^z)$. We solve the TDSE by the Chebyshev polynomial algorithm which is known to yield extremely accurate solutions of the TDSE, independent of the time step used [17–20]. We display the results at time intervals of $\tau = \pi/5J$. We present results for systems containing $N = 26$ spins only. We checked that simulations for $N = 20$ spins (data not shown) yield qualitatively similar results. In our numerical work, we use units such that $\hbar = 1$ and $J = 1$.

First, we study the stability of DWs. The left panel of Fig. 6.1 shows the spin configurations that we take as the initial state ($t/\tau = 0$) in the simulation. All the results shown in this Letter have been obtained using open boundary conditions. We let the system evolve in time according to the Hamiltonian Eq.(6.1) for a long time ($t/\tau = 100$) and find that the motion generates a dynamically stable state with DW(s) (see Fig. 6.1(f,g)). The DW is defined as the boundary between regions of different magnetization but it is not trivial that these boundaries exists in the presence of strong quantum fluctuations. [7] Figure 6.1(e,f,g) shows the dynamically stable spin configurations obtained by starting from the corresponding configuration (a,b,c).

Whether or not quantum fluctuations destroy the DW(s) depends on the value of the anisotropy λ. For the model Eq.(6.1), it is well know [16] that quantum fluctuations destroy the long range order of the ground state if $-1 < \lambda < 1$ (XY-like) or $\lambda = -1$ (Heisenberg antiferromagnet). For $\lambda \geq 1$ (Ising-like) the ground state exhibits long range order. This property is reflected in the stability of configurations that contain one or more DWs, except for $\lambda = 1$. Our numerical simulations show that configurations with a DW are dynamically stable if $\lambda > 1$. For comparison, in Fig. 6.1 we include the case $\lambda = 1$, where the initial DW structure (Fig. 6.1(d)) is destroyed (Fig. 6.1(h)). Not surprisingly, the destructive effect of quantum fluctuations can be suppressed by increasing λ. Having studied systems with different values of λ, we found that $\lambda = 2$ is representative for the quantitative behavior of the anisotropic systems. Therefore, in this chapter, we present results for $\lambda = 2$ only. We also checked the effect of the boundary condition. We found almost the same stable DW structures in the case of periodic boundary conditions (results not shown).

6.2 Spin Wave Propagation

We use the configuration at $t/\tau = 100$ as the initial configuration to study the spin wave dynamics. We generate a spin wave excitation by rotating the left most spin $\mathbf{S}_1$ in Fig. 6.1(e,f,g). For reference, we also consider the dynamics of the ferromagnet (see Fig. 6.1(a,e)). This case without DW can be analyzed analytically, so that it also gives check of precision of numerical calculation. Actually, we found very small difference between the analytical results and numerical ones.

In Fig. 6.2(a) we show the time evolution of $\{\langle S_n^z(t)\rangle\}$ for $n = 1, \ldots N$ after flipping $\mathbf{S}_1$, in the case of the uniform chain. The time evolution of $\{\langle S_n^z(t)\rangle\}$ for $n = 1, \ldots N$ in the chain with one DW at $n = 13, 14$ is depicted in Fig. 6.2(b), and Fig. 6.2(c) shows the results for the chain with one DW at $n = 10, 11$ and another DW at $n = 17, 18$. Hence, we demonstrate that even in the presence of a spin wave, the DW structure remain stable. In the model Eq.(6.1), the magnetization in the z-direction is a conserved quantity. Hence, by flipping one or more spins we change the total magnetization of the initial state. The expectation value of the transverse spin components is identically zero ($\langle S_n^x(t)\rangle = \langle S_n^y(t)\rangle = 0$ for $n = 1, \ldots N$), for all $t > 0$.

From Fig. 6.2, we can deduce how the spin wave is scattered by the DW(s).

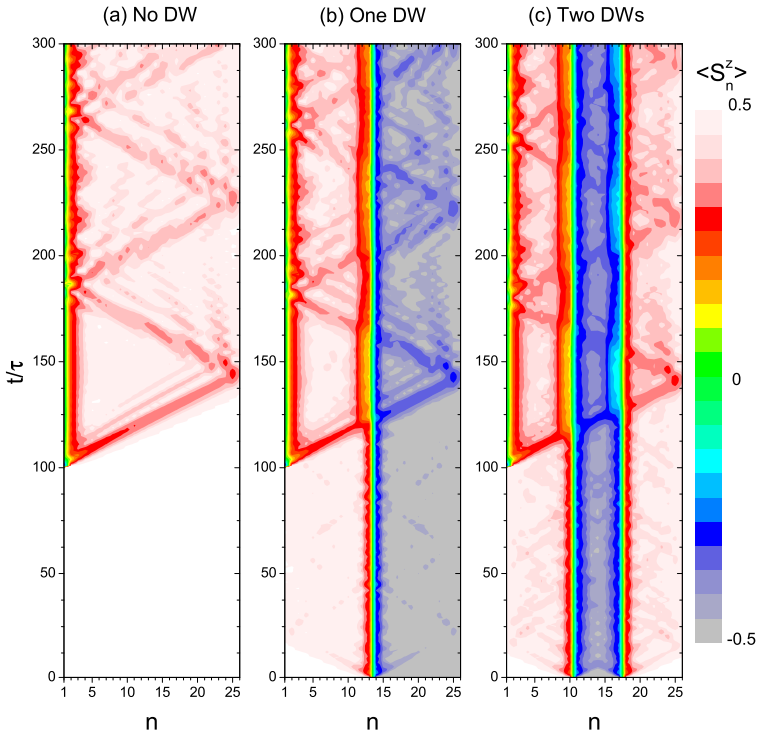

Figure 6.2: (color online) Time evolution of the magnetization $\langle S_n^z(t)\rangle$ of the Ising-like spin chain with $\lambda = 2$. The initial configuration ($t/\tau = 0$) of each panel (a,b,c) is shown in Fig. 6.1(a,b,c), respectively. At the time $t/\tau = 100$, the first spin ($n = 1$) is flipped, generating a longitudinal spin wave.

The triangular pattern in Fig. 6.2(a) merely results from the reflection of the spin flip excitation by the other edge of the chain. The triangular pattern is also present in Fig. 6.2(b), but the presence of the DW causes $\langle S_n^z(t)\rangle$ to change sign if $n > N/2$. Fig. 6.2(b) also demonstrates that the DW itself is extremely robust, even in systems with one spin flipped. A similar behavior is observed for the case of two DWs (see Fig. 6.2(c)), indicating that the change of sign at the DW is generic.

The slope of the line in Fig. 6.2 from the point $(n = 1, t/\tau = 100)$ that connects spin 1 and spin N is directly related to the velocity of the excitation. We can estimate the time of the excitation to propagate from site n to site m by analyzing the infinitely long chain. Starting from an initial state in which

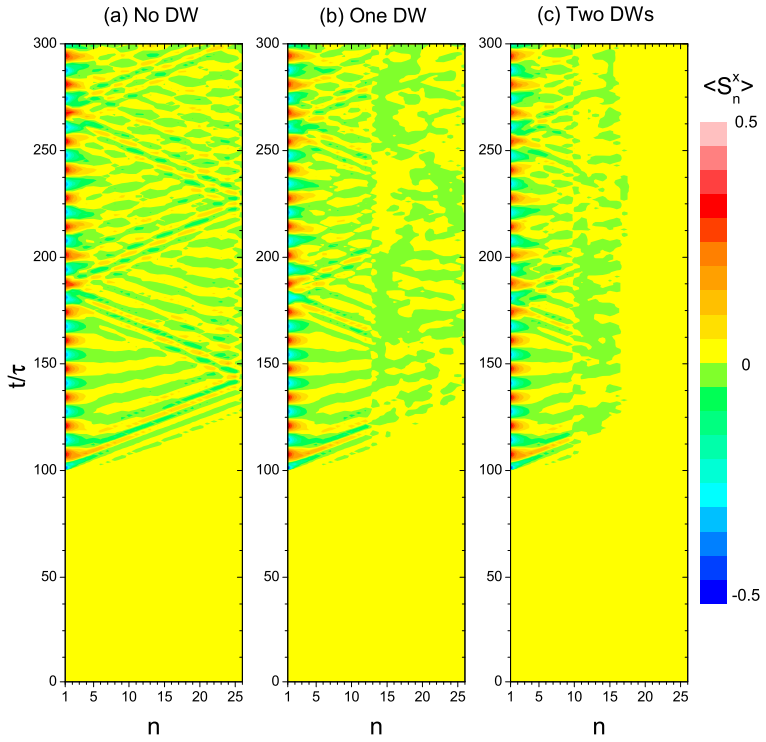

Figure 6.3: (color online) Time evolution of the transverse component $\langle S_n^x(t)\rangle$ of the magnetization, for the same cases as those shown in Fig. 6.2 except that the first spin is rotated by $\pi/2$ about the y-axis (instead of flip) at the time $t/\tau = 100$.

we flip the spin at site n, the magnetization at site m is given by

$$\langle S_m^z(t)\rangle = \lim_{N\to\infty} \frac{1}{2}\left[1 - |\langle n|e^{-itH}|m\rangle|^2\right], \tag{6.2}$$

$$= \frac{1}{2}\left[1 - 2J_{m-n}^2(Jt)\right], \tag{6.3}$$

where $|m\rangle$ denotes the ferromagnet state with a flipped spin at site m and $J_m(x)$ is the Bessel function of the first kind of order m. Although Eq.(6.3) is valid for the infinite chain only, we may expect that it provides a qualitatively correct description of the wave propagation in the finite system. Our numerical calculations (results not shown) demonstrate that for $N \geq 16$, the time for the excitation to travel from $n = 1$ to $m = 26$ agrees within 2% with the first minimum of Eq.(6.3).

Although it is clear that the longitudinal motion of the spin that results from the spin flip can easily propagate through the DW structures, quantum fluc-

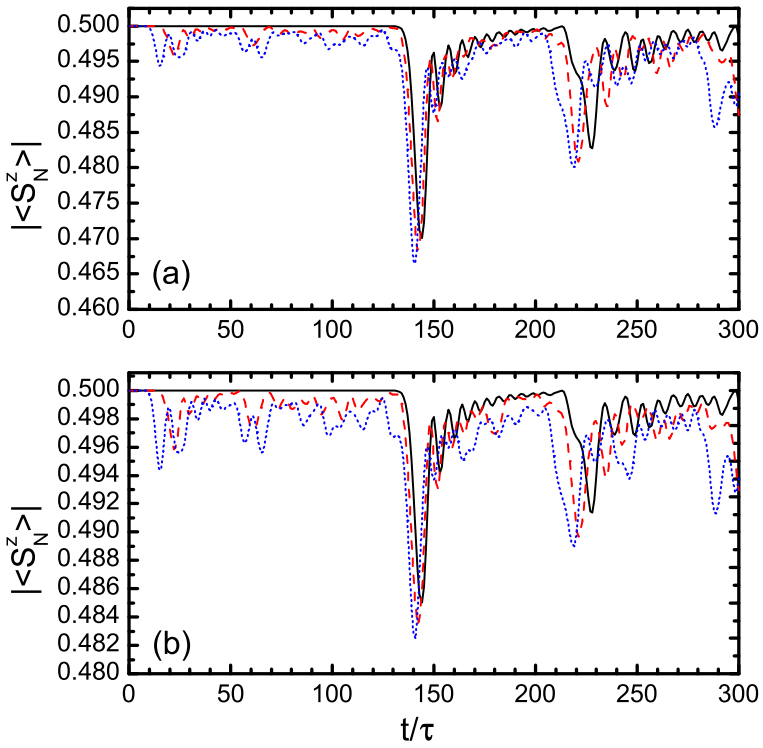

Figure 6.4: (color online) Time evolution of the magnetization $\langle S_N^z(t)\rangle$. (a) spin wave generated by flipping the first spin $\mathbf{S}_1$; (b) spin wave generated by rotating the first spin $\mathbf{S}_1$ by $\pi/2$ about the y-axis. Solid (black) line: No DW, corresponding to the spin configuration Fig. 6.1(e); Dashed (red) line: one DW, corresponding to the spin configuration Fig. 6.1(f). Because $\langle S_N^z(t)\rangle$ is negative in this case, we plot the absolute value to facilitate the comparison; Dotted (blue) line: two DWs, corresponding to the spin configuration Fig. 6.1(g). Comparison of (a) and (b) shows that the times at which the $\langle S_N^z(t)\rangle$ reaches one of the minima does not depend on method by which the spin wave is generated.

tuations reduce the amplitude of the excitation and for $t/\tau > 250$ it becomes difficult to follow the excitation in Fig. 6.2(b,c). As mentioned earlier, we could increase λ to reduce the quantum fluctuations but this does not change the qualitative features that we are interested in.

Next, we study the propagation of the transverse components, that is the x or y components of the expectation values of the spins. At $t/\tau = 100$, we excite the system by rotating the first spin in Fig. 6.1(e,f,g) by $\pi/2$ about the y-axis. After this rotation, the magnetization of spin $\mathbf{S}_1$ is parallel to the x-axis. Starting from this configuration, the time evolution will cause the first spin to rotate about the z-axis (due to the presence of the neighboring spin that is

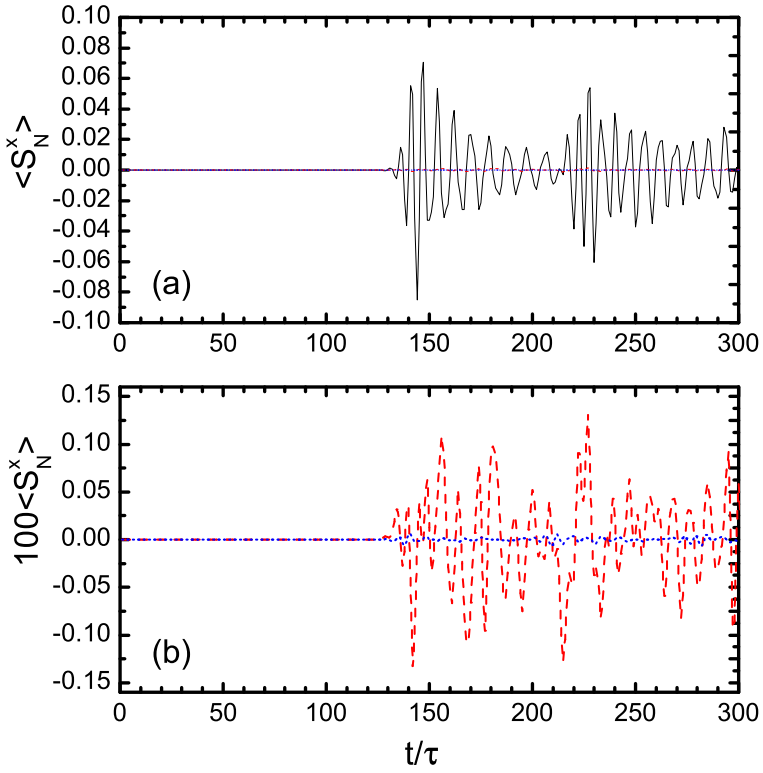

Figure 6.5: (color online) Time evolution of $\langle S_N^x(t)\rangle$ of the same system as in Fig. 6.3, plotted on two different scales. Solid (black) line: No DW, corresponding to the spin configuration Fig. 6.1(e); Dashed (red) line: One DW, corresponding to the spin configuration Fig. 6.1(f). Dotted (blue) line: Two DWs, corresponding to the spin configuration Fig. 6.1(g).

pointing in the z-direction). This then generates spin waves that contain both longitudinal $\{\langle S_n^z(t)\rangle\}$ and transverse ($\{\langle S_n^x(t)\rangle\}$, $\{\langle S_n^y(t)\rangle\}$) components.

The space-time diagram of $\langle S_n^z(t)\rangle$ looks very similar as Fig. 6.2 and therefore we do not show it. Now, we investigate the propagation of the transverse spin waves by considering one of the two components (the actual choice is irrelevant). In Fig. 6.3, we present results for the time evolution of $\langle S_n^x(t)\rangle$ for $n = 1$ to N. In the Ising-like Heisenberg chain without a DW, the transverse spin waves propagate in the same manner as the longitudinal waves. (compare Fig. 6.2(a) and Fig. 6.3(a)). However, from Fig. 6.3(b,c) it is clear that the transverse waves do not propagate through the DW structure but are reflected instead.

For a more quantitative study of the interaction of DW(s) and spin waves in

quantum spin chains, we analyze in detail, the time evolution of the rightmost spin. In Fig. 6.4 we plot $\langle S_N^z(t)\rangle$ as a function of time for the six cases depicted in Figs. 6.2 (Fig. 6.4(a)) and 6.3 (Fig. 6.4(b)).

From Fig. 6.4, we conclude that the propagation of longitudinal spin waves in the two cases is essentially the same, except for the amplitude. Rotating the first spin by $\pi/2$ (instead of π in the case of the spin flip) about the x or y axis generates waves of which the amplitude of the longitudinal component at the site N is half of that of the spin-flip case. Using Eq.(6.3) and the fact that $J_{25}(x)$ has a first maximum at $x \approx 27.4$, we find that $\langle S_{26}^z(t)\rangle$ has a minimum at $t/\tau \approx 144$. This value is in agreement with the time at which the numerical solution for the $N = 26$ chain exhibits a first dip (see black (solid) line in Fig. 6.4(a)). A first conclusion from this analysis is that the qualitative aspects of the interaction of the longitudinal spin wave excitation and the DW(s) does not depend on the transverse components of the spin wave.

Fig. 6.4 also clearly shows that the presence of a DW increases the speed at which the excitation travels through the DW. Comparing the curves for the system without DW, one DW, and two DWs, we conclude that the solid curve lags behind with respect to the dashed curve, and the dashed curve lags behind with respect to the dotted curve. Thus, the longitudinal component of the spin wave excitation is shifted forward as it passes a DW.

Fig. 6.5 shows the time evolution of $\langle S_N^x(t)\rangle$. In contrast to the longitudinal component (see Fig. 6.4), the maximum amplitude of the transverse signals strongly depend on the presence of DW(s) in the system (note the difference in scale between Fig. 6.5(a) and Fig. 6.5(b)). Thus, in the quantum system, the reflection of the transverse spin wave excitation is significantly larger than the reflection of the longitudinal component.

6.3 Summary

Finally, we point out the difference between the continuous model for mesoscale magnetic systems and the present lattice model. In the former, DWs exist as rotation of the spins according to a soliton structure, while in the microscopic quantum system, there is no structure in the transverse spin component and a DW is defined as a dynamically stable structure of the longitudinal components. We found that such DWs exists for $\lambda > 1$ whereas for $\lambda \leq 1$ they are

unstable. We also studied spin wave propagation and found that the longitudinal components of the spin wave speed up when they cross a DW. The transverse components of the spin wave are almost totally reflected by the DW, but this characteristic feature of the microscopic quantum chain is not found in mesoscopic magnetic system, where the transverse components crosse a DW without reflection and with a phase shift of $\pi/2$ [8]. It should be noted that the system described by the LLG equation is fundamentally different from the system that we consider in this Letter. The former treats the magnetic system in the mesoscopic regime as a classical, continuous medium, whereas the present study treats the magnetic system as a microscopic, quantum mechanical system. Which of these two approaches is the most suitable description obviously depends on the specific material. The change of behavior from mesoscopic to microscopic may become important as bottom-up chemical synthesis is providing new ways for further down-sizing of the magnets.

References

[1] D.A. Allwood, G. Xiong, M.D. Cooke, C.C. Faulkner, D. Atkinson, N. Vernier and R.P. Cowburn, Science **296** (2002) 2003.

[2] D. Atkinson, D.A. Allwood, G. Xiong, M.D. Cooke, C.C. Faulkner and R.P. Cowburn, Nature Materials **2** (2003) 85.

[3] E. Saitoh, H. Miyajima, T. Yamaoka and G. Tatara, Nature **432** (2004) 203.

[4] C. Charppert and T. Devolder, Nature **432** (2004) 162.

[5] K. Nakamura and T. Sasada, Phys. Lett. **48A** (1974) 321.

[6] K. Nakamura and T. Sasada, J. Phys. C: Solid State Phys. **11** (1978) 331.

[7] H.J. Mikeska, S. Miyashita and G.H. Ristow, J. Phys.: Condens. Matter **3** (1991) 2985.

[8] R. Hertel, W. Wulfhekel and J. Kirschner, Phys. Rev. Lett. **93** (2004) 257202.

[9] T. Kajiwara, M. Nakano, Y. Kaneko, S. Takaishi, T. Ito, M. Yamashita, A. Igashira-Kamiyama, H. Nojiri, Y. Ono and N. Kojima, J. Am. Chem. Soc. **127** (2005) 10150.

[10] M. Mito, H. Deguchi, T. Tajiri, S. Takagi, M. Yamashita and H. Miyasaka, Phys. Rev. B **72** (2005) 144421.

[11] H. Kageyama, K. Yoshimura, K. Kosuge, M. Azuma, M. Takano, H. Mitamura and T. Goto, J. Phys. Soc. Jpn. **66** (1997) 3996.

[12] A. Maignana, C. Michel, A.C. Masset, C. Martin and B. Raveau, Eur. Phys. J. B **15** (2000) 657.

[13] S. Bose, Phys. Rev. Lett. **9**1 (2003) 207901.

[14] T.J. Osborne and N. Linden, Phys. Rev. A **6**9 (2004) 052315.

[15] M. Christandl, N. Datta, A. Ekert and A.J. Landahl, Phys. Rev. Lett. **9**2 (2004) 187902.

[16] D.C. Mattis, *The Theory of Magnetism I*, Solid State Science Series 17 (Springer, Berlin 1981).

[17] H. Tal-Ezer and R. Kosloff, J. Chem. Phys. **8**1 (1984) 3967.

[18] C. Leforestier, R.H. Bisseling, C. Cerjan, M.D. Feit, R. Friesner, A. Guldberg, A. Hammerich, G. Jolicard, W. Karrlein, H.-D. Meyer, N. Lipkin, O. Roncero and R. Kosloff, J. Comp. Phys. **9**4 (1991) 59.

[19] T. Iitaka, S. Nomura, H. Hirayama, X. Zhao, Y. Aoyagi and T. Sugano, Phys. Rev. E**5**6 (1997) 1222.

[20] V.V. Dobrovitski and H.A. De Raedt, Phys. Rev. E**6**7 (2003) 056702.

Chapter 7

Domain Wall Dynamics near a Quantum Critical Point

This chapter was previously published as
S. Yuan, H. De Raedt, and S. Miyashita, Phys. Rev. B **75**, 184305 (2007).

Recent progress in synthesizing materials that contain ferromagnetic chains [1–4] provides new opportunities to study the quantum dynamics of atomic-size domain walls (DWs). On the atomic level, a DW is a structure that is stable with respect to (quantum) fluctuations, separating two regions with opposite magnetization. Such a structure was observed in the one-dimensional $CoCl_2 \cdot 2H_2O$ chain [5, 6].

In previous chapter, we studied the propagation of spin waves in ferromagnetic quantum spin chains that support DWs. We demonstrated that DWs are very stable against perturbations, and that the longitudinal component of the spin wave speeds up when it passes through a DW while the transverse component is almost completely reflected.

In this chapter, we focus on the dynamic stability of the DW in the Heisenberg-Ising ferromagnetic chain. It is known that the ground state of this model in the subspace of total magnetization zero supports DW structures [8, 9]. However, if we let the system evolve in time from an initial state with a DW structure and this initial state is not an eigenstate, it must contain some excited states. Therefore, the question whether the DW structure will survive in the stationary (long-time) regime is nontrivial.

The question how the DW structure dynamically survives in the stationary (long-time) region is an interesting problem. In particular, we focus on the stability of the DW with respect to the dynamical (quantum) fluctuations as we approach the quantum critical point (from Heisenberg-Ising like to Heisenberg). We show that the critical quantum dynamics of DWs can be described well in terms of conventional power laws. The behavior of quantum systems at or near a quantum critical point is of contemporary interest [10]. We also show that the DW profiles rapidly become very stable as we move away from the quantum critical point.

7.1 Model

The Hamiltonian of the system is given by [8, 9, 11–13]

$$H = -J \sum_{n=1}^{N-1} (S_n^x S_{n+1}^x + S_n^y S_{n+1}^y + \Delta S_n^z S_{n+1}^z), \tag{7.1}$$

where N indicates the total number of spins in the spin chain, and the exchange integrals J and $J\Delta$ determine the strength of the interaction between the x, y and z components of spin 1/2 operators $\mathbf{S}_n = (S_n^x, S_n^y, S_n^z)$. Here we only consider the system with the ferromagnetic ($J > 0$) nearest exchange interaction. It is well known that $|\Delta| = 1$ is a quantum critical point of the Hamiltonian in Eq.(7.1), that is, the analytical expressions of the ground state energy for $1 < \Delta$ and $-1 < \Delta < 1$ are different and singular at the points $\Delta = \pm 1$ [12].

In Ref. [8, 9] Gochev constructed a stable state with DW structure in both the classical and quantum treatments of the Hamiltonian (7.1). In the classical treatment, Gochev replaces the spin operators in Eq.(7.1) by classical vectors of length s

$$S_n^z = s\cos\theta_n, S_n^x = s\sin\theta_n\cos\varphi_n, S_n^y = s\sin\theta_n\sin\varphi_n,$$

and then uses the conditions $\delta E/\delta\theta = 0$ and $\varphi_n = const.$ to find the ground state. In the ground state, the magnetization per site is given by [9]

$$\begin{aligned} S_n^z &= s\tanh(n-n_0)\sigma, \\ S_n^x &= s\cos\varphi\ \mathrm{sech}(n-n_0)\sigma, \\ S_n^y &= s\sin\varphi\ \mathrm{sech}(n-n_0)\sigma, \end{aligned} \tag{7.2}$$

where

$$\sigma = \ln[\Delta + \sqrt{\Delta^2 - 1}], \tag{7.3}$$

φ is an arbitrary constant, and n_0 is a constant fixing the position of the DW. The corresponding energy is

$$E_{DW} = 2s^2 J\Delta\tanh\sigma. \tag{7.4}$$

In the quantum mechanical treatment, Gochev first constructs the eigenfunction of a bound state of k magnons [9]

$$|\psi_k\rangle = A_n \sum_{\{m_l\}} B_{m_1 m_2 \ldots m_k} S^-_{m_1} S^-_{m_2} \ldots S^-_{m_k} |0\rangle\,, \tag{7.5}$$

where

$$B_{m_1 m_2 \ldots m_k} = \prod_{i=1}^{k} v_i^{m_i}, m_i < m_{i+1}, \tag{7.6}$$

$$v_i = \cosh(i-1)\sigma/\cosh(i\sigma), \tag{7.7}$$

$$A^{-2} = \prod_{i=1}^{k} v_i^{2i}/(1-v_i^2), \tag{7.8}$$

and the corresponding energy is given by [9]

$$\epsilon_k = \frac{1}{2} J\Delta\tanh\sigma\tanh k\sigma. \tag{7.9}$$

Then he demonstrated that for the infinite chain, the linear superposition

$$|\phi_{n_0}\rangle = A \sum_{i=-\infty}^{\infty} \exp\left\{-\frac{1}{2}\sigma\left[i + \left(\frac{1}{2} - \alpha\right)\right]\right\} |\psi_{N_0+i}\rangle\,, \tag{7.10}$$

where

$$n_0 = N_0 + \alpha, |\alpha| \le 1/2, N_0 \to \infty, \tag{7.11}$$

$$A^{-2} = \sum_{i=-\infty}^{\infty} \exp\left\{-\frac{1}{2}\sigma\left[i + \left(\frac{1}{2} - \alpha\right)\right]^2\right\}, \tag{7.12}$$

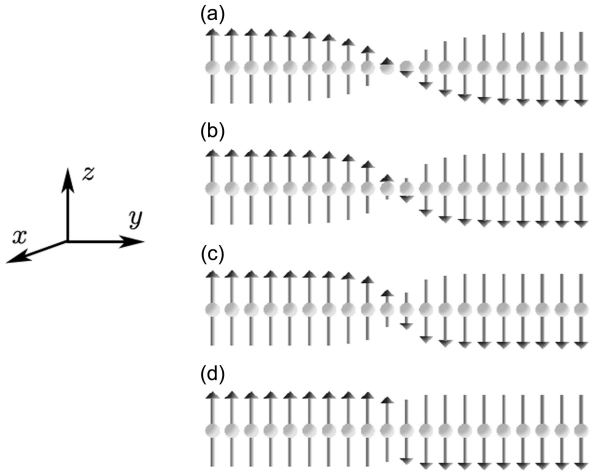

Figure 7.1: The magnetization $\langle S_n^z \rangle$ in the ground state of the subspace of total magnetization $M = 0$, generated by the power method. The parameters are: (a) $\Delta = 1.05$, (b) $\Delta = 1.1$, (c) $\Delta = 1.2$, (d) $\Delta = 2$. The total number of spins in the spin chain is $N = 20$. It is clear that there is a DW at the centre of the spin chain. Furthermore there is no structure in the XY plane, that is, $\langle S_n^x \rangle = \langle S_n^y \rangle = 0$.

is the quantum analog of the classical domain wall, in which $\langle S_n^z \rangle, \langle S_n^x \rangle, \langle S_n^y \rangle$ are given in Eq.(7.2), and the energy coincides with Eq.(7.4).

Gochev's work confirmed the existence of the DW structures in the one-dimensional ferromagnetic quantum spin 1/2 chain. In the infinite chain, the exact quantum analog of classical DW is represented by $|\phi_{n_0}\rangle$. In the finite chain, the DW structure exists as a bound k-magnon state $|\psi_k\rangle$. The main difference between these two states is the distribution of magnetization in the XY plane. In the infinite chain, the change of the magnetization occurs in three dimensions, according to Eq.(7.2), but in the finite chain $\langle S_n^x \rangle = \langle S_n^y \rangle = 0$ for all spins.

Now we consider $\langle S_n^z \rangle$ of the bound state $|\psi_k\rangle$ in the case that the number of flipped spin is half of the total spins, i.e., $k = N/2$ and N is an even number. Even though the formal expression for $|\psi_k\rangle$ is known, the expression for $\langle S_n^z \rangle$ in this state (for finite and infinite chains) is not known. For finite N, the ground state in the subspace of total magnetization $M = 0$ can, in principle, be calculated from Eq.(7.5). However, this requires a numerical procedure and we loose the attractive features of the analytical approach. Indeed, it is more efficient to use a numerical method and compute directly the ground

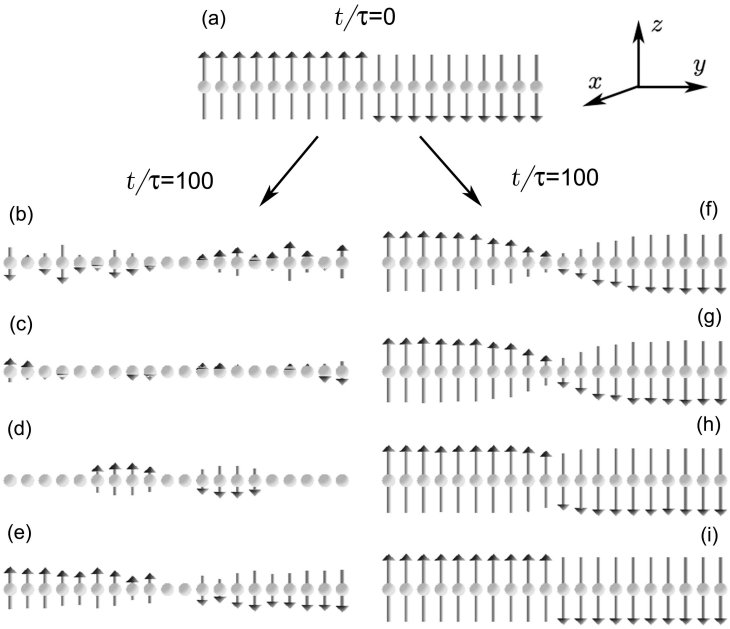

Figure 7.2: Top picture (a): Initial spin configuration at time $t/\tau = 0$; Bottom pictures (b,c,d,e,f,g,h,i): Spin configuration at time $t/\tau = 100$; Bottom left pictures (b,c,d,e): DW structures disappear or are not stable. The parameters are: (b) $\Delta = 0$ (XY model), (c) $\Delta = 0.5$ (Heisenberg-XY model), (d) $\Delta = 1$ (Heisenberg model), (e) $\Delta = 1.05$ (Heisenberg-Ising model); Bottom right pictures (f,g,h,i): DW structures are dynamically stable in the Heisenberg-Ising model. The parameters are: (f) $\Delta = 1.1$, (g) $\Delta = 1.2$, (h) $\Delta = 2$, (i) $\Delta = 20$. The total number of spins in the spin chain is $N = 20$.

state in the subspace of total magnetization $M = 0$. In Fig. 7.1, we show some representative results as obtained by the power method [14] for a chain of $N = 20$ spins. In all cases, the domain wall is well-defined. Obviously, because we are considering the system in the ground state, the magnetization profile will not change during the time evolution.

In fact, a DW can simply be introduced in the spin chain by letting half of the spins up and the other half down (see Fig. 7.2(a) for $N = 20$). This cluster state ($|\Phi\rangle$) contributes mostly in the bound state $|\psi_k\rangle$ with $k = N/2$, because $|B_{m_1 m_2 ... m_k}|^2$ reaches the maximum if $m_i = i$ for all $i = 1, 2, .., N/2$ (note $|v_i| < 1$). It is clear that $|\Phi\rangle$ is not an eigenstate of the Hamiltonian in Eq.(7.1). The relative energy of $|\Phi\rangle$ to the ferromagnetic ground state is $J\Delta/2$, and the spread $\left(\left\langle \Phi \left| H^2 \right| \Phi \right\rangle - \left\langle \Phi \left| H \right| \Phi \right\rangle^2\right)^{1/2} = J/2$, so the relative

Table 7.1: ϵ_k is the relative energy of the ground state in the subspace of total magnetization $M = 0$ (see Fig. 7.1), and $E = J\Delta/2$ is the relative energy of the initial state $|\Phi\rangle$ (see Fig. 7.2(a)), which is the same for different N, and conserved during the time evolution.

Δ	E	ϵ_k $(N = 18)$	ϵ_k $(N = 20)$	ϵ_k $(N = 22)$
1.01	0.505	0.042	0.046	0.050
1.05	0.525	0.148	0.149	0.150
1.1	0.55	0.219	0.219	0.219
2	1	0.856	0.856	0.856
5	2.5	2.439	2.439	2.439

spread is $1/\Delta$. The dynamics of the DW in $|\Phi\rangle$ is still unknown.

In Table 7.1, we list some representative values of the energy in the ground state of subspace $M = 0$ (see Fig. 7.1) and in the initial state (see Fig. 7.2(a)) for a chain of $N = 18, 20$ and 22 spins. For $\Delta \simeq 1$, the difference in energy is sufficiently large, indicating that near the quantum critical point, the initial state contains a significant amount of excited states, it is not longer evident that the DW structure will survive in the long-time regime, so we need computer simulation to explore the dynamics of the DW, and by solving the time dependent Schrödinger equation (TDSE), we can easily see if the DW is dynamically stable or not.

7.2 Dynamically Stable Domain Walls

We solve the TDSE of the whole system with the Hamiltonian in Eq.(7.1) and study the time-evolution of the magnetization at each lattice site. The numerical solution of the TDSE is performed by the Chebyshev polynomial algorithm, which is known to yield extremely accurate independent of the time step used [15–18]. We adopt open boundary conditions, not periodic boundary conditions, because the periodic boundary condition would introduce two DWs in the initial state. In this chapter, we display the results at time intervals of $\tau = \pi/5J$, and use units such that $\hbar = 1$ and $J = 1$.

The initial state of the system is shown in Fig. 7.2(a). The spins in the left part ($n = 1$ to 10) of the spin chain are all "spin-up" and the rest ($n = 11$ to 20) are all "spin-down". Here "spin-up" or "spin-down" correspond to the

eigenstates of the single spin 1/2 operator S_n^z.

Whether the DW at the centre of the spin chain is stable or unstable depends on the value of Δ. In Fig. 7.2(b,c,d,e,f,g,h, and i), we show the states of the system as obtained by letting the system evolve over a fairly long time ($t = 500J/\pi$). It is clear that the DW totally disappears for $0 \leq \Delta \leq 1$, that is, in the XY, Heisenberg-XY and Heisenberg spin 1/2 chain, the DW structures are not stable. For the Heisenberg-Ising model ($\Delta > 1$), the DW remains stable when $t \geq 500J/\pi$ (see Ref. [7]), and its structure is more sharp and clear if Δ is larger, so we will concentrate on the cases $\Delta > 1$. One may note that the values of Δ in Fig. 7.2(e,f,g,h) are the same as in Fig. 7.1(a,b,c,d), but that the distributions of the magnetization are similar but not the same. This is because the energy is conserved during the time evolution and the system, which starts from the initial state shown in Fig. 7.2(a), will never relax to the ground state of the subspace with the total magnetization $M = 0$.

In order to get a quantitative expression of the width of DW, we first introduce quantity $\overline{S_n^z(t_1, t_2; \Delta)}$ ($n = 1, 2, ..., N$) as the time average of the expectation value $\langle S_n^z(t) \rangle$ of nth spin:

$$\overline{S_n^z(t_1, t_2; \Delta)} \equiv \frac{\int_{t_1}^{t_2} \langle S_n^z(t) \rangle \, dt}{t_2 - t_1}. \tag{7.13}$$

We take the average in Eq.(7.13) over a long period during which the DW is dynamically stable. In Fig. 7.3, we show some results of $\overline{S_n^z(t_1, t_2; \Delta)}$ for the Heisenberg-Ising model, where we take $t_1 = 101\tau$, $t_2 = 200\tau$ and various Δ. We find that each curve in Fig. 7.3 is symmetric about the line $n = (N+1)/2$, and can be fitted well by the function

$$\overline{S_n^z(t_1, t_2; \Delta)} \simeq a_\Delta \tanh\left[\frac{n - (N+1)/2}{b_\Delta}\right]. \tag{7.14}$$

The values of Δ we used and the corresponding values of a_Δ, b_Δ are shown in Table 7.2. As we mentioned earlier, Gochev [9] constructed an eigenstate of the one-dimensional anisotropic ferromagnetic spin 1/2 chain in which the mean values S_n^z, S_n^x and S_n^y coincide with the stable DW structure in the classical spin chain, that is

$$\langle S_n^z \rangle = \frac{1}{2} \tanh(n - n_0)\sigma, \tag{7.15}$$

where n_0 is the position of the DW (in our notation, this is $(N+1)/2$). The fitted form of $\overline{S_n^z(t_1, t_2; \Delta)}$ in Eq.(7.14) is similar to Eq.(7.15). From Table

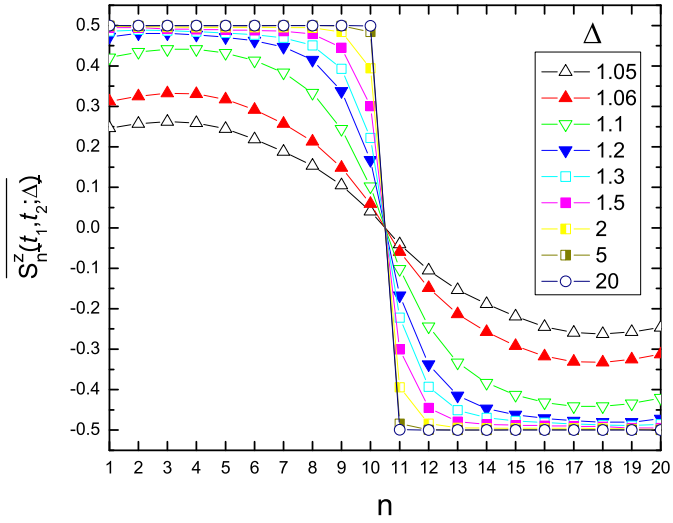

Figure 7.3: (Color online) $\overline{S_n^z(t_1,t_2;\Delta)}$ as a function of n for different Δ. Here $t_1 = 101\tau$, $t_2 = 200\tau$. We show the data for $\Delta = 1.05, 1.06, 1.1, 1.2, 1.3, 1.5, 2, 5$ and 20 only. The total number of spins in the spin chain is $N = 20$.

7.2, it is clear that as Δ increases, $|a_\Delta|$ converges to $1/2$, in agreement with Eq.(7.15). From the comparison of b_Δ and $1/\sigma$ in Fig. 7.4, it is clear that the dependence on Δ is qualitatively similar but not the same. This is due to the fact that Gochev's solution is for a DW in the ground state whereas we obtain the DW by relaxation of the state shown in Fig. 7.2(a).

We want to emphasize that the meaning of $\overline{S_n^z(t_1,t_2;\Delta)}$ in Eq.(7.14) is different from $\langle S_n^z\rangle$ in Eq.(7.15). The former describes the mean value of $\langle S_n^z(t)\rangle$ in a state with dynamical fluctuations, while the latter describes the distribution of $\langle S_n^z\rangle$ in an exact eigenstate without dynamical fluctuations.

Next we introduce a definition of the DW width. From Eq.(7.14), we can find n_1 and n_2 which satisfy

$$\begin{aligned}\overline{S_{n_1}^z(t_1,t_2;\Delta)} &= 1/4,\\ \overline{S_{n_2}^z(t_1,t_2;\Delta)} &= -1/4,\end{aligned} \tag{7.16}$$

that is, when $\left|\overline{S_n^z(t_1,t_2;\Delta)}\right|$ equals half of its maximum value (1/2). Here n_1 and n_2 are not necessarily integer numbers. Now we can define the DW width

Table 7.2: The values of Δ we used in our simulations and the corresponding a_Δ, b_Δ fitted by Eq.(7.14) for a spin chain of $N = 20$ spins.

Δ	a_Δ	b_Δ	Δ	a_Δ	b_Δ
1.05	−0.263	3.659	1.8	−0.493	0.524
1.06	−0.330	3.171	1.9	−0.494	0.488
1.07	−0.377	2.850	2	−0.495	0.460
1.08	−0.406	2.673	2.1	−0.495	0.436
1.09	−0.424	2.534	2.2	−0.496	0.416
1.1	−0.435	2.396	2.5	−0.497	0.370
1.15	−0.462	1.996	3	−0.498	0.322
1.2	−0.471	1.626	4	−0.499	0.270
1.25	−0.476	1.330	5	−0.499	0.240
1.3	−0.479	1.142	6	−0.500	0.220
1.35	−0.481	0.959	7	−0.500	0.206
1.4	−0.483	0.869	8	−0.500	0.195
1.45	−0.485	0.770	9	−0.500	0.187
1.5	−0.487	0.719	10	−0.500	0.179
1.6	−0.489	0.629	15	−0.500	0.156
1.7	−0.491	0.568	20	−0.500	0.141

Table 7.3: The values of ϵ_N, A_N and B_N in Eq.(7.18) for a spin chain of $N = 16$, 18, 20, 22 and 24 spins. For the fit, we used all the data for $\Delta \leq 5$.

N	ϵ_N	A_N	B_N
16	0.065 ± 0.001	2.08 ± 0.10	-0.493 ± 0.142
18	0.052 ± 0.002	2.07 ± 0.11	-0.450 ± 0.152
20	0.045 ± 0.002	2.22 ± 0.09	-0.556 ± 0.133
22	0.040 ± 0.001	2.36 ± 0.08	-0.689 ± 0.140
24	0.033 ± 0.001	2.34 ± 0.06	-0.681 ± 0.127

W as the distance between n_1 and n_2:

$$W = |n_1 - n_2| \,. \tag{7.17}$$

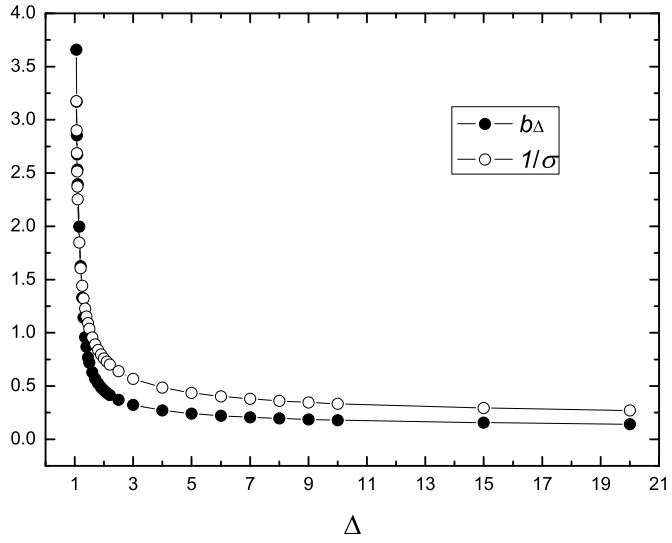

Figure 7.4: Compare of b_Δ and $1/\sigma$ as a function of Δ. The total number of spins in the spin chain is $N = 20$.

Clearly, the width of the DW becomes ill-defined if it approaches the size of the chain. On the other hand, the computational resources (mainly memory), required to solve the TDSE, grow exponentially with the number of spins in the chain. These two factors severely limit the minimum distance $\Delta - 1$ to the quantum critical point $\Delta = 1$ that yields meaningful results for the width of the DW. Indeed, for fixed N, Δ has to be larger than the "effective" critical value for the finite system in order for the DW width to be smaller than the system size. Although the system sizes that are amenable to numerical simulation are rather small for present-day "classical statistical mechanics" standards, it is nevertheless possible to extract from these simulations useful information about the quantum critical behavior of the dynamically stable DW.

In Fig. 7.5, we plot W as a function of Δ ($1.06 \leq \Delta \leq 20$). By trial and error, we find that all the data can be fitted very well by the function

$$W(\Delta) = \frac{A_N}{\ln\left\{\Delta - \epsilon_N + \left[(\Delta - \epsilon_N)^2 - 1\right]^{1/2}\right\}} + B_N, \tag{7.18}$$

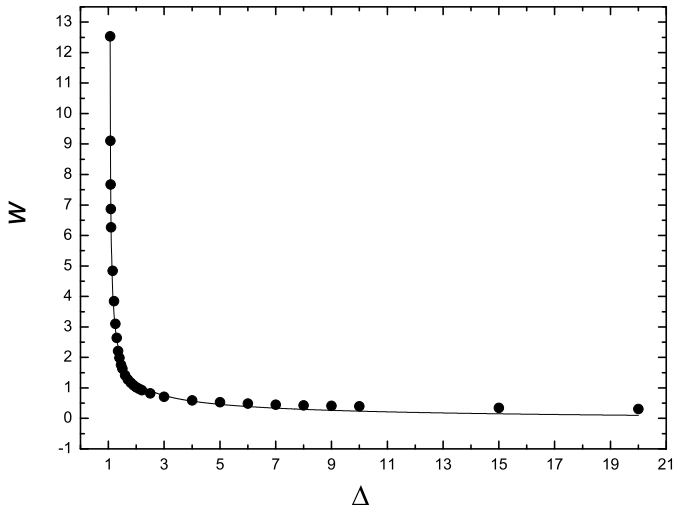

Figure 7.5: The DW width as a function of Δ in a spin chain of $N = 20$ spins. The black dots are the simulation data and the solid line is given by $W(\Delta) = A_N / \ln\left\{\Delta - \epsilon_N + \left[(\Delta - \epsilon_N)^2 - 1\right]^{1/2}\right\} + B_N$ with $\epsilon_N = 0.046 \pm 0.001$, $A_N = 2.16 \pm 0.06$ and $B_N = -0.485 \pm 0.068$.

where ϵ_N, A_N and B_N are fitting parameters. As shown in Fig. 7.6, all the data for $N = 16$, 18, 22, 24 and $\Delta \leq 5$ fit very well to Eq.(7.18). The results of these fits are collected in Table 7.3.

As an check on the fitting procedure, we apply it to the data obtained by solving for the ground state in the $M = 0$ subspace. In view of Eq.(7.13) and (7.14), we may expect that Eq.(7.18) fits the data very well and, as shown in Fig. 7.7, this is indeed the case.

To analyze the finite-size dependence in more detail, we adopt the standard finite-size scaling hypothesis [19]. We assume that in the infinite system, the DW width plays the role of the correlation length, that is, we assume that

$$W(\Delta) \sim W_0(\Delta - 1)^{-\nu}. \tag{7.19}$$

This assumption is supported by the results of Gochev [9] for the ground state for which, from Eq.(7.15), it follows that $\nu = 1/2$. If we identify Δ in the quantum system with the temperature, finite-size scaling predict that the effective critical value Δ_N^* scales as

$$\Delta_N^* \sim 1 + \lambda N^{-1/\nu}, \tag{7.20}$$

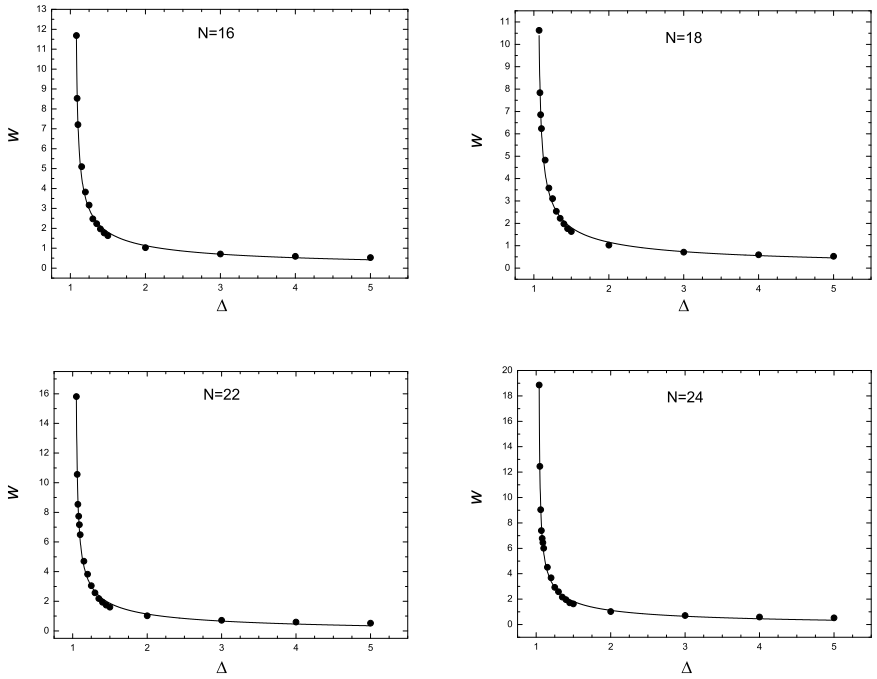

Figure 7.6: The DW width as a function of Δ in a spin chain of $N = 16$, 18, 22, and 24 spins. The black dots are the simulation data and the solid line in each panel is given by Eq.(7.18).

where λ is a model-dependent constant [19]. In Fig. 7.8, we present the results of a fit of all our numerical data to

$$\Delta_N^* = 1 + \epsilon_N \simeq \Delta^* + \lambda N^{-1/\nu}, \tag{7.21}$$

and conclude that the fit is consistent with both the exponent $\nu = 1/2$, and $\Delta^* \sim 1$.

Still considering the finite-size dependence in our model, although the width of the DW as a function of Δ cannot be expressed by Eq.(7.19), it can be fitted well to

$$W(\Delta) = W_0 (\Delta - \Delta_N^*)^{-C}. \tag{7.22}$$

To find the exponent C, we fix the number of spins in the system and fit the DW width as Eq.(7.22) for $\Delta \in [1.06, \Delta_{\max}]$ with different $\Delta_{\max}$. For $N = 20$, the results are shown in Fig. 7.9, from which we can see that as $\Delta_{\max}$ changes

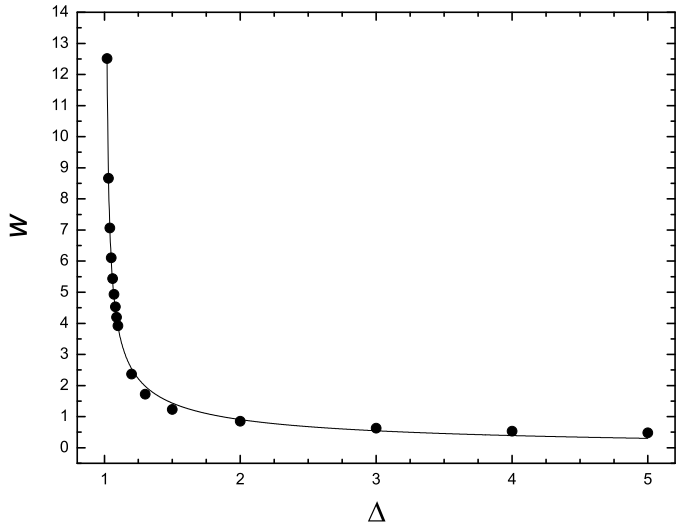

Figure 7.7: The DW width as a function of Δ ($1.06 \leq \Delta \leq 20$) in the ground state of subspace $M = 0$ in a spin chain of $N = 20$ spins. The black dots are the simulation data and the solid line is given by Eq.(7.18), with $\epsilon_N = 0.010 \pm 0.001$, $A_N = 1.87 \pm 0.04$ and $B_N = -0.550 \pm 0.079$.

from 20 to 1.2, the value of C decreases from 0.57 to 0.51, that is, if Δ is close to critical point, then $C \to \nu = 1/2$.

7.3 The Stability of Domain Walls

To describe the stability of the DW structure, we introduce $\delta_n(\Delta)$ ($n = 1, 2, ..., N$):

$$\delta_n(\Delta) = \sqrt{\overline{\left[S_n^z(t_1, t_2; \Delta)\right]^2} - \overline{S_n^z(t_1, t_2; \Delta)}^2}, \tag{7.23}$$

where

$$\overline{\left[S_n^z(t_1, t_2; \Delta)\right]^2} \equiv \frac{\int_{t_1}^{t_2} \langle S_n^z(t)\rangle^2 \, dt}{t_2 - t_1}. \tag{7.24}$$

In order to show the physical meaning of δ_n, we write $\langle S_n^z(t)\rangle$ as

$$\langle S_n^z(t)\rangle \equiv C_n + \Omega_n(t), \tag{7.25}$$

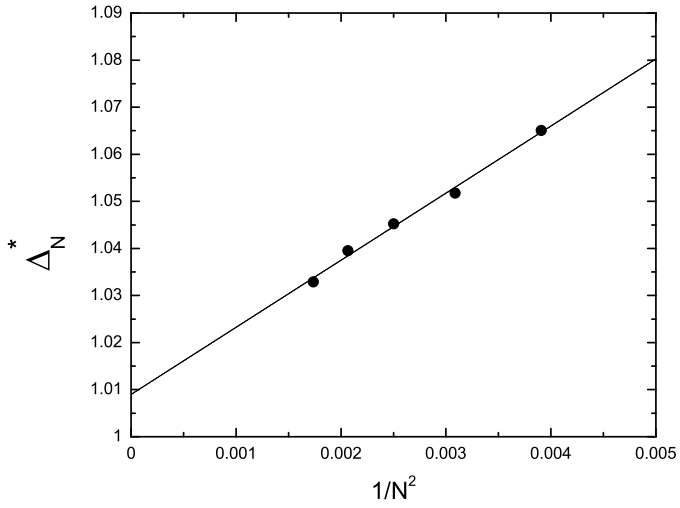

Figure 7.8: Fit of Δ_N^* to $\Delta^* + \lambda \cdot N^{-2}$ with $\Delta^* = 1.009 \pm 0.002$, and $\lambda = 14.253 \pm 0.660$.

where C_n is a constant and $\Omega_n(t)$ is a time-dependent term. Then Eq.(7.23) becomes

$$\delta_n(\Delta) = \left\{ \frac{\int_{t_1}^{t_2} \Omega_n^2(t)\, dt}{t_2 - t_1} - \left[\frac{\int_{t_1}^{t_2} \Omega_n(t)\, dt}{t_2 - t_1} \right]^2 \right\}^{1/2}. \tag{7.26}$$

It is clear that if $\langle S_n^z(t) \rangle$ is a constant in the time interval $[t_1, t_2]$, then $\delta_n(\Delta) = 0$. In general, since the initial state is not an eigenstate of the Hamiltonian Eq.(7.1), the magnetization of each spin will fluctuate and $\Omega_n(t) \neq 0$. If, after long time, the system relaxes to a stationary state that contains a DW, the magnetization of each spin will fluctuate around its stationary value C_n. The fluctuations are given by $\Omega_n(t)$. If $|\Omega_n(t)|$ is large, the difference between the actual magnetization profile at time t and the stationary profile C_n may be large. From Eq.(7.26), it is clear that $\delta_n(\Delta)$ is a measure of the deviation of $\langle S_n^z(t) \rangle$ from its stationary value C_n, averaged over the time interval $[t_1, t_2]$. Thus, $\delta_n(\Delta)$ gives direct information about the dynamics stability of the DW.

Figure 7.10 shows the distribution $\delta_n(\Delta)$ for different values of Δ. We only show some typical results, as in Fig. 7.3. As expected, the distribution of $\delta_n(\Delta)$ is symmetric about the centre of the spin chain ($n = 10.5$).

We first consider how $\delta_n(\Delta)$ changes with Δ for fixed n. From Fig.7.10, we

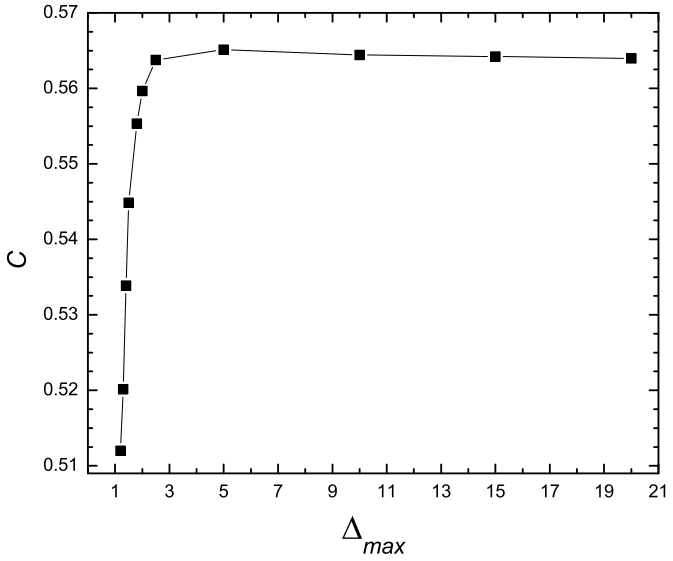

Figure 7.9: The exponent C as a function of $\Delta_{\max}$ in a spin chain of $N = 20$ spins. The exponent C obtained by fitting the DW width to Eq.(7.22), with $\Delta^*_{N=20} = 1.045$ and Δ in the range $[1.06, \Delta_{\max}]$.

conclude the following:

1) For the spins which are not located at the DW centre, i.e., $n \neq 10, 11$, $\delta_n(\Delta)$ decreases if Δ becomes larger. This means that the quantum fluctuations of these spins become smaller if we increase the value of Δ. This is reasonable because with increasing Δ, the initial state approaches an eigenstate of the Hamiltonian for which $\delta_n(\Delta) = 0$ (Ising limit).

2) For the spins at the DW centre, i.e., $n = 10, 11$, when Δ becomes larger and larger, $\delta_n(\Delta)$ first increases and then decreases. Qualitatively, this can be understood in the following way. When Δ is close to 1, the magnetization at the DW centre disappears very fast and remains zero. However, if $\Delta >> 1$, the magnetization at the DW centre will retain its initial direction, hence the behavior of the spin at the DW centre will qualitatively change as Δ moves away from the critical point $\Delta = 1$. In Fig. 7.11, we plot $\delta_{10}(\Delta)$ $(= \delta_{11}(\Delta))$ as a function of Δ. It is clear that $\delta_{10}(\Delta)$ first increases as Δ increases, reaches its maximum at $\Delta = 1.3$, and then decreases as Δ becomes larger.

Now we consider the n-dependence of $\delta_n(\Delta)$ for fixed Δ. Since $\delta_n(\Delta)$ is a

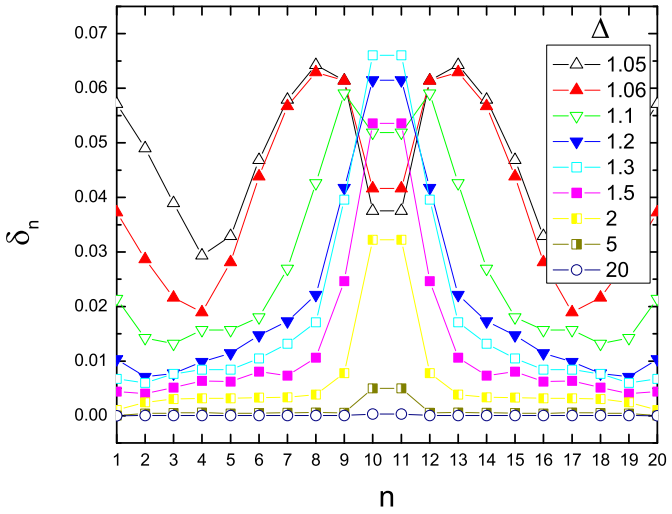

Figure 7.10: (Color online) $\delta_n(\Delta)$ as a function of n for different Δ. Here $t_1 = 101\tau$, $t_2 = 200\tau$. We only show the data for $\Delta = 1.05, 1.06, 1.1, 1.2, 1.3, 1.5, 2, 5$ and 20. The total number of spins in the spin chain is $N = 20$.

symmetric function of n, we may consider only one side of the whole chain, e.g., the spins with $n = 1, 2, ..., N/2$. From Fig.7.10, according to the value of Δ, there are three different regions:

1) $1.05 \leq \Delta \leq 1.3$: starting from the boundary ($n = 1$), $\delta_n(\Delta)$ first decreases, then increases, and finally decreases again as n approaches the DW centre ($n = 10$). As we discussed already, the fluctuation of the magnetization at the DW centre is small when Δ is close to 1. The spin at the boundary only interacts with one nearest spin, so it has more freedom to fluctuate. For the others, because of the influence of the DW structure (or boundary), the fluctuations of the spins which are near the DW (or near the boundary) are larger compared to those of a spin located in the middle of a polarized region. Thus $\delta_n(\Delta)$ is larger if the spin is located near the DW or near a boundary.

2) $1.3 \leq \Delta \leq 5$: $\delta_n(\Delta)$ reaches its maximum at the DW centre. The reason for this is that in this regime the magnetizations of all spins retain their initial direction, therefore the spins that are far from the centre fluctuate little.

3) $5 < \Delta$: in this regime (Ising limit), the initial state is very close to the eigenstate, and the fluctuations are small, even for the spins at the DW.

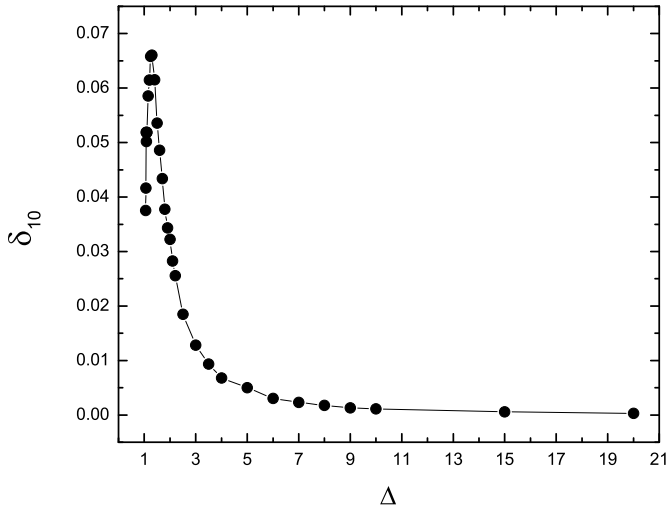

Figure 7.11: $\delta_{10}(\Delta)$ as a function of Δ. Here $t_1 = 101\tau$, $t_2 = 200\tau$. The total number of spins in the spin chain is $N = 20$.

7.4 Summary

In the presence of Ising-like anisotropy, DWs in a ferromagnetic spin 1/2 chain are dynamically stable over extended periods of time. The profiles of the magnetization of the DW are different from the profile in the ground state in the subspace of total magnetization $M = 0$. As the system becomes more isotropic, approaching the quantum critical point, the width of the DW increases as a power law, with an exponent equals to 1/2.

References

[1] T. Kajiwara, M. Nakano, Y. Kaneko, S. Takaishi, T. Ito, M. Yamashita, A. Igashira-Kamiyama, H. Nojiri, Y. Ono and N. Kojima, J. Am. Chem. Soc. **127** 10150 (2005).

[2] M. Mito, H. Deguchi, T. Tajiri, S. Takagi, M. Yamashita and H. Miyasaka, Phys. Rev. B **72**, 144421 (2005).

[3] H. Kageyama, K. Yoshimura, K. Kosuge, M. Azuma, M. Takano, H. Mitamura and T. Goto, J. Phys. Soc. Jpn. **66**, 3996 (1997).

[4] A. Maignana, C. Michel, A.C. Masset, C. Martin and B. Raveau, Eur. Phys. J. B **15**, 657 (2000).

[5] J. Torrance and M. Tinkham, Phys. Rev. **187**, 587 (1969).

[6] D. Nicoli and M. Tinkham, Phys. Rev. B **9**, 3126 (1974).

[7] S. Yuan, H. De Raedt, and S. Miyashita, J. Phys. Soc. Jpn., **75**, 084703 (2006).

[8] I.G. Gochev, JETP Lett. **26**, 127 (1977).

[9] I.G. Gochev, Sov. Phys. JETP **58**, 115 (1983).

[10] S. Sachdev, *Quantum Phase Transitions*, (Cambridge University Press, Cambridge, 1999).

[11] H.J. Mikeska, S. Miyashita and G.H. Ristow, J. Phys.: Condens. Matter **3**, 2985 (1991).

[12] J. des Cloizeaux and M. Gaudin, J. Math. Phys. **7**, 1384 (1966).

[13] D.C. Mattis, *The Theory of Magnetism I*, Solid State Science Series 17 (Springer, Berlin 1981).

[14] J.H. Wilkinson, *The Algebraic Eigenvalue Problem*, (Oxford University Press, Oxford, 1999).

[15] H. Tal-Ezer and R. Kosloff, J. Chem. Phys. **81**, 3967 (1984).

[16] C. Leforestier, R.H. Bisseling, C. Cerjan, M.D. Feit, R. Friesner, A. Guldberg, A. Hammerich, G. Jolicard, W. Karrlein, H.-D. Meyer, N. Lipkin, O. Roncero and R. Kosloff, J. Comp. Phys. **94**, 59 (1991).

[17] T. Iitaka, S. Nomura, H. Hirayama, X. Zhao, Y. Aoyagi and T. Sugano, Phys. Rev. E**56**, 1222 (1997).

[18] V.V. Dobrovitski and H.A. De Raedt, Phys. Rev. E**67** , 056702 (2003).

[19] D.P. Landau and K. Binder, *A Guide to Monte Carlo Simulations in Statistical Physics*, (Cambridge University Press, Cambridge, 2000).

Appendix A

Correlation and Concurrence

We define the correlation function as $\langle \mathbf{S}_1 \cdot \mathbf{S}_2 \rangle$. In order to show the relation between the correlation function and the state of the two-spin system, we denote a general state in the standard basis ($|\uparrow\rangle|\uparrow\rangle$, $|\uparrow\rangle|\downarrow\rangle$, $|\downarrow\rangle|\uparrow\rangle$, $|\downarrow\rangle|\downarrow\rangle$) as

$$|\psi\rangle = a_1|\uparrow\rangle|\uparrow\rangle + a_2|\uparrow\rangle|\downarrow\rangle + a_3|\downarrow\rangle|\uparrow\rangle + a_4|\downarrow\rangle|\downarrow\rangle, \tag{A.1}$$

where a_1, a_2, a_3, a_4 are complex constants. Then a simple calculation gives

$$\begin{aligned}
&\langle S_1^x S_2^x \rangle = \langle\psi|S_1^x S_2^x|\psi\rangle = (\langle\psi|S_1^x)(S_2^x|\psi\rangle) = (a_3^* a_2 + a_4^* a_1 + a_1^* a_4 + a_2^* a_3)/4, \\
&\langle S_1^y S_2^y \rangle = (a_3^* a_2 - a_4^* a_1 - a_1^* a_4 + a_2^* a_3)/4, \\
&\langle S_1^z S_2^z \rangle = \left(|a_1|^2 - |a_2|^2 - |a_3|^2 + |a_4|^2\right)/4,
\end{aligned} \tag{A.2}$$

and we find that the expression of the correlation reads

$$\begin{aligned}
\langle \mathbf{S}_1 \cdot \mathbf{S}_2 \rangle &= \langle S_1^x S_2^x \rangle + \langle S_1^y S_2^y \rangle + \langle S_1^z S_2^z \rangle \\
&= \left[2(a_3^* a_2 + a_2^* a_3) + |a_1|^2 - |a_2|^2 - |a_3|^2 + |a_4|^2\right]/4.
\end{aligned} \tag{A.3}$$

If the central system consists two coupled spins with the Hamiltonian $H_c = -\mathbf{S}_1 \cdot \mathbf{S}_2$, then $\langle \mathbf{S}_1 \cdot \mathbf{S}_2 \rangle$ is a direct measurement of the energy of the central system. If $\langle \mathbf{S}_1 \cdot \mathbf{S}_2 \rangle = -0.75$, then the central system is in the lowest-energy state (singlet state $\frac{1}{\sqrt{2}}(|\uparrow\rangle|\downarrow\rangle - |\downarrow\rangle|\uparrow\rangle)$); if $\langle \mathbf{S}_1 \cdot \mathbf{S}_2 \rangle = 0.25$, then the central system is in the highest-energy state, which could be one of the triplet states ($|\downarrow\rangle|\downarrow\rangle$, $|\uparrow\rangle|\uparrow\rangle$, $\frac{1}{\sqrt{2}}(|\uparrow\rangle|\downarrow\rangle + |\downarrow\rangle|\uparrow\rangle)$) or superposition of these states.

The concurrence, introduced by W.K. Wootters (Phys. Rev. Lett. **8**0, 2245 (1998)), is defined as

$$C(\rho) = \max(0, \lambda_1 - \lambda_2 - \lambda_3 - \lambda_4), \tag{A.4}$$

where the λ_i are the eigenvalues, in decreasing order, of the Hermitian matrix

$$R \equiv \sqrt{\sqrt{\rho}\widetilde{\rho}\sqrt{\rho}}. \tag{A.5}$$

Here ρ is the reduced density matrix of central spin pairs based on the standard basis $|\uparrow\rangle|\uparrow\rangle$, $|\uparrow\rangle|\downarrow\rangle$, $|\downarrow\rangle|\uparrow\rangle$, $|\downarrow\rangle|\downarrow\rangle$, and

$$\widetilde{\rho} = (\sigma_y \otimes \sigma_y)\rho^*(\sigma_y \otimes \sigma_y), \tag{A.6}$$

where $\sigma_y = \begin{pmatrix} 0 & -i \\ i & 0 \end{pmatrix}$ and ρ^* is the complex conjugate on ρ.

In fact, the concurrence C is a measure between the state $|\psi\rangle$ and the state with the two spins filpped $\left|\widetilde{\psi}\right\rangle$ ($C = \left|\left\langle\psi|\widetilde{\psi}\right\rangle\right|$). The singlet state, $|\psi\rangle = \frac{1}{\sqrt{2}}(|\uparrow\rangle|\downarrow\rangle - |\downarrow\rangle|\uparrow\rangle)$ is unchanged under two spins flip, so $C = 1$. Similarly, the triplet state $|\psi\rangle = \frac{1}{\sqrt{2}}(|\uparrow\rangle|\downarrow\rangle + |\downarrow\rangle|\uparrow\rangle)$ is also unchanged under two spins flip, so $C = 1$. For $|\uparrow\rangle|\uparrow\rangle$, $|\uparrow\rangle|\downarrow\rangle$, $|\downarrow\rangle|\uparrow\rangle$, and $|\downarrow\rangle|\downarrow\rangle$, the state is totally different if the two spins flip, so $C = 0$.

In order to get the value of concurrence, we need to know the expressions of ρ and $\widetilde{\rho}$. Our simulation program uses the standard basis, therefore we can easily get the matrix ρ, and according to the expression of ρ, we can find the matrix $\widetilde{\rho}$.

For our central system, the density matrix of the state in Eq.(A.1) is

$$\rho = \begin{pmatrix} |a_1|^2 & a_1^* a_2 & a_1^* a_3 & a_1^* a_4 \\ a_2^* a_1 & |a_2|^2 & a_2^* a_3 & a_2^* a_4 \\ a_3^* a_1 & a_3^* a_2 & |a_3|^2 & a_3^* a_4 \\ a_4^* a_1 & a_4^* a_2 & a_4^* a_3 & |a_4|^2 \end{pmatrix}, \tag{A.7}$$

and the state with two spins flipped is

$$\left|\widetilde{\psi}\right\rangle = \sigma_y \otimes \sigma_y |\psi\rangle = -a_4|\uparrow\rangle|\uparrow\rangle + a_3|\uparrow\rangle|\downarrow\rangle + a_2|\downarrow\rangle|\uparrow\rangle - a_1|\downarrow\rangle|\downarrow\rangle, \tag{A.8}$$

therefore the matrxi $\widetilde{\rho}$ can be expressed as

$$\widetilde{\rho} = \left|\widetilde{\psi}\right\rangle\left\langle\widetilde{\psi}\right| = \begin{pmatrix} |a_4|^2 & -a_4^* a_3 & -a_4^* a_2 & a_4^* a_1 \\ -a_3^* a_4 & |a_3|^2 & a_3^* a_2 & -a_3^* a_1 \\ -a_2^* a_4 & a_2^* a_3 & |a_2|^2 & -a_2^* a_1 \\ a_1^* a_4 & -a_1^* a_3 & -a_1^* a_2 & |a_1|^2 \end{pmatrix}. \tag{A.9}$$

Finally, by directly diagonalizing the matrix R, we can get the eigenvalues $\{\lambda_i\}$ and then the concurrence C.

Appendix B

Spin Wave in a Chain with Free Ends

We consider a spin chain of N spins ($S = 1/2$) with nearest neighbor interaction. The Hamiltonian for a chain with free-end boundary conditions reads

$$H = -J \sum_{k=1}^{N-1} (S_k^x S_{k+1}^x + S_k^y S_{k+1}^y + \lambda S_k^z S_{k+1}^z). \tag{B.1}$$

We take an ansatz for the eigenstate (we will prove that the following expression is only correct when $\lambda = 1$):

$$|k\rangle = \sqrt{\frac{2}{N}} \sum_{j=1}^{N} \left\{ \cos[k(j - \frac{1}{2})] + \delta(k)(\frac{\sqrt{2}}{2} - 1) \right\} |\downarrow_j\rangle , \tag{B.2}$$
$$k = \frac{m\pi}{N}, m = 0, 1, 2, ..., N - 1.$$

Here $m \neq N$ or $k \neq \pi$ otherwise $|k\rangle = 0$, and the normalization constant $\sqrt{N/2}$ follows from the identities :

$$\begin{aligned}
&\frac{2}{N}\sum_{j=1}^{N}\cos[k(j-\frac{1}{2})]^2 \\
&=\frac{1}{N}\sum_{j=1}^{N}\left\{1+\cos\left[\frac{2m\pi}{N}(j-\frac{1}{2})\right]\right\} \\
&=1+\frac{1}{N}\left[\cos(\frac{m\pi}{N})\sum_{j=1}^{N}\cos\left(\frac{2m\pi j}{N}\right)+\sin(\frac{m\pi}{N})\sum_{j=1}^{N}\sin\left(\frac{2m\pi j}{N}\right)\right] \\
&=1, \qquad \text{(B.3)}
\end{aligned}$$

for $k \neq 0$, and

$$\frac{2}{N}\sum_{j=1}^{N}\left(\frac{\sqrt{2}}{2}\right)^2=1, \qquad \text{(B.4)}$$

for $k=0$. Furthermore, we have

$$\begin{aligned}
&\frac{2}{N}\sum_{k=0}^{N-1}\left\{\cos[k(j-\frac{1}{2})]+\delta(k)(\frac{\sqrt{2}}{2}-1)\right\}^2 \\
&=\frac{2}{N}\left\{\frac{1}{2}+\sum_{k=1}^{N-1}\cos^2\left[k(j-\frac{1}{2})\right]\right\} \\
&=\frac{1}{N}\left\{N+\sum_{m=1}^{N-1}\cos\left[\frac{2m\pi}{N}(j-\frac{1}{2})\right]\right\} \\
&=1+\frac{1}{N}\sum_{m=1}^{(N-1)/2}\left\{\cos\left[\frac{2m\pi}{N}(j-\frac{1}{2})\right]+\cos\left[\frac{2\pi}{N}(N-m)(j-\frac{1}{2})\right]\right\} \\
&=1+\frac{1}{N}\sum_{m=1}^{(N-1)/2}\left\{\cos\left[\frac{2m\pi}{N}(j-\frac{1}{2})\right]+\cos\left[\pi+\frac{2m\pi}{N}(j-\frac{1}{2})\right]\right\} \\
&=1. \qquad \text{(B.5)}
\end{aligned}$$

If we let the Hamiltonian H act on $|k\rangle$, we can get :

$$\begin{aligned}
H|k\rangle &= \sqrt{\frac{2}{N}}\sum_{j=1}^{N}\cos[k(j-\frac{1}{2})]H|\downarrow_j\rangle \\
&= \sqrt{\frac{2}{N}}\sum_{j=2}^{N-1}\cos[k(j-\frac{1}{2})]\frac{-(N-3)\lambda J+2\lambda J}{4}|\downarrow_j\rangle \\
&+ \sqrt{\frac{2}{N}}\sum_{j=1,N}\cos[k(j-\frac{1}{2})]\frac{-(N-2)\lambda J+\lambda J}{4}|\downarrow_j\rangle \\
&- \sqrt{\frac{2}{N}}\sum_{j=1}^{N-1}\cos[k(j-\frac{1}{2})]\frac{J}{2}|\downarrow_{j+1}\rangle - \sqrt{\frac{2}{N}}\sum_{j=2}^{N}\cos[k(j-\frac{1}{2})]\frac{J}{2}|\downarrow_{j-1}\rangle \\
&= \frac{J}{\sqrt{2N}}\sum_{j=1}\left[\cos[k(j-\frac{1}{2})]\frac{-(N-3)\lambda}{2}-\cos[k(j+\frac{1}{2})]\right]|\downarrow_j\rangle \\
&+ \frac{J}{\sqrt{2N}}\sum_{j=2}^{N-1}\left[\cos[k(j-\frac{1}{2})]\frac{-(N-5)\lambda}{2}-\cos[k(j-\frac{3}{2})]-\cos[k(j+\frac{1}{2})]\right]|\downarrow_j\rangle \\
&+ \frac{J}{\sqrt{2N}}\sum_{j=N}\left[\cos[k(j-\frac{1}{2})]\frac{-(N-3)\lambda}{2}-\cos[k(j-\frac{3}{2})]\right]|\downarrow_j\rangle\,, \qquad \text{(B.6)}
\end{aligned}$$

or

$$\begin{aligned}
H|k\rangle &= \frac{J}{\sqrt{2N}}\sum_{j=1}\cos[k(j-\frac{1}{2})]\left[\frac{-(N-5)\lambda}{2}-\lambda-\frac{\cos[k(j+\frac{1}{2})]}{\cos[k(j-\frac{1}{2})]}\right]|\downarrow_j\rangle \\
&+ \frac{J}{\sqrt{2N}}\sum_{j=2}^{N-1}\cos[k(j-\frac{1}{2})]\left[\frac{-(N-5)\lambda}{2}-2\cos k\right]|\downarrow_j\rangle \\
&+ \frac{J}{\sqrt{2N}}\sum_{j=N}\cos[k(j-\frac{1}{2})]\left[\frac{-(N-5)\lambda}{2}-\lambda-\frac{\cos[k(j-\frac{3}{2})]}{\cos[k(j-\frac{1}{2})]}\right]|\downarrow_j\rangle\,.
\end{aligned} \qquad \text{(B.7)}$$

For $j=1$ we have

$$\begin{aligned}
1+\frac{\cos[k(j+\frac{1}{2})]}{\cos[k(j-\frac{1}{2})]} &= \frac{\cos[k(j-\frac{1}{2})]+\cos[k(j+\frac{1}{2})]}{\cos[k(j-\frac{1}{2})]} \\
&= 2\cos kj = 2\cos k, \qquad \text{(B.8)}
\end{aligned}$$

and for $j = N$ we find

$$\begin{aligned} 1 + \frac{\cos[k(j-\frac{3}{2})]}{\cos[k(j-\frac{1}{2})]} &= \frac{2\cos[k(j-1)]\cos\frac{k}{2}}{\cos[k(j-\frac{1}{2})]} \\ &= \frac{2\cos\left(m\pi - \frac{m\pi}{N}\right)\cos\frac{m\pi}{2N}}{\cos\left(m\pi - \frac{m\pi}{2N}\right)} \\ &= 2\cos k. \end{aligned} \tag{B.9}$$

Equation (B.7) becomes

$$\begin{aligned} H\left|k\right\rangle &= \frac{J}{\sqrt{2N}}\sum_{j=1}^{N}\cos[k(j-\frac{1}{2})]\left[\frac{-(N-5)\lambda}{2} - 2\cos k\right]\left|\downarrow_j\right\rangle \\ &\quad + \frac{J}{\sqrt{2N}}\sum_{j=1,N}\cos[k(j-\frac{1}{2})]\,(1-\lambda)\left|\downarrow_j\right\rangle \\ &= J\left[\frac{-(N-5)\lambda}{4} - \cos k\right]\left|k\right\rangle + \frac{J\,(1-\lambda)}{\sqrt{2N}}\sum_{j=1,N}\cos[k(j-\frac{1}{2})]\left|\downarrow_j\right\rangle, \end{aligned} \tag{B.10}$$

it clear that only for $\lambda = 1$ the second term in above expression is zero, therefore we have

$$H\left|k\right\rangle = J\left[\frac{-(N-5)\lambda}{4} - \cos k\right]\left|k\right\rangle \equiv E_k\left|k\right\rangle, \tag{B.11}$$

where

$$E_k = E_0 + J\,(1-\cos k)\,; \tag{B.12}$$

$$E_0 = \frac{-(N-1)J}{4}; \tag{B.13}$$

$$k = 0, 1, 2, ..., N-1. \tag{B.14}$$

Now we consider the time evolution of the system ($\lambda = 1$), that initially is in a state with all spins up except for spin j which is down. We denote this state by $\left|t=0\right\rangle = \left|\downarrow_j\right\rangle$. The state at time t is given by

$$
\begin{aligned}
|t\rangle &= e^{-itH}\,|\downarrow_j\rangle \\
&= \sum_{k=0}^{N-1} e^{-itE_k}\,|k\rangle\,\langle k|\,|\downarrow_j\rangle \\
&= \sqrt{\frac{2}{N}}\sum_{k=0}^{N-1} e^{-itE_k}\,|k\rangle \sum_{m=1}^{N}\left\{\cos[k(m-\frac{1}{2})]+\delta(k)(\frac{\sqrt{2}}{2}-1)\right\}\langle\downarrow_m\mid\downarrow_j\rangle \\
&= \sqrt{\frac{2}{N}}\sum_{k=0}^{N-1} e^{-itE_k}\,|k\rangle\left\{\cos[k(j-\frac{1}{2})]+\delta(k)(\frac{\sqrt{2}}{2}-1)\right\} \\
&= \frac{2}{N}e^{-i(E_0+J\lambda)}\sum_{n=1}^{N}\sum_{k=0}^{N-1}\exp\left(iJt\cos k\right)\left\{\cos[k(j-\frac{1}{2})]+\delta(k)(\frac{\sqrt{2}}{2}-1)\right\} \\
&\times\left\{\cos[k(n-\frac{1}{2})]+\delta(k)(\frac{\sqrt{2}}{2}-1)\right\}|\downarrow_n\rangle \\
&= \frac{1}{N}e^{-i(E_0+J\lambda)}\sum_{n=1}^{N}\sum_{k=0}^{N-1}\exp\left(iJt\cos k\right) \\
&\times\left\{\cos k(j+n-1)+\cos k(j-n)-\delta(k)\right\}|\downarrow_n\rangle\,. \qquad \text{(B.15)}
\end{aligned}
$$

The time evolution of the $m-th$ spin $< S_m^z >$ is

$$
\begin{aligned}
< S_m^z > &= \langle t|\,S_m^z\,|t\rangle = \langle\downarrow_j|\,e^{itH}S_m^z e^{-itH}\,|\downarrow_j\rangle \\
&= \sum_{q,p=1}^{N}\langle\downarrow_j|\,e^{itH}\,|\downarrow_q\rangle\,\langle\downarrow_q|\,S_m^z\,|\downarrow_p\rangle\,\langle\downarrow_p|\,e^{-itH}\,|\downarrow_j\rangle\,, \qquad \text{(B.16)}
\end{aligned}
$$

and as

$$
S_m^z\,|\downarrow_p\rangle = \{\begin{array}{c} -\frac{1}{2}\,|\downarrow_p\rangle\,, m=p \\ \frac{1}{2}\,|\downarrow_p\rangle\,, m\neq p\end{array} = \frac{1}{2}\left[1-2\delta(m-p)\right]|\downarrow_p\rangle\,, \qquad \text{(B.17)}
$$

we have

$$
\begin{aligned}
< S_m^z > &= \sum_{q,p=1}^{N}\langle\downarrow_j|\,e^{itH}\,|\downarrow_q\rangle\,\langle\downarrow_q|\,\frac{1}{2}\left[1-2\delta(m-p)\right]|\downarrow_p\rangle\,\langle\downarrow_p|\,e^{-itH}\,|\downarrow_j\rangle \\
&= \sum_{p=1}^{N}\frac{1}{2}\left[1-2\delta(m-p)\right]\langle\downarrow_j|\,e^{itH}\,|\downarrow_p\rangle\,\langle\downarrow_p|\,e^{-itH}\,|\downarrow_j\rangle \\
&= \frac{1}{2}\left[1-2\left|\langle\downarrow_m|\,e^{-itH}\,|\downarrow_j\rangle\right|^2)\right] \\
&= \frac{1}{2}\left[1-2\left|\langle\downarrow_m\,|t\rangle\right|^2)\right]. \qquad \text{(B.18)}
\end{aligned}
$$

By using the expression of $|t\rangle$ in Eq.(B.15), we find

$$\begin{aligned}\langle S_m(t)\rangle &= \frac{1}{2} - \frac{4}{N^2}\left|\sum_{k=0}^{N-1}\exp\left(iJt\cos k\right)\left\{\cos[k(j-\frac{1}{2})] + \delta(k)(\frac{\sqrt{2}}{2}-1)\right\}\right. \\ &\left.\left\{\cos[k(m-\frac{1}{2})] + \delta(k)(\frac{\sqrt{2}}{2}-1)\right\}\right|^2 \\ &= \frac{1}{2} - \frac{1}{N^2}\left|\sum_{k=0}^{N-1}\exp\left(iJt\cos k\right)\left[\cos k(j+m-1) + \cos k(j-m) - \delta(k)\right]\right|^2 .\end{aligned} \tag{B.19}$$

Summary

From a large collection of simulation results for a ferromagnetic and antiferromagnetic Heisenberg system coupled to a variety of different spin-bath environments that are initially prepared in the ground state or random state, we establish the conditions under which the central system relaxes from the initial spin-up - spin-down state towards its ground state or other pointer states. In general, it turns out that the relaxation to the ground (pointer) state(s) is a more complicated process, than the one one would naively expect, depending essentially on the ratio between parameters of the interaction and environment Hamiltonians. Changing the internal dynamics of the environment may change the qualitative features of the decoherence of the central spin system.

The central system more easily evolves to its ground state when the latter is less entangled (e.g., up-down state compared to the singlet), and constraints on the system such as existence of additional integrals of motion can make the evolution to the ground state more efficient. At the first sight, the latter statement looks a bit counterintuitive since it means that it may happen that a more regular system exhibits faster relaxation than a chaotic one. The reason that this may happen is that the larger the dimensionality of the available Hilbert space for the central system is, the more complicated the decoherence process is due to appearance of the whole hierarchy of decoherence times for different elements of the reduced density matrix.

We found that environments that exhibit some form of frustration, such as spin glasses or frustrated antiferromagnets, might be very effective as a decoherence mechanism. We demonstrated that the efficiency of the decoherence process decreases drastically with the type of environment in the following order:

1) Spin glass and random coupling of all spins to the central system;

2) Frustrated antiferromagnet (triangular lattice with nearest-neighbor inter-

actions);

3) Bipartite antiferromagnet (square lattice with nearest-neighbor interactions);

4) One-dimensional ring with nearest-neighbor antiferromagnetic interactions.

Furthermore, we observed that for a fixed system size of the environment and in those cases that the decoherence is effective, different realizations of the random parameters do not significantly change the results. The use of spin-glass or frustrated thermal bath is indeed a very efficient way to simulate decoherence processes. Environments containing $14 - 16$ spins are sufficiently large to induce a complete decay of the Rabi oscillations, this in sharp contrast to environments that have a more simple structure, such as spin-chains or square lattices.

We believe that these results can stimulate further development and clarification of the "decoherence program". Assuming that the interaction with an environment is weak enough, a hypothesis that the pointer states should be the eigenstates of the Hamiltonian of the central system was proposed, with the very ambitious aim to explain the basic phenomenon of "quantum jumps". Our results confirm that if the interaction between the central system and environment is much smaller than the coupling between the spins in the central system, the pointer states are the eigenstates of the central system. However, our results also demonstrate the nongeneric character of the decoherence, casting doubts on the general applicability of the decoherence program.

In the presence of Ising-like anisotropy, domain walls in a ferromagnetic spin $1/2$ chain are dynamically stable over extended periods of time. The profiles of the magnetization of the domain wall are different from the profile in the ground state in the subspace of zero total magnetization. As the system becomes more isotropic, approaching the quantum critical point, the width of the domain wall increases as a power law, with an exponent equal to $1/2$.

We also studied the propagation of spin wave through the domain wall in the quantum spin $1/2$ chain, and found that the longitudinal components of the spin wave speed up when they cross a domain wall. The transverse components of the spin wave are almost totally reflected by the domain wall, but this characteristic feature of the microscopic quantum chain, obtained by solving the time-dependent Schrödinger equation, is not found in mesoscopic magnetic systems, where the transverse components cross a domain wall without

reflection and with a phase shift of $\pi/2$. The system described by the Landau-Lifshitz-Gilbert equation treats the magnetic system in the mesoscopic regime as a classical, continuous medium, whereas our study treats the magnetic system as a microscopic, quantum mechanical system. Which of these two approaches is the most suitable description obviously depends on the specific material. The change of behavior from mesoscopic to microscopic may become important as bottom-up chemical synthesis is providing new ways for further down-sizing of the magnets.

Samenvatting

Aan de hand van een grote verzameling simulatieresultaten voor een ferro- en antiferromagnetisch Heisenberg systeem, gekoppeld aan verschillende spin-bad omgevingen geprepareerd in de grondtoestand, hebben we de voorwaarden bepaald waaronder het centrale Heisenberg systeem evolueert van de initiële spin-up - spin-down toestand naar zijn grondtoestand of naar andere "pointer" toestanden. We hebben vastgesteld dat de evolutie naar de grondtoestand of een pointer toestand een aanzienlijk gecompliceerder proces is dan wat men zou verwachten. De evolutie hangt op een essentiële, niet-intuïtieve manier af van de verhouding van de sterkte van de interaktie en van het type spin-bad Hamiltonianen. Veranderen we de interne dynamica van de omgeving (= spin-bad) dan verloopt de decoherentie van het centrale systeem meestal, maar niet altijd, anders.

Het centrale systeem relaxeert gemakelijker naar zijn grondtoestand indien deze laatste minder verstrengeld (entangled) is, zoals bij de spin-up - spin-down toestand en de singlet toestand. Heeft het systeem bijvoorbeeld extra behouden grootheden dan kan de evolutie naar de grondtoestand sneller verlopen. Op het eerste zich lijkt dit laatste een beetje vreemd omdat het zou suggereren dat een meer regulier systeem sneller zou kunnen relaxeren dan een meer chaotisch systeem. Een verklaring voor dit gedrag is te vinden in het feit dat in de afwezigheid van extra behouden grootheden, het decoherentieproces veel gecompliceerder is, met verschillende decoherentietijden voor de verschillende elementen van de dichtheidsmatrix, en dit omdat de toegankelijke Hilberruimte groter is.

We hebben gevonden dat omgevingen die op één of andere manier "gefrustreerd" zijn, zoals bvb, een spin-glas of een antiferromagneet op een driehoekig rooster, aanleiding geven tot een zeer effectief decoherentieproces. We hebben laten zien dat de efficiëntie van het decoherentieproces drastisch afneemt indien we het type van spin-bad als volgt kiezen:

1) Spin-glas en random waarde voor de koppelingsterkte van de spins met alle spins in het centrale systeem;

2) Gefrustreerde antiferromagneet (driehoekig rooster met naaste-nabuur interacties);

3) Bipartiete antiferromagneet (vierkant rooster met naaste-nabuur interacties);

4) En-dimensionale ring met naaste-nabuur interacties.

Verder hebben we aangetoond dat voor een spin bad omgeving met een vast aantal spins en in die gevallen waarin het decoherentieproces efficiënt is, verschillende realisaties van de random parameters geen significant effect geeft. Gebruiken we het spin-glas of de gefrustreerde magneet als omgeving dan blijkt dat dit een zeer effectieve manier is om het decoherentieprocessen to simuleren. Omgevingen met 14 tot 16 spins zijn dan voldoende groot om de Rabi oscillaties volledig te onderdrukken, dit in tegenstelling met spin bad omgevingen die een eenvoudigere struktuur hebben, zoals een ketting of vierkant rooster van spins.

Onze resultaten zijn een stimulans om het zogenaamde "decoherence program" verder te ontwikkelen en verhelderen. Indien we aannemen dat de interacties met de omgeving zwak genoeg zijn dan is de stelling dat de "pointer" toestand een eigentoestand van de Hamiltoniaan van het centrale systeem moet zijn, met het ambitieuze doel om het fenomeen van de zogenaamde "quantum jumps" te verklaren. Onze resultaten bevestigen dat onder de genoemde condities de "pointer" toestanden inderdaad de eigentoestanden zijn van het centrale systeem. Anderzijds tonen onze resultaten ook aan dat de decoherentie verre van generiek is, wat dan de algemene toepasbaarheid van het "decoherence program" sterk in vraag stelt.

In de aanwezigheid van Ising-achtige anisotrope interacties blijken domeinmuren in ferromagnetische spin-1/2 systemen dynamisch stabiel te zijn over zeer lange tijden. Het magnetisatieprofiel van de domeinmuur verschilt van het profiel van de grondtoestand in de deelruimte met totale magnetisatie nul. Als het systeem meer isotroop wordt en het in de buurt van het quantum kritische punt wordt gebracht dan divergeert de breedte van de muur als een macht van de afstand tot het kritisch punt en met kritische exponent 1/2.

Ten slotte hebben we de propagatie van spingolven door domeinmuren in quantum spin-1/2 kettingen bestudeerd. We hebben gevonden dat de longitudinale component van de spingolf versnelt bij het doorboren van een domeinmuur.

De transverse component wordt echter bijna volledig gereflecteerd. Dit gedrag, afgeleidt uit de oplossing van de tijdsafhankelijke Schrödinger vergelijking, is eigen aan het quantum spin model, dit in tegenstelling met het gedrag in mesoscopische magnetische systemen. Deze laatste worden veelal beschreven door de Landau-Lifschitz-Gilbert vergelijking die het mesoscopische magnetische systeem als een klassiek continue medium beschrijft en waarin de transverse component van de spingolf zonder reflectie maar met een faseverschuiving van 90^0 aan de andere kant van de domeinmuur verschijnt. Welke van de twee beschrijvingen het meest geëigend is hangt uiteraard af van het specifieke materiaal. Echter, het verschil in het gedrag tussen een mesoscopisch en een microscopisch systeem kan van belang worden nu het met hedendaagse bottom-up synthetische chemie mogelijk wordt om magnetische materialen steeds kleiner te maken.

Publications

[1] S. Yuan, M.I. Katsnelson, and H. De Raedt, *Giant enhancement of quantum decoherence by frustrated environments*, JETP Letters. **84**, 99-103 (2006).

[2] S. Yuan, H. De Raedt, and S. Miyashita, *Quantum Dynamics of Spin Wave Propagation Through Domain Walls*, J. Phys. Soc. Jpn. **75**, 084703 (2006).

[3] S. Yuan, M.I. Katsnelson, and H. De Raedt, *Evolution of a quantum spin system to its ground state: Role of entanglement and interaction symmetry*, Phys. Rev. A **75**, 052109 (2007).

[4] S. Yuan, H. De Raedt, and S. Miyashita, *Domain Wall Dynamics near a Quantum Critical Point*, Phys. Rev. B **75**, 184305 (2007).

[5] S. Yuan, M.I. Katsnelson, and H. De Raedt, *Importance of bath dynamics for decoherence in spin systems*, arXiv:0707.2372.

Acknowledgments

During the last fours years, I enjoyed the study and daily life in the computational physics group in University of Groningen. I still remember that when I first visited Groningen as a PhD candidate, I had a feeling that this is the place I should be. Now, it is a great pleasure to acknowledge all colleagues and friends at the end of my PhD study.

I am greatly indebted to my supervisor Prof. Hans De Raedt for his continuous encouragement and invaluable guidance of my research.

I would like to give special thanks to Prof. Seiji Miyashita and Prof. Mikhail I. Katsnelson. I am very grateful for their support and supervision.

Many thanks go to the former and current colleagues in our group, Dr. K.F.L. Michielsen, Dr. Chuan-Jian Shen, Dr. M.T. Figge, K. Keimpema, and Fengping Jin, for many nice discussions and help in daily life.

I would like to thank the reading committee for carefully reading this thesis and for giving me a lot of good advice and comments.

Finally, I would like to give my warm thanks to my parents and my wife, Shuang Zhao, for their continuous care and support. I also want to thank my little baby, Zi Xuan as she brings me many memorable moments from the very moment that she was born.